Max-Planck-Institut
für Meteorologie

MAX-PLANCK-GESELLSCHAFT

The Water Cycle in the Mediterranean Region and the Impacts of Climate Change

Alberto Elizalde Arellano

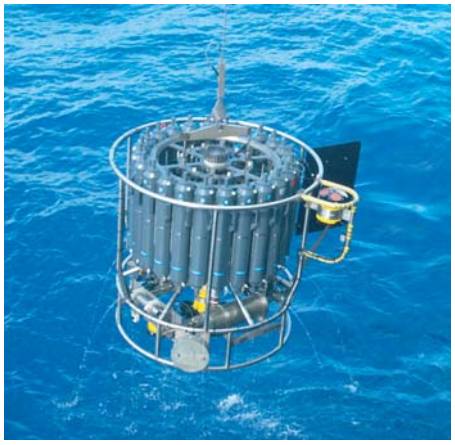

Berichte zur Erdsystemforschung 103/2011

Reports on Earth System Science

Hinweis

Die Berichte zur Erdsystemforschung werden vom Max-Planck-Institut für Meteorologie in Hamburg in unregelmäßiger Abfolge herausgegeben.

Sie enthalten wissenschaftliche und technische Beiträge, inklusive Dissertationen.

Die Beiträge geben nicht notwendigerweise die Auffassung des Instituts wieder.

Die "Berichte zur Erdsystemforschung" führen die vorherigen Reihen "Reports" und "Examensarbeiten" weiter.

Notice

The Reports on Earth System Science are published by the Max Planck Institute for Meteorology in Hamburg. They appear in irregular intervals.

They contain scientific and technical contributions, including Ph. D. theses.

The Reports do not necessarily reflect the opinion of the Institute.

The "Reports on Earth System Science" continue the former "Reports" and "Examensarbeiten" of the Max Planck Institute.

Anschrift / Address

Max-Planck-Institut für Meteorologie
Bundesstrasse 53
20146 Hamburg
Deutschland

Tel.: +49-(0)40-4 11 73-0
Fax: +49-(0)40-4 11 73-298
Web: www.mpimet.mpg.de

Layout:

Bettina Diallo, PR & Grafik

Titelfotos:
vorne:
Christian Klepp - Jochem Marotzke - Christian Klepp
hinten:
Clotilde Dubois - Christian Klepp - Katsumasa Tanaka

Berichte zur Erdsystemforschung 103/2011

The Water Cycle in the Mediterranean Region and the Impacts of Climate Change

Alberto Elizalde Arellano

aus México D.F., México.

Hamburg 2011

Reports on Earth System Science 103/2011

ISSN 1614-1199

Alberto Elizalde Arellano
Max-Planck-Institut für Meteorologie
Bundesstrasse 53
20146 Hamburg
Germany

Als Dissertation angenommen
vom Department Geowissenschaften der Universität Hamburg

auf Grund der Gutachten von
Prof. Dr. Martin Claußen
und
Prof. Dr. Daniela Jacob

Hamburg, den 14. Juli 2011
Prof. Dr. Jürgen Oßenbrügge
Leiter des Departments für Geowissenschaften

ISSN 1614-1199

The Water Cycle in the Mediterranean Region and the Impacts of Climate Change

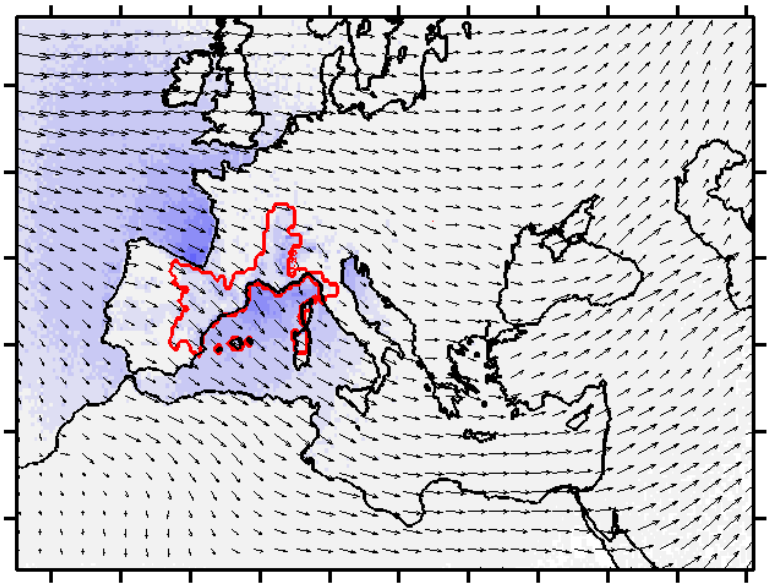

Alberto Elizalde Arellano

Hamburg 2011

Abstract

The water cycle acts as an integrator within the Mediterranean climate system. The climate variability is controlled by several phenomena involved in the water cycle processes such as precipitation, evaporation, cloud formation, ocean-atmosphere and land-atmosphere interactions, moisture advection, atmospheric circulation, etc. These processes, together with the geographical location and morphology of the Mediterranean region, form complex weather systems on different time and spatial scales. The Mediterranean Sea also plays an important role in the hydrology system. The basin is a source of moisture due to its excess of evaporation and, in a long term average, it warms the low atmosphere due to heat loss at the air-sea interface. A comprehensive understanding of the mechanisms involved in the hydrological cycle is necessary. Furthermore, the region has been identified as one of the most sensitive areas to raising temperatures conditions in future climate projections, which implies changes in the hydrological cycle, water availability and therefore in the human activity.

Several works have studied the Mediterranean water cycle. Although large progress has been achieved, there are still open issues regarding the assessment of the hydrological cycle components, like, e.g., the evaporation over the Mediterranean Sea. The estimations of the freshwater loss from different data sets show a large range of discrepancies. This uncertainty can be attributed to several factors: data quality, time and spatial coverage, spatial resolution, and misrepresentation of physical processes, like air-sea interaction.

To overcome some of the previous deficiencies, a new high resolution modeling tool has been developed, which joins the atmosphere, ocean and hydrology components with the purpose to simulate the feedback mechanisms within the water cycle components. In the new model the regional climate model REMO, the ocean model MPI-OM and hydrology model HDmodel are fully coupled. Two experiments have been carried out, one using the coupled model and the other using the REMO model in stand-alone version. These experiments have been driven by ERA40 reanalysis data for model validation. A third run has been performed using the emissions scenario A1B to assess the climate change impact in the Mediterranean water cycle. The resolution used for the simulations are ~25 x 25 km^2 of REMO and ~10 x 10 km^2 for the MPI-OM.

Results show that the high resolution of the model improves, on the one side, the representation of the orographic precipitation processes through a finer description of the topography. This produces a more realistic precipitation pattern compared with coarse resolution data. On the

other side, a high resolution of the sea surface temperature (SST) and an active air-sea interaction improve the correlation of the marine evaporation with its driving components, especially at areas near the coast.

With regard to the role of the Mediterranean Sea in the hydrological cycle, it has been detected that the evaporation produced at the Mediterranean Sea contributes partially to precipitation over land through moisture advection by atmospheric eddy transport. This contribution varies throughout the year. Larger contribution takes place during winter than in summer. The opposite behavior is found for the terrestrial evaporation contribution. Nevertheless, it has been found that up to 53% of the water is recirculated within the Mediterranean hydrological cycle independent of the exchanged roles of the terrestrial and marine evaporation sources.

Concerning the impact of Climate Change, as a direct consequence of decreased precipitation, the deficit in the land water budget in the Mediterranean catchment induces a decrease up to 23% in the total river discharge into the Mediterranean Sea with respect to present climate conditions. Regarding the freshwater flux into the Mediterranean basin, the freshwater loss increases up to 21%. The magnitudes of such deficits agree with previous studies from other authors, but the projected signal of the individual water budget components differ in this study.

The models analyzed here are able to reproduce the sea surface fluxes and the main characteristics of the physical processes involved in the Mediterranean hydrological cycle, including the air-sea feedbacks in the case of the coupled model. Another degree of freedom is introduced when SSTs are calculated in the coupled model, which can be considered as an advantage with regard to the assessment of the Climate Change response. The coupled model keeps more independence from the SSTs signal of its driving model in future climate simulations.

Contents

Chapter 1

Introduction

The Mediterranean water cycle is determined by a variety of complex processes that affect the region. Evidence of this variety is the spread of climate types that are present in the Mediterranean area. According to the Köppen-Geiger climate classification, the Mediterranean climate is defined as dry summer subtropical, but in fact, the variety of the climates is much larger: arid climate in northern Africa, continental climate at the border between Greece and Turkey, tundra climate in the Alpine highlands, among others (Peel et al. 2007; McKnight and Hess 2000). Such a variety and the strong weather regionality are consequences of the geographical location and morphology of the Mediterranean region.

Several studies have been carried out to yield a better understanding of the processes involved in the Mediterranean water cycle. Different approaches have been used to address these issues based on satellite data, surface measurements and model simulated data. The studies achieve a wide comprehension of the Mediterranean Climate, but, there are still open issues like e.g. the disagreement in the assessments of the water cycle components due to the large range of uncertainty in the data and the misrepresentation or simply lack of information related to unresolved processes.

This Chapter describes the main factors that affect the Mediterranean water cycle, some of the gaps in the current knowledge and, finally, expose challenging questions to be addressed within this study to advance the understanding of the Mediterranean Climate.

1.1 Motivation

The climate and weather in the Mediterranean region is under the influence of two large-scale atmospheric circulation phenomena: the subsidence of the Hadley Cell and the direct effect of large-scale air masses driven by the Atlantic Jet Stream (Xoplaki et al. 2003; Alpert et al. 2006). Meanwhile in the first case the descending motion reduces the air moisture, the second one governs transport of water vapor in and out of the Mediterranean region (Gimeno et al. 2010; Schicker et al. 2010). The seasonal changes of the moisture transport are directly dependent

on the seasonal variability of the large-scale circulation (Millán et al. 2002; Josey et al. 2011), like in the case of the moisture stagnation during the summer season (Schicker et al. 2010).

In a similar way, the Mediterranean climate variations are a direct consequence of the interannual variability of the large-scale circulation (Mariotti et al. 2002; Lionello and Sanna 2005; Josey et al. 2011). Large-scale pressure systems, northern fronts and extratropical cyclones from the Atlantic affect Europe and the western Mediterranean region (Reale et al. 2001), as shown by the strong correlation between the precipitation in these areas and the North Atlantic Oscillation index (NAO) (Fernández et al. 2003). Under certain circumstances, the large-scale circulation could lead to specific extreme events (Hurrell 1995). Even though it is not completely understood, the high temperature and air dryness produced during the heat wave in summer 2003 seems to be a consequence of the large-scale variation (Black and Sutton 2007).

The complex orography is the key factor that explains the regionality of the weather regimes (Bojariu and Giorgi 2005). High mountains steer the air masses deviating or channeling the wind flow through valleys or sea straits. Even though the inflow and outflow to the Mediterranean region are influenced by the seasonality of the pressure systems, the orography steers the airstreams in predominant wind currents: an inflow stream takes place mainly at the channel between the Alps and Pyrenees mountain ranges, and outflow streams occur at the straits of Gibraltar, Dardanelles and over the Red Sea, Mesopotamia region and the plain between the highlands of Iran and Arabia (Schicker et al. 2010). The mechanical forcing of the wind dynamics is also responsible for limiting the moisture transport (Fernández et al. 2003). In the case of the Alps and Pyrenees mountains, the deposition of water vapor is done by the forced ascent of the eastward air flow due to such mountain ranges, hence, the inflow of moisture into the Mediterranean region is reduced (Fernández et al. 2003; Sodemann and Zubler 2010). At the lee side of the mountains, the water vapor is recirculated locally by the turbulent flow. In this way, the northern and southern Alpine slopes present different hydrological regimes which are connected to Atlantic and Mediterranean water masses respectively (Sodemann and Zubler 2010).

Besides the local wind systems, the intricate coastal line and the sea surface temperature (SST) interact to create very local weather regimes (Millán et al. 2002, 2005). As discussed in Millán et al. (2005), during autumn, warm Mediterranean SST and relative cold air produce strong evaporation in the basin. The moist air at the coast is lifted by winds following the terrain profile upslope producing strong rainfall when cold air pools are found at high levels. Thereby, the water cycle budget is influenced by processes at local scale in coastal areas. These phenomena have been described for the western Mediterranean coast, but they are present in many parts of the basin. Since the Mediterranean region has a very extensive coastal line (47,027 km), such local-scale processes have an important influence on the whole Mediterranean hydrological cycle.

The difficulty to interpret at large scales changes detected at the local scale in the Mediterranean

region has already been underlined by several authors (Spagnoli et al. 2002; Svensson et al. 2005; Neppel et al. 2011). Therefore, fine scale information is needed to resolve small scale features, e.g., on the moisture transport (Schicker et al. 2010).

The Mediterranean Sea plays an active role in the regional climate through the air-sea exchange of moisture and heat. There are strong feedbacks between the atmospheric and the oceanic components. The Mediterranean Sea is driven by the atmosphere through the exchange of moisture, momentum and heat at the surface. The heat gained or lost at the surface is transported to deeper ocean layers by turbulent diffusion and advection processes. The temporal scale of these internal heat-exchange processes in the sea is larger if compared with the respective temporal scale in the atmospheres. Therefore it may be said that the ocean has a larger thermal inertia that acts as a source or sink of heat modifying the thermal characteristics of the low atmosphere. Both components, the atmosphere and the Mediterranean Sea, are external driving forcings for each other and their interaction oscillates in a none stationary state throughout the year.

The Mediterranean Sea has a deficit on the heat and water surface budgets (Mariotti et al. 2002; Sanchez-Gomez et al. 2011). On the one hand, the loss of heat and moisture is the forcing mechanism responsible for the Mediterranean thermohaline circulation (MTHC). On the other hand, the Mediterranean Sea can be seen as a heat and moisture source for the climate system.

The marine evaporation is determined by different conditions that affect the surface: SST, atmospheric circulation, humidity, air temperature and wind speed. The spatial distribution and the time variability of these factors produce a very characteristic evaporation pattern. The water vapor produced by the evaporation is transported to land areas by advection becoming part of the local precipitation. In the Mediterranean catchment, the influence of Atlantic and Mediterranean evaporation on land rainfall largely depends on the area location, the season, the atmospheric conditions and circulation (Schicker et al. 2010).

The influence of the marine evaporation produced over the Mediterranean sea area is not limited only to the Mediterranean sea. The more direct influences are seen in Europe originating from the western Mediterranean basin, and in the Middle East and northern Africa by the eastern one (Schicker et al. 2010). Gimeno et al. (2010) show that the precipitation in the whole Northern Hemisphere is formed, even in a low fraction, with moisture from the Mediterranean Sea, and Li (2006) reports significant effects of Mediterranean sea surface changes on the global atmospheric circulation.

The influence of the Mediterranean Sea over the mesoscale to large-scale atmospheric dynamic has been addressed in previous works. Studies about the wave heat over Europe in 2003 come to the conclusion that Mediterranean SST anomalies have a significant influence on the large-scale atmospheric circulation, and the Mediterranean Sea plays an active role in the European Climate (Black and Sutton 2007). Contrary to this, Jung et al. (2006) concluded that

the Mediterranean plays a minor role in maintaining the anomalous atmospheric circulation.

The Mediterranean region has been identified as the area in which the mean precipitation and the surface temperatures are some of the most responsive variables to climate change (Giorgi 2006). A decrease in precipitation and an increase in temperature have been detected to occur under climate change conditions (Gibelin and Déqué 2003; Ulbrich 2006; Sheffield and Wood 2008; Mariotti et al. 2008; Giorgi and Lionello 2008; Somot et al. 2008).

Global warming, and the large-scale changes derived from it, may also have consequences. The increase of water vapor transport from low to high latitudes is influencing the hydrological cycle in the future climate of the Mediterranean region (IPCC 2007). Signals of trends for temperature and salinity of the Mediterranean Sea have already been detected at the end of the 20^{th} century (Rixen et al. 2005). These may have a large negative impact on the environment and on the social-economical activities.

Current efforts to understand and assess the water cycle in the Mediterranean region utilized observational or reanalysis data sets with low spatial resolution (~83 to ~125 km) (Colacino and Dell'Osso 1977; Mariotti et al. 2002; Jin and Zangvil 2009; Romanou et al. 2010), or coarse resolution (~150 km) from global atmosphere-ocean coupled model data (Mariotti et al. 2008). It became clear that there are still large uncertainties concerning the observations of the various terms of the heat and water budgets of the Mediterranean Sea. Sanchez-Gomez et al. (2011) analyzed the air-sea fluxes reproduced in high resolution simulations (~25 to ~55 km) from stand-alone regional climate models (RCMs), which were driven by coarse resolution SSTs (125 km). They conclude that inside the model ensembles, not all RCMs yield significant improvements of such fluxes. A successful simulation of the Mediterranean Sea has been achieved by Somot et al. (2008) using a regional atmosphere-ocean coupled model. The air-sea feedbacks were represented using a heat flux correction to improve the estimations of the atmospheric model. The resolution of the atmospheric model was ~50 km. However, no detailed studies about the water cycle were carried out with the Somot et al. (2008) model results.

This study pretends to improve the understanding and assessment of the Mediterranean water cycle through a better representation of small-scale processes and air-sea feedbacks using a new regional atmosphere-ocean-hydrology coupled model with a high spatial resolution (~25 km for the atmosphere, ~10 km for the ocean).

1.2 Objectives of this study

To overcome previous deficiencies of existing climate simulations, a high resolution coupled atmosphere-ocean-hydrology modeling tool has been developed to fulfill the following objectives:

- Better representation of local scale processes through a detailed SST pattern
- Improvement of the surface fluxes through an interactive air-sea feedback
- Simulation of the hydrological cycle in a closed system

In this context, this study contributes to the understanding of the processes involved in the Mediterranean water cycle and to estimate the role that the Mediterranean Sea plays in it. With these primary goals, the hydrological cycle and its components are analyzed in a climatic framework to address the following questions:

- What are the impacts of the improved resolution and the inclusion of the air-sea feedbacks on the simulation of the water budget?
- What is the role of the Mediterranean Sea for precipitation in the Mediterranean region?
- How is the Mediterranean hydrological cycle affected by anthropogenic climate change?

The new tool, developed within this framework, includes the coupled components of the atmospheric regional climate model REMO (Jacob 2001) with the ocean model MPI-OM in a limited area version (Mikolajewicz 2011) and the hydrological model HDmodel (Hagemann and Dümenil 1998) as a river routing scheme for an interactive river discharge. The new configuration can be considered as a Regional Climate System Model (RCSM) and as part of a new generation of modeling tools for regional climate simulation purposes.

1.3 Outline

After the background given in Chapter 1, the content of the thesis comprises the following considerations:

In Chapter 2, the RCSM is presented with a detailed description of the model components and the coupling strategy. Besides this, a description of the different data sets, based on the observations, satellite data and reanalysis products, which have been used in this work as references is given. In Chapter 3, the validation of the RCSM is performed with a focus on the simulated hydrological components and air-sea fluxes, and the role of the water vapor and clouds in the solar radiation budget under climate change conditions is studied. In this chapter the oceanic response of the coupled system with regard to the Mediterranean water masses is addressed as well. Chapter 4 includes an analysis of the moisture divergence and advection, together with an assessment of the evaporations sources that contribute to the land precipitation over the Mediterranean catchment. In Chapter 5, the influence of the Mediterranean Sea on the atmospheric dynamics in the case of the heat wave event in summer 2003 as simulated by the RCSM is explained. Conclusions of the main findings are summarized in Chapter 6 and possible steps for future research are proposed.

Chapter 2

Model description and data

In Chapter 1 the necessity of using a high resolution atmosphere-ocean coupled model for a better representation of the climate in the Mediterranean region has been discussed. Here a new tool is presented to perform such simulations based on the coupling of three models: the REgional atmosphere MOdel (REMO), the Max-Planck-Institute for Meteorology ocean model (MPI-OM) and the Hydrological Discharge Model (HD model). All models have been developed at the Max-Planck-Institute for Meteorology. The OASIS3 software has been used as a coupler for the atmosphere and ocean components. To achieve the connection between the three earth components: land-atmosphere-ocean. Therefore, the new tool can be considered as a Regional Climate System Model (RCSM).

Figure 2.1 shows the domain of each model, and for the first time in the Mediterranean Sea simulations, the Black Sea has been included in the oceanic domain. Hence, the internal physics of the Black Sea is present in the inflow's signal to the Mediterranean Sea through the Bosphorus Strait.

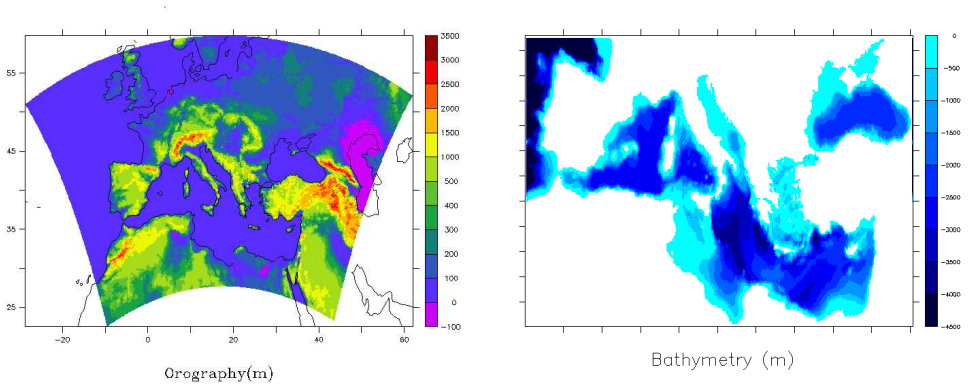

Figure 2.1: Domain of each model component: left panel shows the orography of the atmosphere model (REMO) and right panel shows the bathymetry of the oceanic component (MPI-OM). Units are meters

2.1 Atmospheric model

REMO (Jacob and Podzun 1997; Jacob 2001) is a three-dimensional, hydrostatic atmospheric circulation model which solves the discretized primitive equations of atmospheric motion. It is based on the 'Europa-Modell' of the German Weather service (Majewski 1991) and the physical parameterizations are taken from the global climate model ECHAM-4 (Roeckner et al. 1996). REMO is a hydrostatic model and can be used for an horizontal resolution up to 10km, in this case a 25 km resolution domain is established.

For horizontal discretization REMO uses a spherical Arakawa-C grid in which all variables, except the wind components, are defined in the center of the respective grid box. The grid box centers are defined on a rotated latitude-longitude coordinate system. In the vertical, variations of the prognostic variables (except surface pressure) are represented by a hybrid vertical coordinate system and 31 vertical levels are used for this experiment.

As a Limited Area Model, REMO needs lateral boundary forcing data like temperature, wind, surface pressure and moisture. These boundary conditions can be prepared using reanalysis data for validation simulations or from global climate models for climate simulation scenarios. For the surface boundary, the treatment of soil hydrology is based on a simple bucket scheme, whereas, over the sea, REMO uses the sea surface temperature (SST) whether they be prescribed or calculated on-line by the oceanic component. In this case, they are calculated only for the Mediterranean Sea and Black Sea, and prescribed for the rest of the oceanic surface.

2.2 Oceanic model

The oceanic component is the Max-Planck-Institute Ocean Model (MPI-OM, formerly C-HOPE (Maier-Reimer 1997; Marsland et al. 2003)), which is a primitive equation model (z-level, with Boussinesq and incompressibility assumptions) formulated on an orthogonal curvilinear Arakawa C-grid. The model includes a dynamic-thermodynamic sea ice model with viscous-plastic rheology (Hibler 1979). It has a free surface and uses a mass flux boundary condition for salinity.

For the Mediterranean domain the MPI-OM model uses a bipolar orthogonal spherical coordinate system. Orthogonal meridians and parallels are constructed according to the choice of zonal and meridional resolution and are used to define the spatial mesh. A simple bottom boundary layer scheme is included as well as the standard set of subgrid scale parameterizations (e.g. isopycnal diffusion, Richardson number dependent vertical diffusivities, a simple mixed layer scheme including the effect of wind mixing at the surface). The horizontal resolution is ~9 km. 29 vertical levels are used (the average of the depths between two consecutive

levels in meters: 6 17 27 37 48 60 74 92 113 136 161 192 228 272 325 389 466 559 671 806 969 1165 1401 1686 2029 2416 2841 3316 3816).

The original global model was modified and limited to the Mediterranean Sea Area (Mikolajewicz 2011). The oceanic domain includes both the Mediterranean and Black basins. The Atlantic box is used as a sponge zone, where oceanic temperature and salinity are restored. The Mediterranean Sea is connected to the Atlantic through the Gibraltar Strait which has been simulated with 4 grid boxes long (~36 km), 3 grid boxes wide (~27 km) with a narrower section of 2 grid boxes (~18 km). The depth is 270 m represented by the firsts 14 levels with one grid box channel at the bottom. The connection between the Mediterranean Sea and the Black Sea takes place through the Bosphorus Strait which has 3 grid boxes long (~27 km) and one grid box wide (~9 km), the maximum depth is 12 m.

2.3 Hydrological model

The HD Model (Hydrological Discharge) is a routing scheme, which has been developed at the Max Planck Institute for Meteorology (Hagemann and Dümenil 1998). It accounts for the lateral waterflow on the land surface in global climate model applications. Inside the coupled model it delivers freshwater from the river system to the ocean component. The model describes the translation and retention of the lateral discharge within the river system as a function of spatially distributed land surface characteristics.

The HD Model is applied on a regional scale with a fixed horizontal resolution of 1/2° on a regular, non-rotated spherical grid, corresponding to an average grid box size of about 55 km x 55 km . The model requires surface runoff and subsurface drainage as input parameters. These quantities are interpolated from the REMO model grid to the 1/2° grid used by the HD Model (Hagemann and Dümenil 1999; Hagemann and Jacob 2007).

The atmospheric domain covers the Mediterranean and Black Sea catchments for all Mediterranean and Black Sea rivers discharge calculation, except for the Nile river. The Nile discharge has been heavily antropogenized and its hydrological system is disconnected from meteorological processes, so a prescribed value of 1829.5 m^3/s has been used. This value corresponds to the mean of the last three decades of observed discharge according with river discharge observations database from Global Runoff Data Centre (GRDC) (Dümenil Gates et al. 2000).

2.4 Coupling strategy

The Figure 2.2 shows a scheme of the coupling strategy. The coupling between the REMO atmosphere model and the MPI-OM ocean model was carried out using the OASIS coupler

developed by CERFACS (Valcke 2006). OASIS is used for variables exchange and for coupling time synchronization only. A conservative bilinear interpolation routine is integrated in the MPI-OM model to interpolate fields between REMO and MPI-OM model grids. In the HDmodel a different interpolation for REMO fields is used.

In REMO heat, freshwater and momentum fluxes are calculated for each grid box and SST, sea ice thickness and compactness are received from the ocean model. The atmosphere-ocean coupling frequency is set to 6 hours and the calculation of the river routing is every 24 hours. A similar configuration without the river routing has been used for Indonesian rainfall simulations (Aldrian et al. 2005) and Arctic Sea ice studies (Mikolajewicz et al. 2005).

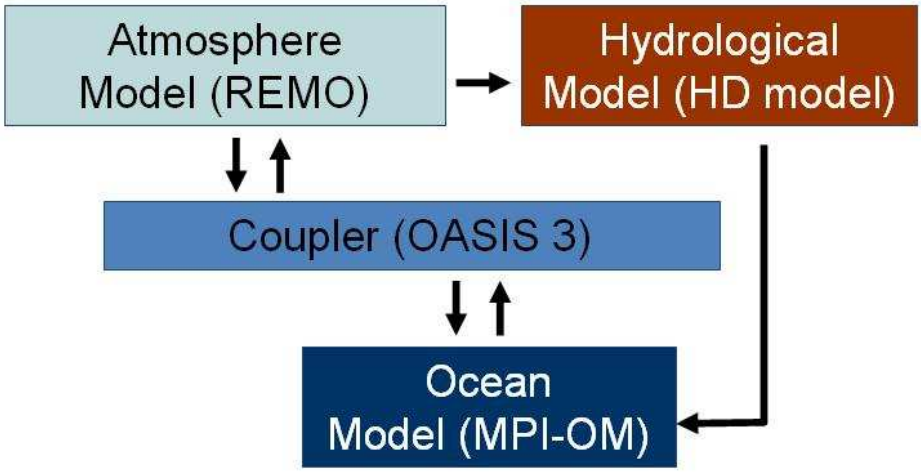

Figure 2.2: Scheme for the coupling of the model components

2.5 Description of the experiments

A total of four simulations have been conducted for this study. To investigate the air-sea feedback in the Mediterranean climate system, two atmospheric simulations have been performed. One simulation was done using the atmosphere regional climate model REMO only (hereinafter referred to as ARCM), in which the SSTs are prescribed. A second simulation was carried out with the coupled model RCSM, in which SSTs only at the Mediterranean and Black Seas are interactive. The Atlantic SSTs are prescribed as in the ARCM. Each of these two simulations consists on 41 years for present climate from 1958 to 2001. Perfect boundary conditions from the ERA40 reanalysis data by the European Center for Middle range Weather Forecast (ECMWF) (Uppala et al. 2005) have been used as lateral forcings for the REMO model and the Levitus et al. (1998) data set for the MPI-OM in the case of the RCSM simulation. In the case of the ARCM simulation, SSTs from the ERA40 data set were used as surface

conditions.

A third simulation was performed to study the impact of the coupling on the development of the water masses formation at Mediterranean Sea. The simulation was carried out with the uncoupled version of the Limited-Area Ocean Model MPI-OM (LAOM in the following). The same lateral boundary data was used as in the RCSM case, but the variables used to calculate the surface fluxes calculated from bulk formulae are obtained from the ARCM simulation, therefore. The simulation consist of 41 years in the same period (1958-2001).

A forth simulation is dedicated to investigate the hydrological cycle under climate change conditions. The scenario simulation was performed with the RCSM with exactly the same set-up as used in the simulation forced with reanalysis data, but driven by an experiment realized by the Instituto Nazionale di Geosifica e Vulcanologia (INGV) for the EU CIRCE project using the global coupled model ECHAM5/MPI-OM. The climate change conditions correspond to the A1B emissions scenario defined in the Special Report on Emissions Scenarios at the Third Assessment Report by the Intergovernmental Panel for Climate Change (SRES 2000). A period of 101 years from 1950 to 2050 was simulated. Throughout this work, past and future climate conditions are compared. For that purposes, a historical climate period is defined from 1961 to 1990, and a future climate scenario refers to the period from 2021 to 2050.

2.5.1 Initial conditions and spin-up

A 60 years spin-up run was performed with the stand-alone ocean model using Levitus et al. (1998) data set as initial conditions. The simulation was forced with a perpetual year forcings conditions. Temperature and salinity were restored to Levitus et al. (1998) data set values at the sponge zone and OMIP data (Röske 2006) were used for the surface forcings.

The final state of the 60 years Mediterranean simulation has been used as initial conditions for a second spin-up using the LAOM and RCSM set-ups. The second spin-up consists in 20 years (driven by the first 20 year from ERA40). Its final state was used as initial conditions of the definitive experiments. In the case of the scenario simulation the spin-up period was 40 years driven by the first 40 years from the GCM.

2.6 Data

The data sets used as references throughout this work are briefly presented.

CRU Climate Research Unit TS3.1. The resolution is 0.5 degree with a regular grid and global coverage over land only. A period from 1901 to 2006 is available. The data are

time series of monthly means (CRU 2008). Precipitation and evaporation data have been used in this work.

WILLMAT Willmott and Matsuura from the University of Delaware. The resolution is 0.5 degree with a regular grid and global coverage over land only. A period from 1986 to 2000 is available. The data are time series of monthly means (Willmott and Matsuura 2001)

GPCP Global Precipitation Climatology Project from the National Aeronautics and Space Administration. The resolution is 2.5 degree with a regular grid and global coverage. A period from 1979 to 2000 is available. The data are time series of monthly accumulated values (Adler et al. 2003). Precipitation data have been used in this work.

GRDC Observed Historical Discharge Data From Major Rivers For Climate Model Validation from the Global Runoff Data Center and Max Planck Institute. The period depends on the river. The data are time series of monthly means (Dümenil Gates et al. 2000).

ERA40 The ECMWF Re-analyses for 40 years from European Centre for Medium-Range Weather Forecasts. The resolution is 1.125 degree with a regular grid and global coverage. It is a data set of assimilated data which provides atmospheric analyses. A period from mid-1957 to 2001 is available. The data are time series of 6 hourly frequency values (Uppala et al. 2005). Surface heat fluxes, evaporation, precipitation, wind speed data have been used in this work.

HOAPS3 HOAPS Surface Flux Dataset v3.0 (Hamburg Ocean Atmosphere Parameters and Fluxes from Satellite Data) from Hamburg University and Max Planck Institute for Meteorology. The resolution is 0.5 degree with a regular grid and global coverage over ocean only (Information near the coast is not included). A period from 1987 to 2005 is available. The data are time series of monthly means. It is based on pure satellite data for parameters related to heat and freshwater fluxes over the sea (Andersson et al. 2010). Turbulent heat fluxes, evaporation and wind speed data have been used in this work.

NOCS NOCS Surface Flux Dataset v2.0 from the National Oceanography Centre, Southampton (NOCS). The resolution is 1 degree with a regular grid and global coverage over ocean only. A period from 1973 to 2009 is available. The data are time series of monthly means (Berry and Kent 2009). Radiative and turbulent fluxes have been used in this work.

ISCCP International Satellite Cloud Climatology Project as part of the World Climate Research Programme. The resolution is 1 degree with a regular grid and global coverage over ocean only. A period from 1958 onwards. The data are time series of monthly means. This product is a global analysis of satellite-based high-resolution for ocean surface variables. (Yu et al. 2008). Radiative fluxes have been used in this work.

OAFlux Objectively Analyzed air-sea fluxes from Woods Hole Oceanographic Institute. The resolution is 1 degree with a regular grid and global coverage over ocean only. A period from 1958 onwards. The data are time series of monthly means. This product is a global analysis of satellite-based high-resolution for ocean surface variables (Yu et al. 2008). Turbulent heat fluxes, evaporation and wind speed have data been used in this work.

MEDATLASII Mediterranean and Black Sea database of temperature salinity and biochemical parameters from MEDAR Group. The resolution is 0.36 degree with a regular grid and 21 vertical levels over Mediterranean and Black Seas. The data are climatological values. The computation is made from the observed data (MEDAR/MEDATLAS. 2002). Volumetric water temperature and salinity have been used in this work.

Chapter 3

Water cycle in the Mediterranean region

3.1 Introduction

This Chapter presents the performance of the RCSM and the ARCM. A model validation is carried out by the comparison of the model results with reference data sets of different nature. In addition, the model skills to reproduce the physical processes involved in the water cycle are discussed. The analysis is done on a climatological basis with a focus on seasonal changes for summer (June-July-August) and winter (December-January-February). These seasons were chosen since they include the extremest weather conditions throughout the year.

Throughout this Chapter, results from the scenario simulation are discussed too, and differences in the hydrological cycle components are shown. Two periods were selected for the climate change analysis: a past climate period (hereinafter referred to as historical period) from 1961 to 1990, and a future climate period from 2021 to 2050.

In the Section 3.2, the impact of the interactive SST (in the RCSM) versus the prescribed SST (in the ARCM) on the air-sea fluxes is discussed. Section 3.3 analyzes the response of the river system to the simulated precipitation and evaporation balance over land in both experiments. In Section 3.4, a validation of the individual components of the heat and freshwater fluxes over the Mediterranean Sea is performed. Section 3.5 investigates the influence of the hydrological cycle on the radiation budget under climate change conditions. Finally, a brief discussion of the oceanic response and water masses formation is given in Section 3.6.

3.2 Surface feedbacks

The water loses or gains energy through the radiative and turbulent fluxes at the air-sea interface. The net surface heat flux largely depends on the temperature gradient between the air and the sea. A positive net surface heat flux induces an air-to-sea energy transport, which is distributed to the deeper layers of the sea by turbulent diffusion and mixing processes. The

energy transport is reversed (sea-to-air) when the air temperature becomes colder than the sea temperature. Anyhow, the temporal scale of these internal heat-exchange processes in the sea is larger if compared to the respective temporal scale in the atmosphere. It may be said that the ocean has a greater thermal inertia that acts as a source or sink of heat and modifies the thermal characteristics of the low atmosphere. This interaction between both components, the atmosphere and the Mediterranean Sea, oscillates in a none stationary state throughout the year. However, the moisture exchange at the surface is a direct consequence of the thermal conditions at the interface and constrained by the air dryness and momentum. At the same time, a negative feedback is induced when the evaporation process extracts energy as latent heat modifying the thermal state of the thin surface layer.

Such a feedback is misrepresented in ARCM simulations, and it has been shown that it has an impact on the climate and its variability at large scales (Zhang et al. 2010). The response of the atmosphere and water exchange to the prescribed SST, in the ARCM experiment, and the fully prognostic SST, in RCSM one, is addressed in this section.

The moisture flux over water J in the atmospheric component is calculated using the bulk aerodynamic formula derived from Monin-Obukhov Similarity approach:

$$J = \rho C_h v_h \Delta q \tag{3.1}$$

with

$$\Delta q = (q_v - q_s)$$

Where, ρ is the surface air density, C_h is the transfer coefficient for heat, that depends on the atmospheric stability conditions, v_h is wind velocity and the humidity difference Δq composed by q_v water vapor pressure of the air near the surface and q_s saturated water vapor pressure. q_v depends on the air moisture and temperature, whereas q_s depends on the surface pressure and temperature. Therefore, the wind speed, thermodynamic conditions and dryness of the air layer just above the surface, regarding to the water surface conditions, determine the moisture transfer into the atmosphere.

The response of both models in this relation is shown in the Figure 3.1. Values over the Mediterranean Sea have been horizontally averaged and the annual cycle has been calculated for wind speed, SST, 2-meter temperature and evaporation.

Figure 3.1a shows the annual cycle for the wind speed from observations, analysis and model data. The large difference between HOAPS and OAFlux observations data sets is due to the lack of data along the coastal line in the HOAPS data set, which, in the case of the Mediterranean region, plays a very important role due to its large extension. ERA40 reanalysis data seems to underestimate the wind speed, whereas RCSM and ARCM simulate it satisfactorily. Both experiments are very close to the observed values from the OAFlux data set. Slight differences

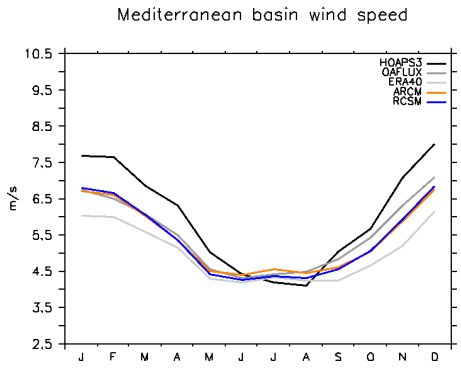

(a) Wind Speed

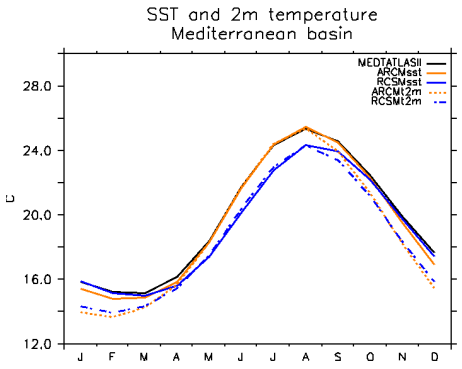

(b) SST

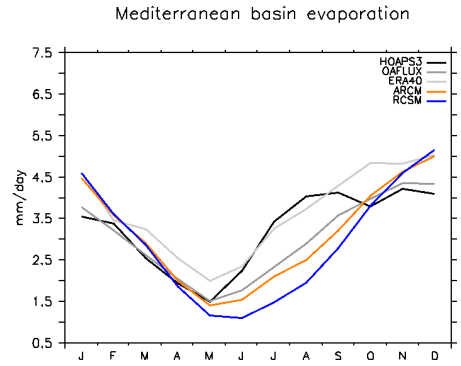

(c) Evaporation

Figure 3.1: Annual cycle averages over the Mediterranean basin. Observational data sets HOAPS3 (1988-2005), OAFlux (1958-2002), ERA40 (1958-2001), MEDATLASII (1958-2001) and simulation ARCM and RCSM (1958-2001)

between the models are observed mainly during Summer as a result of changes on the air surface pressure conditions (not shown). These differences are restricted to water areas, and caused by the thermal expansion/contraction of the atmospheric low level prompted by the different SST (Figure 3.1b).

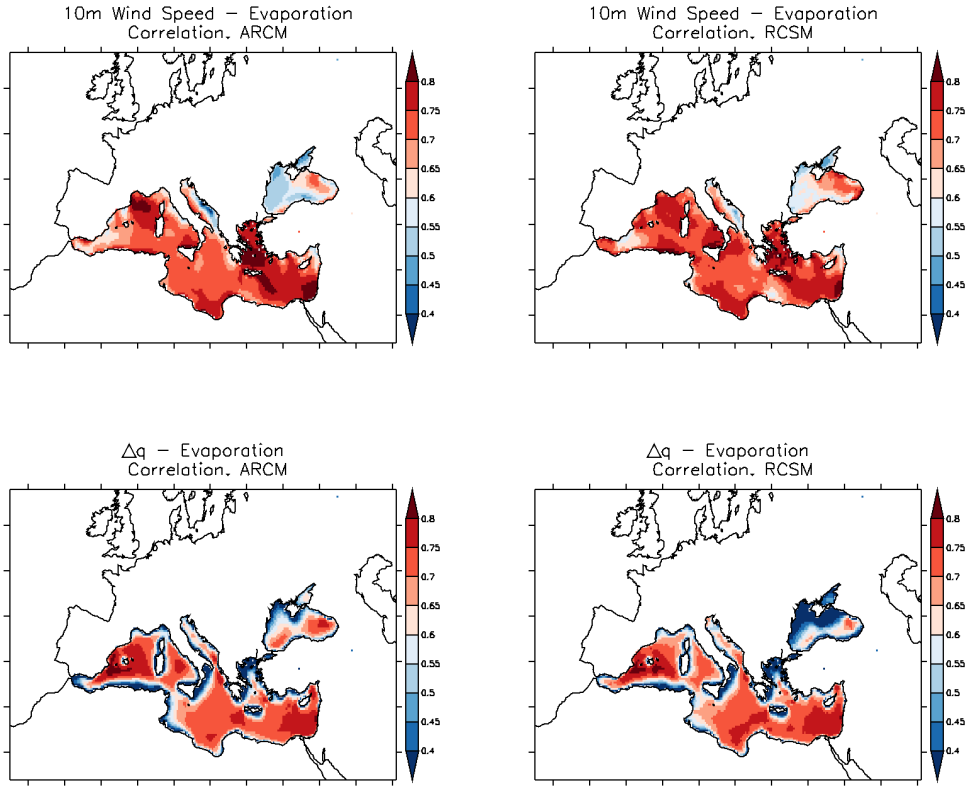

Figure 3.2: Spatial correlations of evaporation with respect to wind speed (upper row) and water vapor pressure gradient (lower row) using annual means. Left column panels show results of the ARCM and right column panels of the RCSM

The difference of the evaporation observed in summer (Figure 3.1c) can be easily attributed to the dynamic in part since the mean wind speed differs between models, and to the thermodynamical processes at the surface interface due to the differences in SST. At the RCSM experiment, the air temperature becomes warmer than the water temperature which produces saturation vapor pressure conditions at the near surface air, and therefore a cut off for the evaporation. The air-sea negative thermal gradient is not observed at the ARCM simulation. During winter, both the wind component and the positive thermal gradient trigger the moisture transport rate into the atmosphere, and leads to similar results in the RCSM and the ARCM.

The correlations between evaporation and wind speed and between evaporation and the gradient

of water vapor pressure (Δq) are shown in Figure 3.2. No large differences are found between the model versions. It has to be noted that the temperature used as SST in the RCSM does not refer to the skin water temperature, but to the averaged value of the first model layer with a thickness of 12 meters.

The wind is highly correlated to the evaporation in the Mediterranean basin but not in the Black Sea. The pattern is determined by the prevailing wind flows and high wind speed. Maximum correlation is found at the Gulf of Lions due to the Mistral wind blowing between Pyrenees and Alps mountains throughout Rhone valley, and at the south of Aegean Sea driven by the Etesian winds during summer, which usually blows forward in south-east direction and contributes to the eastern Levantine evaporation.

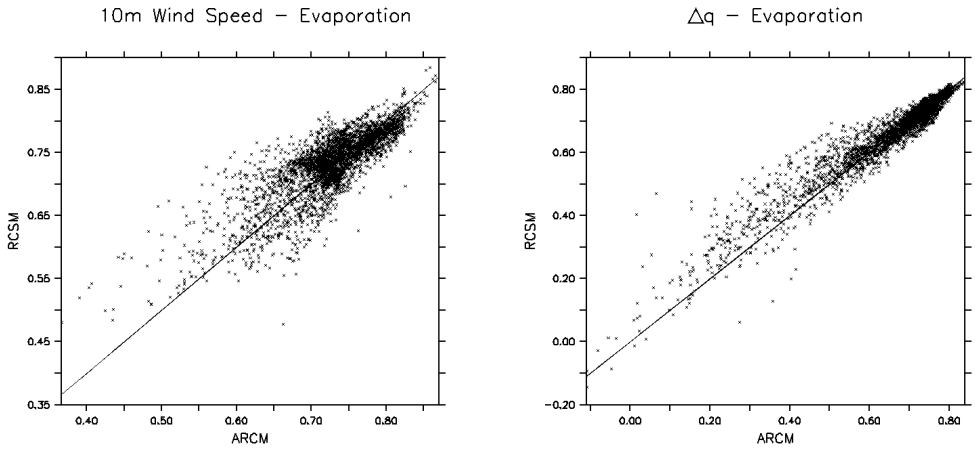

Figure 3.3: Correlation comparison between ARCM and RCSM. The values correspond to those shown in Figure 3.2 for the Mediterranean Sea only, without distinction of the seasons. The left panel shows the correlation of evaporation with the 10-meter wind speed and the right panel the correlation of evaporation with the water vapor pressure gradient

The correlation of evaporation with Δq is high at the open-sea areas and low near the coastal regions. Similar to the wind speed, the Δq is higher correlated to evaporation at the Mediterranean Sea than in the Black Sea basin. The spatial correlation has a strong seasonal cycle (not shown), and is positive during summer and negative during winter. Figure 3.3 shows a comparison between the ARCM and the RCSM only for the Mediterranean basin. The low correlated values in Figure 3.3 correspond to the regions near coast, bluish areas in Figure 3.2. In general, both evaporation driven parameters, wind speed and Δq, are better connected to the evaporation at the RCSM, but specially at the coastal areas, where the correlation increases as a consequence of the higher resolution of the SSTs and the active air-sea feedbacks.

Near to coastal areas, the evaporation is better correlated with the wind speed than the Δq. But at the open-sea there is no predominant role of any of the both parameters visible. However,

the evaporation is triggered by thermal and dynamic processes.

3.3 Land surface water budget

The land surface water balance is calculated as follows:

$$\frac{\partial W}{\partial t} = P - E - R \tag{3.2}$$

where W is the surface water storage, P corresponds to the precipitation, E is total evaporation which includes, surface evaporation, evapotranspiration and sublimation, and R is the total river runoff as the sum of surface runoff plus drainage. In a long therm, the averaged fluctuations of W tends to be zero, therefore the land water budget P-E is directly represented by R.

In this section, the model skills on reproducing the precipitation and the evaporation over land are discussed. Furthermore, the river discharge from individual rivers is used as a validation for the land water budget over smaller areas like the river catchments as well as for the entire Mediterranean catchment.

3.3.1 Precipitation

The Southern Europe precipitation pattern is characterized by enhanced values over the windward side of the mountains. In these areas, the air is mechanically lifted and cooled adiabatically in its raising movement, this forces the condensation of moisture and eventually forms precipitation. The deposition of water vapor by the orographically induced processes limits the moisture transport in the atmosphere.

From Figure 3.4, where precipitation pattern from the CRU observational data set and ARCM and RCSM experiments are shown. It can be seen that these processes take place in the western part of the Mediterranean region caused by northern face of the Cantabric and Pyrenees mountain ranges, at the center Mediterranean region by the north-western side of the Alps, western Dinarish, and Carpathian mountains, and at the eastern Mediterranean caused by at the Kaukasus mountains and all along the coast at the Turkey mountain ranges. At the Black Sea this is visible in the eastern coast.

The structure of the precipitation pattern from both experiments is consistent with the pattern characteristics of CRU. A detailed spatial distribution of the model results is a consequence of its higher resolution and a better representation of the orography. Moreover, it has to be considered that the distribution of station data over mountain regions in the CRU data set might not be dense enough to provide such detailed information. Therefore, it is difficult to assess the

model biases in such regions. Nevertheless, the model precipitation pattern seems to be more realistic.

The major bias of both models is located at the north and east of Europe in plain regions, with an overestimation up to 50% to 100% in both seasons. Although this region is relative far from the Mediterranean region, it influences the Mediterranean hydrological cycle when the runoff from this area reaches the Black Sea and passes through the Dardanelles Strait adding freshwater to the Mediterranean Sea.

The precipitation pattern in the ARCM and RCSM experiments shows slight differences (Figs. 3.4e and 3.4f). During summer, up to 20% less precipitation is simulated along the Mediterranean and Black Seas coast line with some exceptions that reach up to 15% more precipitation on the Greek and Turkey coastal areas. The negative bias shown at the African coast is not significant since almost no precipitation takes place in this region. During winter season, more precipitation is simulated by the RCSM mainly at the upwind side of the mountains (Figure 3.5). The larger precipitation is in connection with the moisture uptake at the Mediterranean and Black Seas, that is transported to land areas. The water vapor transport is analyzed in more detail in the Chapter 4.

In general, the yearly variability of precipitation is well represented by both versions of the model. Figure 4.2 shows the time series of averaged precipitation over the Mediterranean catchment for both seasons summer and winter. The results from both models have positive biases in the wetter years during winter, but precipitation is well simulated during the relative dry conditions. In summer, the variability is well captured. The RCSM tends to simulate more precipitation during winter and less during summer compared to ARCM. The sources of such differences are discussed in detail in the Section 4.4.1.

3.3.2 Evaporation

The ERA40 reanalysis data set has been selected as a reference for land evaporation since no observational gridded data sets exist for long time series. Evaporation shows a similar spatial distribution as precipitation but a different seasonal regime (Figure 3.5).

The winter precipitation and summer rainfall showers over Europe contribute to keep the soil moistened. The soil moisture is eventually evaporated when dry and warm conditions are met in summer and vegetation becomes more active. Some regions in South Europe reach evaporation rates up to 3 mm/day. During winter, lower temperatures and the decrease of vegetation activity are mainly responsible for the reduction of the evaporation.

In both seasons at the African region, the low levels of precipitation throughout the year are not enough to irrigate the land areas and therefore no evaporation is produced. The high values of evaporation near the coasts are an artifact of the interpolation due to the low resolution of

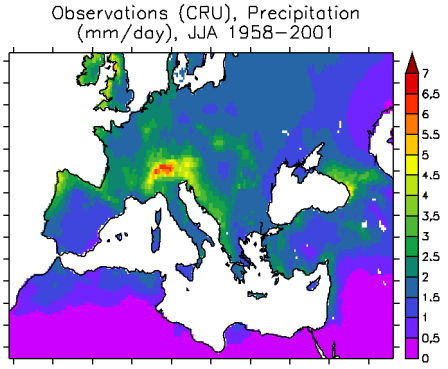

(a) CRU summer

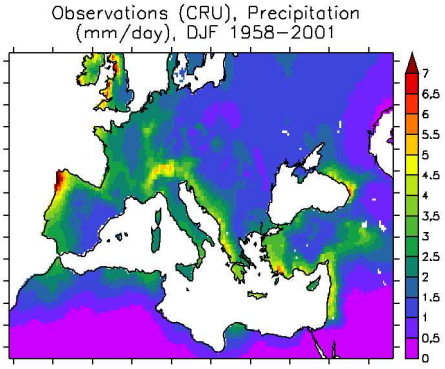

(b) CRU winter

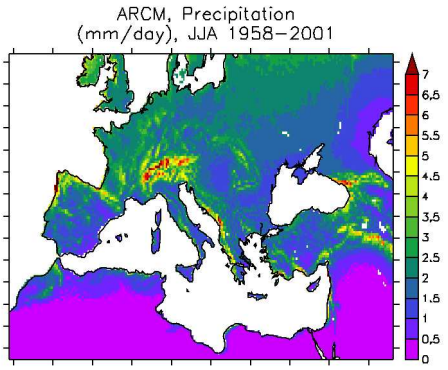

(c) ARCM summer

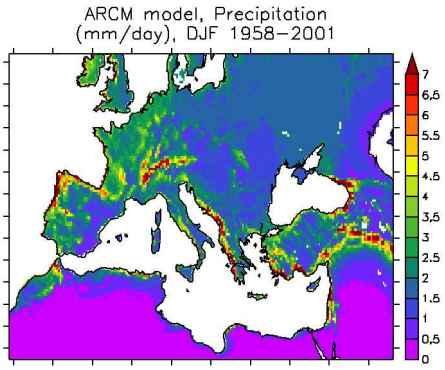

(d) ARCM winter

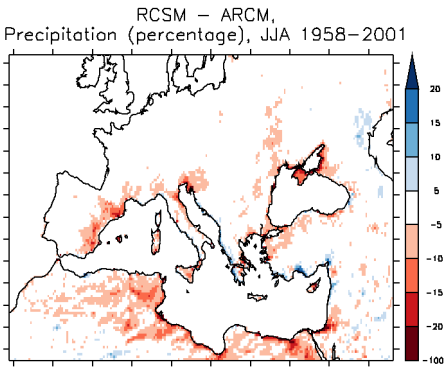

(e) RCSM - ARCM summer

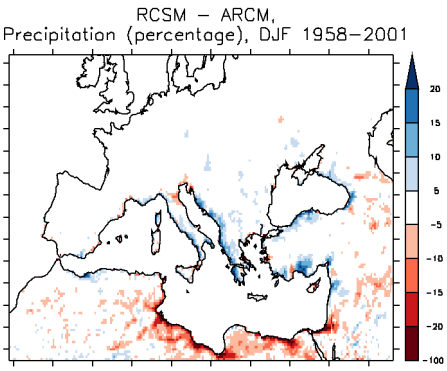

(f) RCSM - ARCM winter

Figure 3.4: Seasonal mean precipitation (mm/day) over 1958-2001. Left column refers to summer season and right to winter season. The CRU observational data set is represented at the top row, ARCM results at the middle, and the relative difference between RCSM minus ARCM experiments at the bottom (in percentage)

the ERA40 data set (125 km x 125 km) (Figure 3.5b). Evaporation over water is mixed with values over land at the coastal line and therefore this data should not be considered.

The ARCM and RCSM produce realistic land evaporation patterns. Figures 3.5c and 3.5d show the seasonal evaporation distributions for the ARCM (very similar to the RCSM, not shown). Summer maximum evaporation rate matches with the orographic precipitation pattern.

In general, results from both models show a similar response and no large differences between them. Results of the RCSM show lower evaporation rates. Similar to precipitation, larger percentages on the relative differences are in connection with low values of evaporation but this percentages are not significant.

Climate change signal in the land water budget

Seasonal differences for future climate with respect to present climate for the land water budget are shown at Figure 3.6. A north-south gradient pattern is simulated over land, with slight changes over the sea. In general, the water budget has decrease of around 20% over the Mediterranean catchment. During winter, the water deficit is more pronounced in the areas of orographic precipitation. Over water, the western basin of the Mediterranean Sea and at the Atlantic near the Spanish Coast a negative difference between 5-20% is calculated. During summer the water deficit is generalized to the whole Mediterranean catchment, with almost no change over the Black Sea catchment. Over water, a slight positive difference can be seen at the center of the basin and Levantine region.

3.3.3 River discharge

An evaluation of both precipitation and evaporation over land regions is done through the analysis of the simulated runoff. Horizontal integrated runoff over the river catchment areas from model data is comparable to river discharge values from measurements. However, it should be considered that some of the measurement stations are not located on the mouth of the river but inland near to the coast. This increases the level of uncertainty of the discharge values, nevertheless it is a good approximation for the runoff.

To analyze model runoff, the HD model is used to calculate river discharge values from fast and slow runoff simulated by the atmospheric model. The values obtained are compared with the GRDC observational data set. Five main rivers were selected: Rhone, Po and Ebro which discharge to the Mediterranean Sea and Danube and Don which discharge to the Black Sea. Seasonal mean values and their standard deviation are shown in Table 3.1 for winter and summer.

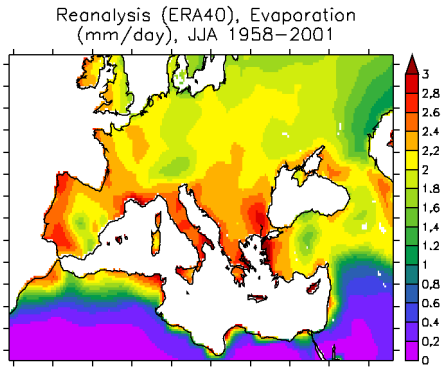

(a) ERA40 summer

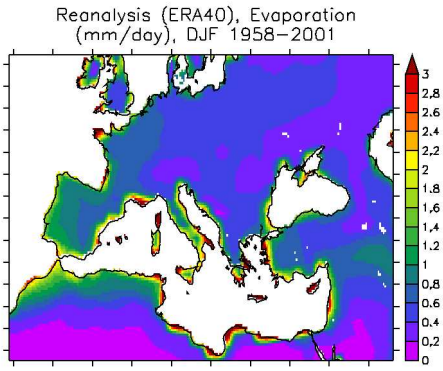

(b) ERA40 winter

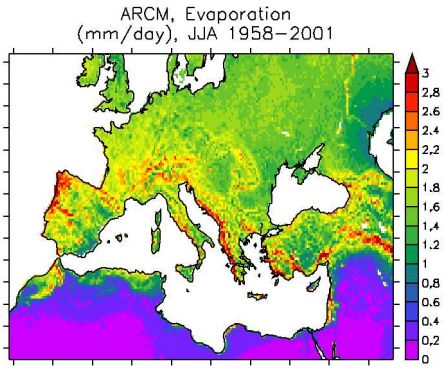

(c) ARCM summer

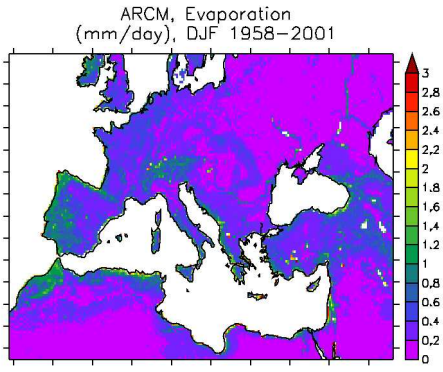

(d) ARCM winter

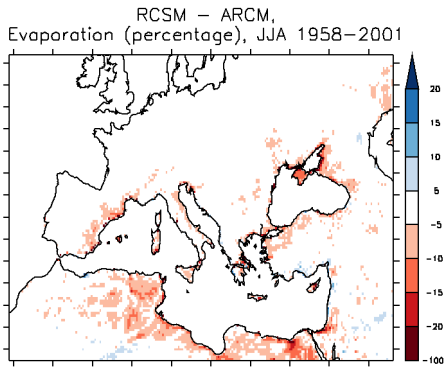

(e) RCSM - ARCM summer

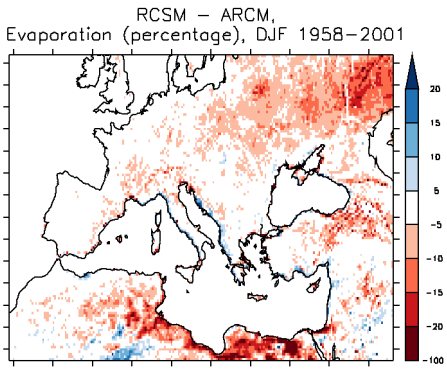

(f) RCSM - ARCM winter

Figure 3.5: Same as figure 3.4 for evaporation (mm/day). Reanalysis ERA40 has been used as the reference data set

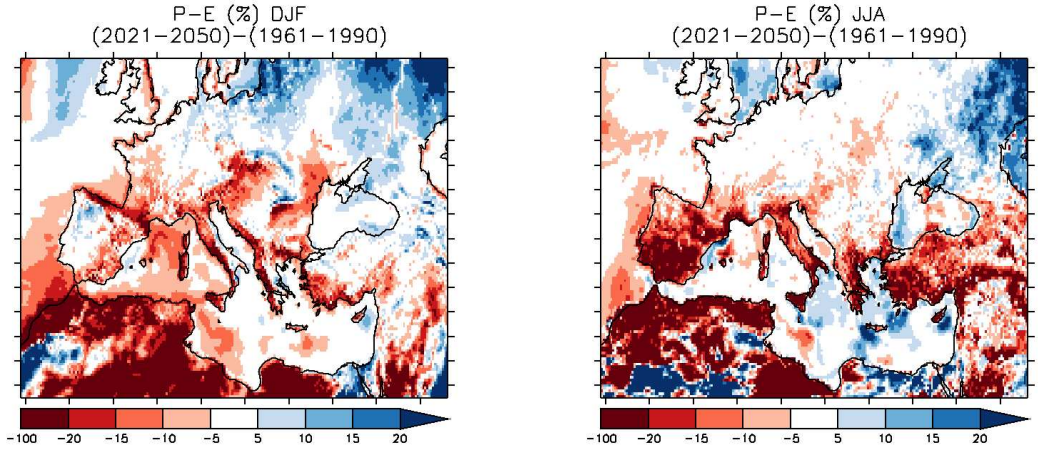

Figure 3.6: Changes in the water budget (precipitation (P) minus evaporation (E)) in the period 2021-2050 with respect to 1961-1990

The Rhone and Ebro rivers follow the hydrological regime that characterize the Mediterranean climate (wet winters and dry summers). Their catchments are under the influence of the north-west fronts that bring moisture from the Atlantic during winter. During summer, changes in the circulation and surface conditions decrease the water budget over the rivers catchments (Figures 3.4 and 3.5) and reduce river discharge. The Rhone river discharge rate is decreased from 1300 m^3 s^{-1} in winter to 800 m^3 s^{-1} in summer, and for the Ebro river from 2700 m^3 s^{-1} to 1200 m^3 s^{-1}, respectively. The results from both models show a positive bias at the Rhone catchment in winter, but good estimations during summer. The Ebro discharge is strongly underestimated in the results from the models.

The Po river discharge does not show the typical Mediterranean hydrological regime, even though it is also located in the center of the Mediterranean region. Its discharge has two maxima through the year, in spring and fall, of approximately 1640 m^3 s^{-1}, and two minima in winter and summer of around 1300 m^3 s^{-1}. For this river, the simulated values from both models underestimate the discharge in winter and summer with a deficit of 500 m^3 s^{-1}.

The catchments of the Black Sea rivers are located outside of the influence of Mediterranean climate. The Danube is the major river which contributes to freshwater into the Black Sea. Its discharge during summer season is approximately 6200 m^3 s^{-1}, and 6900 m^3 s^{-1} during winter. Results from the ARCM and RCSM underestimates the expected discharge, their deficits are around 1000 m^3 s^{-1} during winter and up to 3800 m^3 s^{-1} in summer. These biases represent 50% less than observed. The Don river has a smaller observed discharge of approximately 440 m^3 s^{-1} and 660 m^3 s^{-1} in winter and summer respectively. In the opposite direction to the Danube model results, the Don discharge is largely overestimated by the ARCM and RCSM,

especially during winter up to 3200 m^3 s^{-1}, as a consequence of the larger precipitation bias in its catchment.

Table 3.1: River discharge average and standard deviation (10^3 m^3 s^{-1}) for winter and summer seasons. GRDC observations data set, ARCM, RCSM, historical and future climate scenario. The values refer to the common period of the observations database and the simulations, except for the future climate scenario simulation. *-Indicates that the difference in the averaged values between ARCM and RCSM or historical and scenario simulations are statistically significant with a 95% significance level

Winter						
River	**(Period)**	**GRDC**	**ARCM**	**RCSM**	**Historical**	**Scenario**
		Observations period			1961-1990	2021-2050
Rhone	(1958-1979)	1.3±0.41	2.0±0.61	1.9±0.60*	2.1±0.48	1.9±0.64
Po	(1958-2001)	1.4±0.39	1.0±0.40	0.9±0.41*	1.0±0.39	0.8±0.37
Ebro	(1958-1962)	2.7±0.66	0.4±0.12	0.3±0.12*	0.2±0.12	0.2±0.07
Danube	(1958-1990)	6.2±1.18	5.1±1.42	5.1±1.38	5.2±1.54	4.3±1.45*
Don	(1958-1984)	0.4±0.15	3.2±0.94	3.2±0.92	2.9±0.68	3.3±0.59
Summer						
River	**(Period)**	**GRDC**	**ARCM**	**RCSM**	**Historical**	**Scenario**
		Observations period			1961-1990	2021-2050
Rhone	(1958-1979)	0.8±0.22	0.8±0.25	0.7±0.21*	0.9±0.30	0.6±0.17*
Po	(1958-2001)	1.3±0.38	0.8±0.30	0.7±0.25*	0.5±0.20	0.4±0.13*
Ebro	(1958-1962)	1.2±0.20	0.1±0.03	0.1±0.02*	0.1±0.02	0.0±0.02*
Danube	(1958-1990)	6.9±1.74	3.8±1.58	3.5±1.28*	2.5±0.91	2.5±0.86
Don	(1958-1984)	0.7±0.19	1.3±0.65	1.3±0.66	0.8±0.28	0.9±0.33

The yearly variability is not reproduced properly by the models either for most of the rivers (Figure 3.7). Both simulations tend to enlarge the yearly variability in the case of the Rhone and Don rivers. The Ebro river is misrepresented due to strong deficit in the precipitation. Po is the best river represented by the model despite the turbulent and complex atmospheric dynamics of its catchment.

The past climate period in the scenario simulation has similar values for river discharge as the ARCM and RCSM simulations in the Mediterranean catchment (Table 3.2). Major differences are found for the rivers inside the Black Sea catchment, which mean values show even larger deficit of the runoff than in the ARCM and RCSM simulations during summer.

The scenario simulation in the future climate period has, in general, a deficit in the discharge for all rivers in both seasons, except for the Don river in summer and the Ebro in winter. Nevertheless, not all the projected changes are significant.

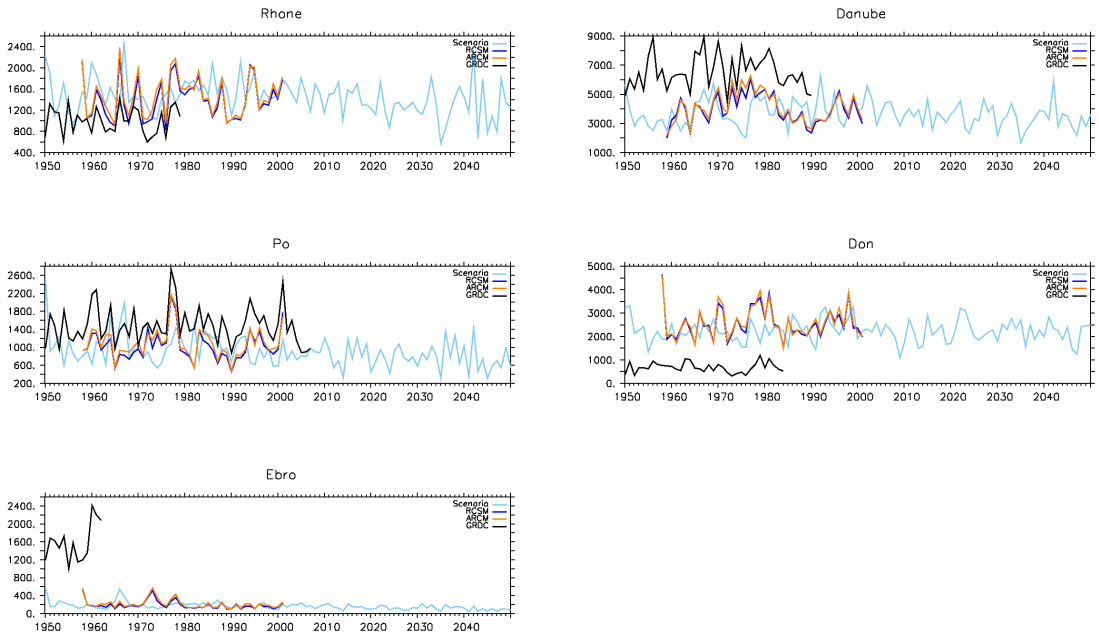

Figure 3.7: Yearly time series for discharge (m^3 s^{-1}) of Mediterranean rivers (left column) and Black Sea rivers (right column)

Total discharge over the basins

The river discharge contributes to almost 20% to the total freshwater flux into the Mediterranean Sea (Mariotti et al. 2002). According to observations (Table 3.2), the annual mean lies between 8.1-16.0 10^3 m^3 s^{-1}. The range of uncertainty is as large as the value of the smaller estimation of the total discharge. This disagreement to the observations could be based on the damming of the rivers along the time by human activity. Nevertheless, Struglia et al. (2004) have estimated the upper bound of the total river discharge into the Mediterranean Sea. Their estimated value is 10.4 10^3 m^3 s^{-1}, based on the total area of the Mediterranean catchments including small catchments that usually are neglected. The simulated values by both model versions are approximately 10.9 10^3 m^3 s^{-1}. These values fit very well to the maximum discharge estimation by Struglia et al. (2004), despite the poor model performances for some of the individual rivers.

The annual mean river discharge in the observations data sets is more consistent for the Black Sea. The estimated value is approximately 9.1 10^3 m^3 s^{-1}. Simulated discharges from both models overestimate the expected value in around 38%. These biases are produced by the positive biases in the precipitation in the north of the Black Sea.

Table 3.2: Annual mean river discharge for the Mediterranean and Black Sea catchments (10^3 m^3 s^{-1}). (1) Kara et al. (2008), (2) Perry et al. (1996), (3) RivDis (Vorosmarty et al. 1998), (4) UCAR, (5) NRL (Barron and Smedstad 2002), (6) Sanchez-Gomez et al. (2011), (7) Struglia et al. (2004), (8) Lionello et al. (2006b). *-Indicates that the difference in the averaged values between RCSM and ARCM and the historical and scenario simulation are statistically significant with a 95% significance level

Catchment	**Observations**	**ARCM** (1958-2001)	**RCSM** (1958-2001)	**Historical/Scenario** (1961-1990) / (2021-2050)
Black Sea (66 river mouths)	9.13 (1)(2) 9.16 (1)(3) 9.01 (1)(4) 9.15 (1)(5)	12.52	12.69*	12.51 / 11.85
Mediterranean Sea (240 river mouths)	10.3 (6) 8.1–10.4 (7) 16.0 (8) 13.6 (8) 16.0 (8) 11.0 (8)	10.91	10.88	11.27 / 8.65*

3.4 Air-sea fluxes

3.4.1 Net surface freshwater flux

The freshwater budget at the Mediterranean Sea is calculated as follows:

$$G = E - P - D - B \tag{3.3}$$

Where G is the net volume transport at Gibraltar strait, E and P are the evaporation and precipitation over the Mediterranean Sea surface, D is the total river discharge and B is the inflow from the Black Sea corresponding to net volume transport at the Bosphorus Strait. In a long term, G is balanced with the freshwater input (E-P-D-B) at the Mediterranean Sea.

The assessment of the freshwater flux balance has been the objective of several studies in which a deficit on the freshwater flux integrated over the Mediterranean Sea was concluded (e.g., Mariotti et al. 2002; Sanchez-Gomez et al. 2011). The negative freshwater budget determines the amount of moisture produced through the evaporation at the Mediterranean Sea. This moisture is transported by advection to the land regions and contribute to land precipitation. Regarding to the Mediterranean Sea, the freshwater flux determines the salinity levels on the upper layers of the sea, and it is a key part of the driving processes of the sea circulation.

A very detailed analysis of the Mediterranean freshwater flux has been done by Sanchez-Gomez et al. (2011). They have been analyzed observational data sets and regional climate models output (RCMs) in stand-alone version from the EU-FP6 ENSEMBLES project (Hewitt and Griggs 2004). Sanchez-Gomez et al. (2011) have reported that the range of uncertainty on the freshwater flux assessment is still large.

The yearly mean time series for the Mediterranean freshwater flux and its components are analyzed for ARCM and RCSM experiments and observational data sets. Results from the scenario simulation are included as well. Yearly mean time series for the Mediterranean Sea are shown in Figure 3.8. A surface area of 2.5x10^{12} m^2 is assumed for the Mediterranean basin.

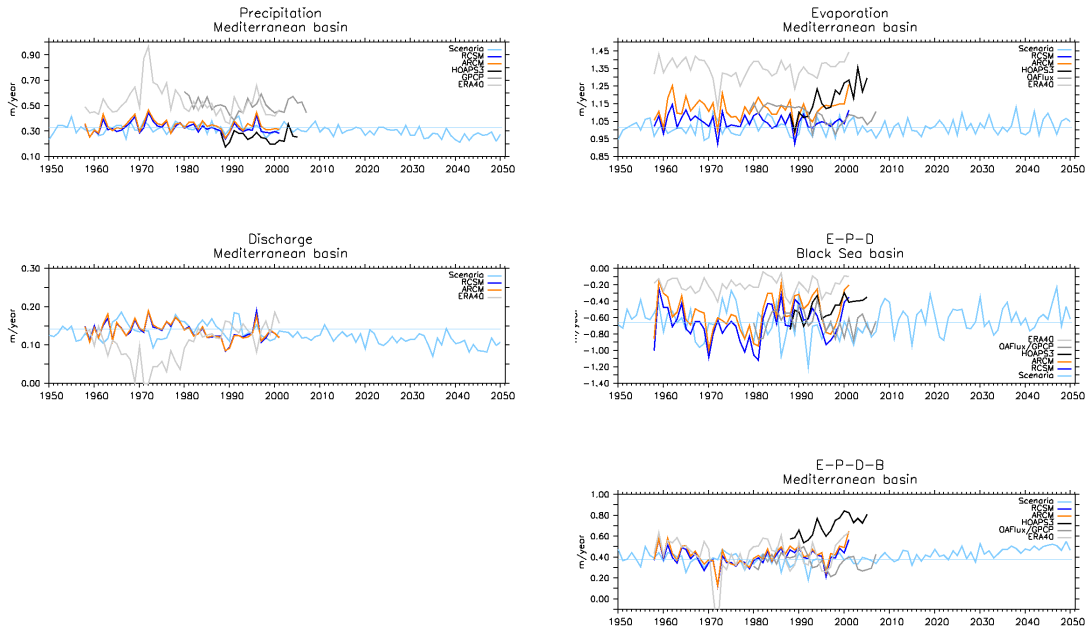

Figure 3.8: Yearly time series of the horizontal integration of the freshwater flux components over the Mediterranean Sea. Observations and reanalysis data sets have been included as a references in gray

Precipitation

The discrepancy of precipitation values over the Mediterranean Sea in the observational data sets has been pointed out by Sanchez-Gomez et al. (2011). The HOAPS3 data sets mean and standard deviation are 0.252 $\pm$ 0.044 m/year, meanwhile the same values for GPCP data set are 0.503 $\pm$ 0.055 m/year. This disagreement can be explained by the limited spatial coverage of the first data set and the low resolution of the second. Besides the fact that they do not cover the same period. For the ERA40 reanalysis data the values are higher than observed, 0.529 $\pm$

0.12 m/year. This data set presents unrealistic large precipitation at the beginning of the 1970s (Figure 3.8). These values are outside of the interval reported by Mariotti et al. (2002), between 0.331-0.447 m/year. ARCM and RCSM experiments means are inside the reference interval, 0.345 $\pm$ 0.046 m/year for ARCM and 0.327 $\pm$ 0.043 m/year for RCSM. Their interannual variabilities are very similar among each other and to the references data sets.

Results from the historical period (1961-1990) are in agreement with those obtained from the ARCM and RCSM experiments. The mean precipitation for the historical period is 0.326 $\pm$ 0.039 m/year, very similar to what was obtained in the RCSM experiment but it shows a smaller yearly variability. For the future climate period (2021-2050) a decrease of precipitation 0.279 $\pm$ 0.035 m/year is detected. It represents 14% of water deficit with respect to the historical period, this difference is significant with a 95% of significance level. The signal is in good agreement with what has been reported in previous works (Mariotti et al. 2008; Giorgi and Lionello 2008; Somot et al. 2008; Sanchez-Gomez et al. 2009).

Evaporation

Similar discrepancies as for annual mean values of precipitation are found for the evaporation over the Mediterranean basin. Sanchez-Gomez et al. (2011) report annual mean intervals between 1.095 $\pm$ 0.08 m/year and 1.167 $\pm$ 0.05 m/year among the reference data sets and 1.066 $\pm$ 0.06 m/year and 1.618 $\pm$ 0.07 m/year for the RCMs. Mean values for HOAPS3, OAFlux and ERA40 are 1.176 $\pm$ 0.09 m/year, 1.090 $\pm$ 0.05 m/year and 1.349 $\pm$ 0.06 m/year, respectively. The ERA40 data set overestimates the evaporation compared to the two other observational data sets (Figure 3.8). A significant difference between the ARCM experiment (1.121 $\pm$ 0.06 m/year) and the RCSM experiment (1.049 $\pm$ 0.04 m/year) has is basis in the different state of the air-water interface as explained in Section 3.2.

The HOAPS3 and OAFlux data sets differ in their trends after the year 1990. HOAPS3 shows a positive trend in a similar way as the ARCM experiment, meanwhile not such a trend is observed in OAFlux data set and RCSM experiment. Further analysis should be done to address this behavior.

The annual mean evaporation of the historical period (1.018 $\pm$ 0.05 m/year) is low in comparison to the reference data sets and ARCM and RCSM experiments. Mariotti et al. (2008) reported an increase in evaporation between 10% and 24% in the future climate period depending on the season, and 4% according to Sanchez-Gomez et al. (2009). Nevertheless, for the future period the signal is very weak, a no significant difference of approximately 1% (1.029 $\pm$ 0.05 m/year) compared to the historical period is simulated.

Discharge

Discharge values calculated from reanalysis ERA40 data show a poor performance mainly in the first 25 years of the simulated period. The poor quality of this data set has been addressed by Hagemann et al. (2005).

As shown in the previous Section 3.3.3, annual mean discharge is well captured by ARCM and RCSM models. The difference in their interannual variability respect to each other is not significant (Figure 3.8). Regarding the changes in the future climate projection, as shown on Table 3.1, the total river discharge has a significant decrease up to 23% with respect to the present climate period. The strong decrease is related to the changes of the water budget over land due to a decrease in precipitation and warmer temperatures that affect the hydrology regime of the Mediterranean region (see Section 3.3).

Black Sea water budget

Similar to the Mediterranean Sea, evaporation exceeds precipitation in the Black Sea basin by around 17%, but this deficit is largely compensated by river runoff. Stanev et al. (2000) estimates an annual mean for the total freshwater of -0.12 m/year based on altimeter and gauge data. The negative sign indicates larger freshwater input than output.

In this study, the Black Sea freshwater flux is calculated from the evaporation and precipitation from OAFlux and GPCP data sets, respectively. In the case of HOAPS3 and ERA40, each data set provides both variables. Due to the low performance of ERA40 data over land, the possibility to calculate the total river discharge at the Black Sea from land precipitation and evaporation was dismissed. Instead, a value of 0.1 m/year is used according with Stanev et al. (2000). A total area of 467,712 km^2 is assumed for the Black Sea (including the Sea of Azov).

The annual mean of the net surface freshwater flux obtained from the reference datasets: HOAPS3, OAFlux/GPCP and ERA40 are -0.043 $\pm$ 0.12 m/year, -0.213 $\pm$ 0.13 m/year and 0.234 $\pm$ 0.09 m/year respectively. Except ERA40 mean, these values differ from the value -0.12 m/year obtained by Stanev et al. (2000). The ARCM and RCSM means compare well with the reference values, -0.218 $\pm$ 0.04 m/year and -0.188 $\pm$ 0.03 m/year respectively. The interannual variability is much larger in the reanalysis data than in model data (Figure 3.8) as one can see from the standard deviation.

The annual mean of the historical period is -0.171 $\pm$ 0.03 m/year. No significant change is seen on the future climate period -0.180 $\pm$ 0.03 m/year.

Freshwater flux

The summary done by Sanchez-Gomez et al. (2011) for total freshwater flux values over the Mediterranean basin sets a range between 0.39 m/year and 1.15 m/year. The range of uncertainty can be considered large, mainly due to the quality, methods and mismatch of time periods on the existing data sets. From the results using a composite of gridded satellite and reanalysis data sets, an interval from 0.28 ± 0.11 m/year to 0.66 ± 0.11 m/year can be calculated and from 0.42 ± 0.13 m/year to 0.72 ± 0.10 m/year using simulated data from the RCMs. An estimation of the freshwater loss from the volume transport balance at the Gibraltar Strait (Lionello et al. 2006b) determines the interval between 0.50 m/year and 1.13 m/year. The annual means of the reference data sets HOAPS3, OAFlux/GPCP and ERA40 are 0.692 ± 0.09 m/year, 0.355 ± 0.07 m/year and 0.425 ± 0.17 m/year respectively. They are not the same as reported by Sanchez-Gomez et al. (2011) since different estimations of total river discharge and Black Sea outflow are used. Nevertheless, the values are consistent within the interval given, except for the combination OAFlux/GPCP that has a too low value due to the overestimation of precipitation in GPCP data set. The mean annual value simulated by ARCM is 0.421 ± 0.08 m/year, this value is slightly higher than in the RCSM experiments 0.390 ± 0.08 m/year. Both time series are at the lower bound of reported intervals but consistent with the reference data sets. The yearly variability is well captured with a smaller amplitude in the signal if compared with ERA40.

A significant increase in the freshwater loss of 21% is simulated at the future climate projection, this is caused by the decrease of the freshwater input from precipitation and river discharge. This increase is in agreement with previous estimations. Sanchez-Gomez et al. (2009) reported an increase between 20% and 60% for the total freshwater flux, and (Mariotti et al. 2008) 24% for the difference E-P only.

3.4.2 Net surface heat flux

The net surface heat flux Q_t is calculated as follows:

$$Q_t = Q_{SR} - Q_{LR} - Q_{lh} - Q_{sh} \tag{3.4}$$

where Q_{SR} is the net surface solar radiation, Q_{LR} is the net surface thermal radiation, Q_{lh} is the net surface sensible heat and Q_{sh} is the net surface latent heat. The first two terms at the right-hand side of the equation are the so-called radiative fluxes, and the last two terms are the turbulent fluxes.

A reference value for the net surface heat flux estimation is obtained from the net heat transport at the Gibraltar Strait, approximately +5 W m^{-2} (Sannino et al. 2009), which is in balance, in

the long term, with the averaged energy exchange at the surface. The estimated net surface heat flux has a large range of uncertainty. Sanchez-Gomez et al. (2011) report from previous studies values between -15 and +30 W m^{-2}. Their own findings estimate this interval between -15 $\pm$ 6 and +9 $\pm$ 8 W m^{-2} using updated observational and reanalysis data sets, and between -40 $\pm$ 3 and +21 $\pm$ 3 W m^{-2} using regional climate model data, with an ensemble mean of -9 $\pm$ 21 W m^{-2}. The mean net surface heat flux is: -4.1 $\pm$ 4.8 W m^{-2} for the ARCM model and -6.1 $\pm$ 5.8 W m^{-2} for the RCSM model.

The annual cycles for the net surface heat flux and its individual components are displayed in Figure 3.9. The Q_{SR} is very similar for both models and in good agreement with data from the ERA40 data set. Nevertheless these values are underestimated according to the observational data sets ISCCP and NOCS. The mean bias is approximately -32 W m^{-2}.

The biases of the Q_{LR} are difficult to estimate, since there is a clear disagreement among the reference data (Figure 3.9). The two observational data sets differ in magnitude and in the annual cycle fluctuation. The annual means for ISCCP and NOCS data sets are 75.4 $\pm$ 4.2 and 62.3 $\pm$ 2.8 W m^{-2}, respectively. The annual mean for the ERA40 reanalysis is closer to the ISCCP mean value, 78 $\pm$ 2.4 W m^{-2}, but the annual cycle is different. In fact, there is no agreement among the reference data sets in the months where maxima and minima values occur. The annual means for ARCM and RCSM are closer to the NOCS data set, 63.5 $\pm$ 4.2 and 64.3 $\pm$ 5.1 W m^{-2}. Contrary to what one might expect from the difference in the SST between the models (Figure 3.1), the simulated net surface longwave flux does not differ in summer but in winter. The summer case shows the equilibrium between the water vapor and clouds effects on the downward longwave radiation and the SST which is used for the upward longwave radiation calculation according to the Stefan-Boltzmann law. In winter, the SST is similar for the models and it might be that the representation of the clouds is responsible for the difference in the downward component of the longwave radiation.

The reference data sets show good consistency for the estimated values for Q_{lh}. All the data sets give a mean annual estimation of approximately 90 W m^{-2} with a standard deviation of 26 W m^{-2}. The exception is the ERA40 reanalysis, which has its mean at 84.4 $\pm$ 22.9 W m^{-2}. The difference between the models is the largest among all heat fluxes. The annual means are 88.7 $\pm$ 34.2 W m^{-2} for the ARCM and 82.9 $\pm$ 39.3 W m^{-2} for the RCSM. The amplitude of the annual signal reproduced by the models is larger than the observed, with a larger negative bias by the RCSM model during summer (Figure 3.9). The difference between the models is attributed to the slightly weaker winds and to the inversed thermal gradient at the air-sea interface. Both are consequence of the difference in SST in the RCSM model. This behavior, in connection with the evaporation, which is derived from the Q_{lh}, is discussed in detail in Section 3.2.

With regard to Q_{sh}, the larger range of uncertainty in the reference data sets occurs during summer season. The annual mean values are 12 $\pm$ 12.5, 8.7 $\pm$ 6.8 and 14.1 $\pm$ 6.2 W m^{-2}

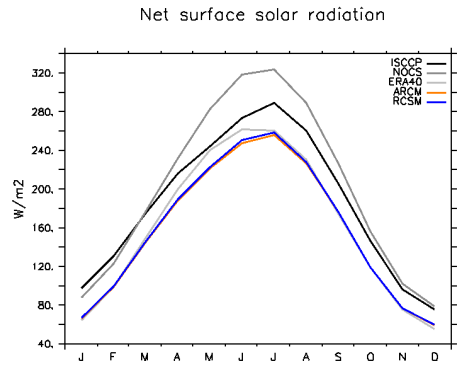

(a) Q_{SR}

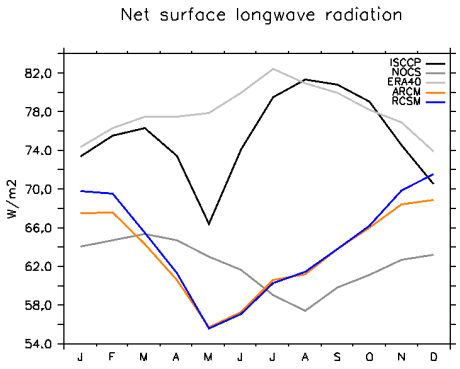

(b) Q_{LR}

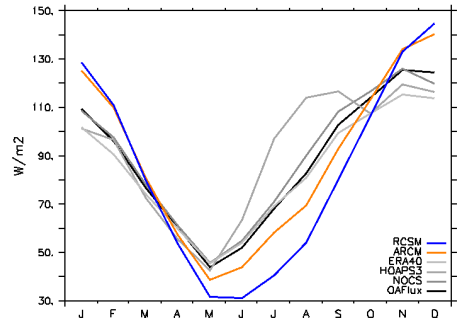

(c) Q_{lh}

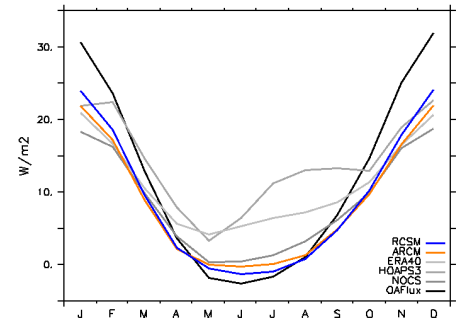

(d) Q_{sh}

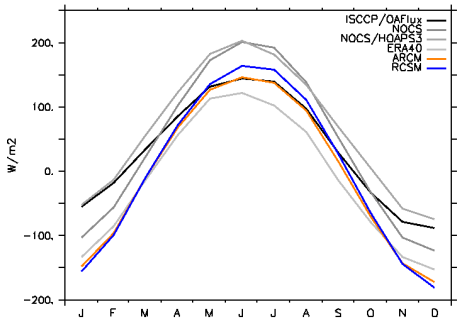

(e) Q_t

Figure 3.9: Annual cycles of the heat fluxes components (W m^{-2})

for the OAFlux, NOCS and HOAPS3 data sets respectively, and 11.17 $\pm$ 5.8 W m^{-2} for the ERA40 data. The models compare very well with NOCS data in the annual cycle, with a slight overestimation during winter, and to the annual mean values, which are 8.7 $\pm$ 8.3 and 9.1 $\pm$ 9.3 W m^{-2} for the ARCM and RCSM simulations. The response of models is similar to the behavior of the Q_{lh}, since both turbulent fluxes are a function of wind speed and the air-sea thermal gradient.

The interannual variability of the heat flux components are shown in Figure 3.10. One can see from the Figure that the ARCM and RCSM models variabilities are close to the ERA40 data set. This relation is expected, since the specific humidity is one of the prescribed variables, determines the moisture content in the atmosphere and has a large impact in the radiation budget.

The historical period (1961-1990) of the scenario simulation shows almost no difference in the average to the ARCM and RCSM experiments: slightly less surface shortwave (approximately 1 W m^{-2}) and less latent heat (approximately 3 W m^{-2}). The total heat flux for the ARCM and RCSM experiments is very similar, -4.1 $\pm$ 4.8 W m^{-2} and -6.07 $\pm$ 5.8 W m^{-2}, respectively. Similar to the RCSM experiment, in the historical period the total heat flux is -6.2 $\pm$ 8.6 W m^{-2}, but the signal at the end of the scenario simulation becomes weaker, -4.1 $\pm$ 7.4 W m^{-2}.

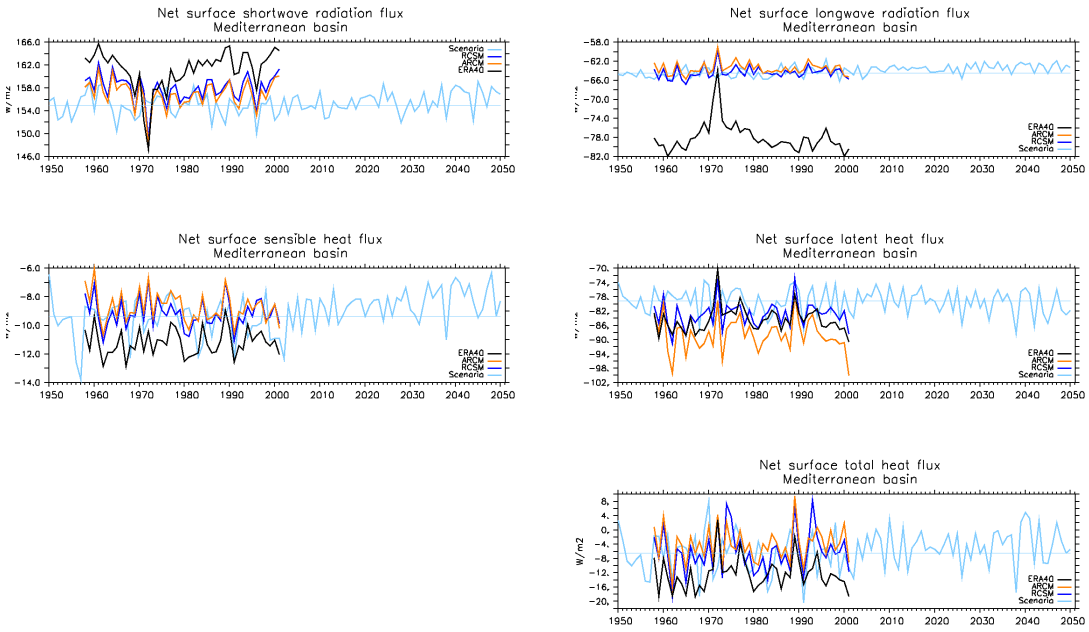

Figure 3.10: Yearly time series of the yearly mean heat fluxes over the Mediterranean Sea. Observations and reanalysis data sets have been included as a references in gray

3.5 Analysis of the radiation budget under a climate change scenario

This section addresses changes of the radiation budget for a future climate scenario simulation compared to historical climate conditions. Climate warming as a consequence of an increase of greenhouse gasses (GHG) concentrations induces a change of the atmospheric radiation balance. The sources of these changes are associated with the components which incoming solar radiation interacts. They are GHG, aerosols and water vapor (Kim and Ramanathan 2008). A modification of the quantities of these components influences the clouds and cloud formation processes through the feedback: solar radiation - surface temperature - surface evaporation - atmospheric water content - clouds. Changes in the balance of such a feedback impacts directly on the hydrological cycle (Ramanathan et al. 2001; Roderick and Farquhar 2002; Ohmura and Wild 2002)).

It has been shown in Section 3.4 that the water budget deficit increases in the Mediterranean during the middle of the 21st century. These results are in agreement with recent studies (Mariotti et al. 2008). A decrease in precipitation and an increase in evaporation leads to a larger amount of water vapor in the atmosphere, which produces changes in cloud properties and atmospheric radiation absorption/reflection capabilities. It is our interest, to analyze the radiation components under climate change conditions and their impact on the hydrological cycle in the Mediterranean region and more precisely over the Mediterranean Sea.

3.5.1 Solar radiation

To estimate the atmospheric influence in the radiation budget, the absorbed and/or reflected solar radiation (Q_{ARSR}) is calculated as follows:

$$Q_{ARSR} = Q_{dsw}^{TOA} - Q_{dsw}^{surf} \tag{3.5}$$

where Q_{dsw}^{TOA} and Q_{dsw}^{surf} are the downward solar radiation at the top of the atmosphere (TOA) and at the surface, respectively. The mean value and standard deviation for the Q_{dsw}^{TOA} over the Mediterranean Sea in the historical period (1961-1990) is 342.9 $\pm$ 0.2 W/m^2, the maximum value reaches 370.8 W/m^2 during summer and the minimum 142.4 W/m^2 during winter.

The mean and standard deviation for Q_{ARSR} has been calculated over the area of the Mediterranean Sea as well. The percentage of the Q_{ARSR} with regards to Q_{dsw}^{TOA} for the historical period is 54.1$\pm$0.6% (185.5$\pm$2 W/m^2), basically more than half of the incoming radiation is absorbed and/or reflected. For the future climate period, this percentage decreases to 53.6$\pm$0.5% (183.8$\pm$1.7 W/m^2). Under clear sky conditions (no presence of clouds) this behavior is reversed: in the historical period the percentage is 36.7$\pm$0.3% (125.8$\pm$1 W/m^2). This value is

slightly smaller than for the future period, 37.1±0.5% (127.2±1.7 W/m^2). The increase of Q_{ARSR} takes place during the last two decades (Figure 3.11). These results suggest two facts: first, an increase of the atmospheric water content increases the shortwave absorption, as shown for clear sky situations, but at the same time, a decrease in cloud formation impacts on both albedo and atmospheric absorption producing a decrease of Q_{ARSR} under cloudy conditions.

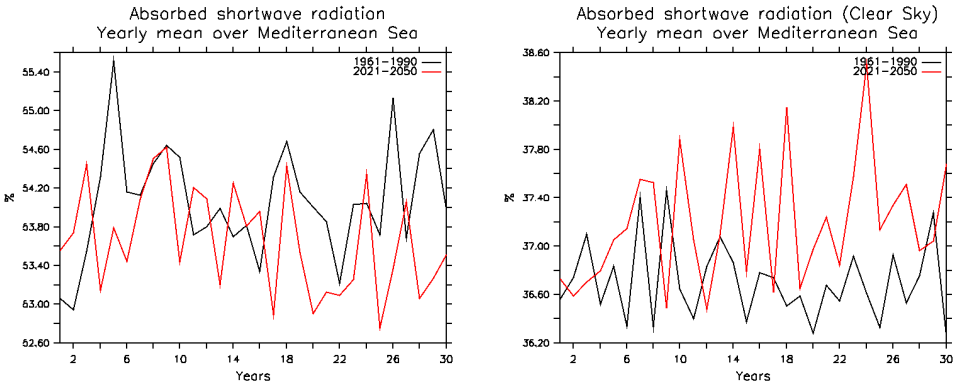

(a) Normal conditions **(b)** Clear Sky

Figure 3.11: Time series of the mean absorbed/reflected solar radiation over the Mediterranean Sea, including clouds (left) and under clear sky conditions (right)

The seasonality and spatial distribution changes between the future and present climate of the Q_{ARSR} are shown in Figure 3.12. Since the model has horizontal uniform distribution of aerosols and GHG, these patterns are only attributed to the atmospheric water content and cloud distribution. During summer, a negative difference is observed over the Atlantic, Spain, France, Black Sea and the west basin of the Mediterranean Sea. Minimum values are located over the Cantabric Range and West French Plain.

During winter, a north-south gradient is observed. An increase of Q_{ARSR} is located mainly at the north of the domain over land areas, and a decrease over the central and eastern basin of the Mediterranean Sea and surroundings.

3.5.2 Cloud cover and water content

The spatial distribution of cloud cover (not shown) corresponds very well with the patterns of the Q_{ARSR} in Figure 3.12. Figure 3.13 shows the yearly average time series over the Mediterranean Sea. A clearly negative trend takes place after the year 2030 up to the end of the simulation. Nevertheless, the decrease in cloud cover is not generalized. As shown in the fractional cloud cover distribution (Figure 3.14), the frequency of occurrences of large fractional

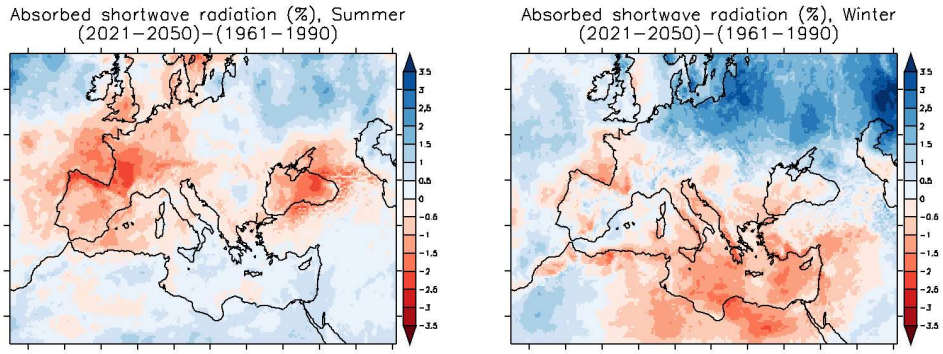

(a) Summer **(b)** Winter

Figure 3.12: Seasonal changes for the spatial distribution of the ARSR including clouds between future (2021-2050) and present climate (1961-1990). Summer (left) and winter (right)

cloud cover is indeed reduced in the scenario simulation. But smaller fractional cloud cover and clear ska conditions occurrences have increased.

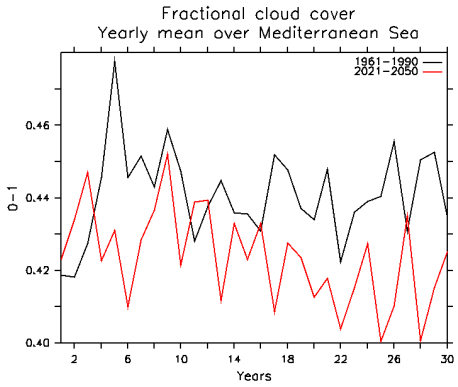

Figure 3.13: As Figure 3.11 for cloud cover over the Mediterranean Sea

No significant change is detected in the vertically integrated liquid water content (Figure 3.15), but the amount water vapor shows an increase of 1.3 Kg/m^2 in the future climate period. This is in agreement with the results discussed for the solar radiation in the previous section.

One can expect that, as a consequence of the general decrease in cloud cover, more solar radiation could reach the surface. Nevertheless this relation is not observed in the simulation over the Mediterranean Sea. The downward surface solar radiation does not show a similar change as the cloud cover. One possible explanation could be that the decrease in reflected

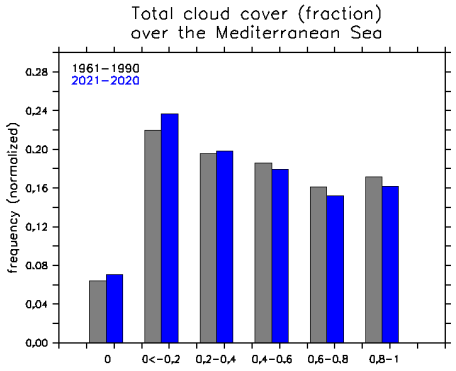

Figure 3.14: Frequency of cloud cover distributed over the Mediterranean Sea. First bin shows clear sky occurrences

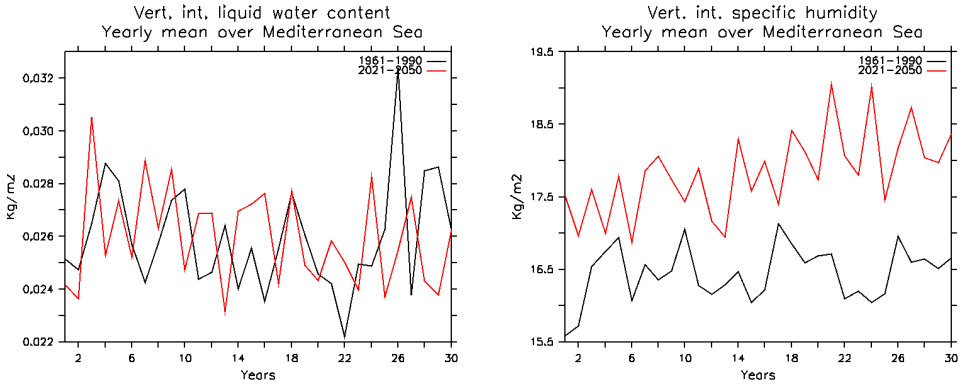

(a) Vert. int. water content

(b) Vert. int. specific humidity

Figure 3.15: As Figure 3.11 for vertically integrated liquid water content (left) and vertical integrated specific humidity over the Mediterranean Sea

solar radiation due to the lack of clouds is compensated by a larger absorption due to a larger concentration of GHG and water vapor in the atmosphere, leading to an unchanged downward surface solar radiation.

At the surface of the Mediterranean Sea, the net water budget (P-E) has a larger deficit, of around 10% (0.2 Kg/m^2). In future climate compared to the present climate period. The evaporation is slightly increased, but the major difference is found in a decrease of precipitation (Section 3.4). Nevertheless, changes in the fresh water flux at the Mediterranean Sea are not enough to explain the increase in the water content over the basin itself. Therefore, more water vapor advection into the basin is taking place. Indeed, according to the observed atmospheric circulation, the evaporation uptake from the Atlantic (under similar thermal air-sea conditions as in the Mediterranean Sea) is transported south-eastward (see Chapter 4) and supplies the water vapor to the region.

3.6 Oceanic response

3.6.1 Water masses

The Mediterranean Sea is characterized by an active thermohaline circulation driven by the surface heat and freshwater fluxes. Changes in surface temperature and salt concentration, produced by heat and freshwater loss, create a water density gradient at the upper layer which induces deep water formation.

The thermohaline structure simulated in the different experiments is represented in Figure 3.16. It shows the profile of the potential density anomaly (σ_θ) calculated from horizontally integrated temperature and salinity over the Mediterranean Sea, and the temperature versus salinity diagram. Three data sets are shown: the observational data set MEDATLASII (MEDAR/MEDATLAS. 2002), the LAOM and the RCSM experiments.

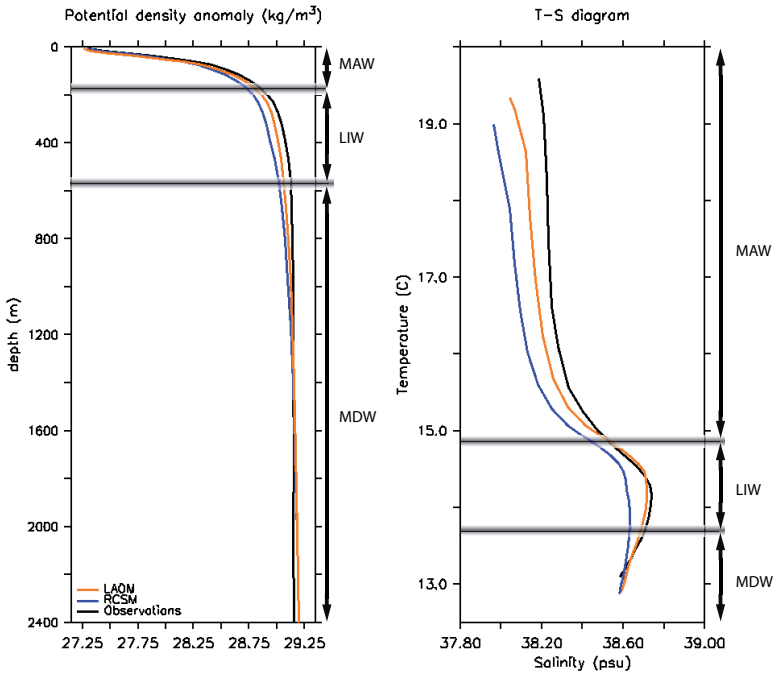

Figure 3.16: Vertical profile of the potential density anomaly and temperature vs salinity diagram for the Mediterranean Sea. The represented data correspond to the LAOM and RCSM experiments and the MEDATLASII observational data. The modeled values are averages for the period 1958 to 2001

The depth reached by the convective plumes of the new deep water varies depending on the surface fluxes conditions. In the Mediterranean Sea, the deep water formation takes place in the late winter between February and April. The major areas of deep water formation are: the

Gulf of Lions, the Levantine region and the south of the Adriatic Sea.

The inflow at the Strait of Gibraltar introduces relative cold (~15.5 °C) and fresh (~36.2 psu) water from the Atlantic (Hopkins 1999). The inflowing water becomes warmer and saltier (up to 19.5 °C and ~38 psu) (Malanotte-Rizzoli et al. 1997) along its travel eastwards to the Levantine basin. It is limited to depths between 0-200 m and it is known as Modified Atlantic Water (MAW) (Malanotte-Rizzoli and Bergamasco 1991).

The simulated MAW by the two models are slightly fresher (Table 3.3), the volumetric salinity average for the MAW shows a negative bias of -0.07 psu for the LAOM simulation and -0.16 psu for RCSM run. The temperature bias between the models is of opposite sign. Nevertheless the deviations can be considered small.

Table 3.3: Biases of potential temperature, salinity and density anomalies with respect to the MEDATLASII for the three main water masses: Modified Atlantic Water (MAW), Levantine Intermediate Water (LIW) and Mediterranean Deep Water (MDW) as the sum of the deep water from the eastern basin and the western one. The period corresponds to 1958-2001

	Δ LAOM / Δ RCSM		
	Potential temperature (°C)	Salinity (psu)	Density anomaly (Kg m^{-3})
MAW	0.12 / -0.07	-0.07 / -0.16	-0.08 / -0.10
LIW	0.21 / 0.20	-0.02 / -0.12	-0.06 / -0.13
MDW	0.02 / -0.02	0.02 / -0.01	0.007 / -0.007

The MAW at the eastern Mediterranean basin can form either Levantine Deep Water (LDW) or Levantine Intermediate Water (LIW). The formation of LIW usually takes place in the Northern Levantine Basin, where Rhodes gyre meets the surface conditions to form denser water (Buongiorno Nardelli and Salusti 2000). The LIW sits in the layer between 200 and 500 m depth, and is the saltiest water mass in the Mediterranean Sea. Its averaged salinity is ~38.72 psu with an averaged temperature of ~14.1 °C, according to MEDATLASII. The Southern Aegean Sea and Northern Levantine are places where eventually dense water can form (Wüst 1961; Theocharis et al. 2002). It circulates westwards towards the west basin (Millot 1999) and finally leaves the Mediterranean Sea as a subsurface flow through the Strait of Gibraltar (Tsimplis and Bryden 2000).

The models are able to reproduce LIW in a good agreement with observations regarding to the water properties (Fig 3.16) and averaged values (Table 3.3). The biases in temperature and salinity produce less denser water than observed. The larger bias is in the temperature which is about 0.2 °C warmer, in both experiments, and a fresher water mass at the RCSM one.

Not all the MAW passes through the Strait of Sicily, but a branch circulates along the northern coast of the Western Mediterranean basin (Millot 1999). The Mistral winds, channeled by the Pyrenees and Alps mountain ranges, induces the water mixing that triggers the deep water

formation process as in the Gulf of Lions. Through the combining effects of the weak stratification driven by the wind, large-scale cyclonic gyre, the entrainment of highly saline LIW from bellow, and the buoyancy loss at the surface due to winter cooling, the Western Mediterranean Deep Water (WMDW) is formed. The dense surface water mixes with the saltier and warmer subsurface water, which induces deep convection that sometimes reaches the ocean bottom down to a depth of 2500 m.

At the Adriatic Sea, deep water formation can take place in the northern and in the southern areas. The northern dense water propagates southwards along the bottom and joins the dense water formed at the open sea in the south of the Adriatic to form the Adriatic Deep Water (ADW) (Manca et al. 2002). Both ADW and LDW contribute to form the Eastern Mediterranean Deep Water (EMDW)

In the case of the Mediterranean Deep Water mass (MDW, WMDW plus EMDW), the models do not show a significant bias in temperature nor salinity (Table 3.3). Nevertheless, it should be considered that 41 years of simulation are not enough to replace entirely the deep water masses from the deep Mediterranean basin. Therefore, the MDW characteristics remain close to the initial conditions characteristics, which are based on observational data.

3.7 Discussion and conclusions

The capabilities of the RCSM and ARCM to simulate the water cycle in the Mediterranean Region have been analyzed.

A higher correlation between the evaporation and its driving components in the RCSM results compared with the ARCM data, demonstrates that an active interaction of the simulated thermal and dynamic processes at the air-sea interface, and the high resolution on the SSTs, are important for the assessment of the evaporation processes, and therefore, for the air-sea heat exchange as well. Moreover, it has been shown that the detailed information of the SSTs improve the air-sea feedback processes especially in areas near to the coast. Particularly for the evaporation processes induced by the thermal state of the air-sea interface. This issue can be considered as an improvement with regard to the low resolution prescribed SSTs experiments. However, the RCSM results show a cold bias on SST during summer, which implies a larger negative bias for evaporation in that season. The impact of the SST bias is also influencing the dynamics of the low level atmosphere over the sea surface. At the open-sea, the high correlations of the evaporation with both, the wind and Δq, determine that they are equally important for the evaporation process. Therefore, the evaporation could have either a dynamic or thermal origin in the open-sea.

A detailed representation of the orography in the models improve the representation of the precipitation distribution. Nevertheless, precipitation is one of the most difficult variables to

simulate, and it is the main reason for the biases in the water budget over land areas. Although some individual rivers present biases in their simulated discharge, the total river discharge in the Mediterranean catchment is very well caught by the models. The impact of the active air-sea flux exchange on the land precipitation can be seen in the areas near the coast, and mainly at the mountain ranges where orographic precipitation forms. A decrease in the land water budget in the future climate scenario causes a decrease on the freshwater input into the Mediterranean Sea. This contributes to an even higher deficit of the net freshwater flux than in the present climate.

The simulated values for the net surface freshwater and heat fluxes over the Mediterranean region are in a good agreement with those from observations. Considering that the SSTs in the RCSM are simulated, these results are a good achievement by the coupled model.

For some of the surface fluxes components, the validation of the model is a difficult task due to the large discrepancy among the observational data sets. This applies in particular to the evaporation and longwave heat fluxes, in which the observational data differ in magnitude of the averaged values, variability and trends.

An increased freshwater loss is simulated at the future climate projection. The negative trend is attributed to the decrease in precipitation and river discharge, but not to evaporation which shows a weak negative signal. These results differ from what Mariotti et al. (2002) states, who attributes the deficit to the increase of evaporation as well.

Regarding to the net surface heat flux in the future climate, the increasing weak signal of the heat loss through the latent heat flux in the evaporation process is largely compensated by the decreasing signal of the heat loss due to the sensible heat flux. For the radiation fluxes, the effects on the incoming solar radiation by the increased concentration of the aerosols, greenhouse gases and water vapor and the decrease of clouds formation cancel each other and yield to unchanged net surface solar radiation. For the net longwave radiation flux a decreasing weak signal is predicted. Hence, the total heat loss in the future climate period is reduced, which induces a warming of the Mediterranean Sea.

As a final conclusion, the models are able to reproduce the main characteristics of the physical processes involved in the Mediterranean hydrological cycle, the sea surface fluxes and the water masses of the Mediterranean Sea. The RCSM improves the representation of the air-sea feedbacks, which are important for the simulation of the surface fluxes. But another source of uncertainty is introduced into the climate simulation due to the intrinsic model variability and internal model errors. Nevertheless, this study is considered to be the first step towards the use of a new modeling tool and further model development will overcome these issues.

Chapter 4

Water vapor transport and precipitation over the Mediterranean region as simulated by a coupled atmosphere-ocean regional climate model[1]

The Mediterranean hydrological cycle using a regional atmosphere-ocean coupled climate model is investigated. Climatological evaporation sources for precipitation are analyzed for winter and summer seasons in the period from 1961 to 2001. Air parcels are tracked backwards to identify moisture sources that contribute to local precipitation over the Mediterranean and Black Sea catchments.

High resolution datasets (0.22° x 0.22°) from three different climate simulations are used in this analysis. The simulations were carried out using regional atmosphere (REMO) and limited area ocean (MPI-OM) models. The first simulation was carried out using the stand-alone version of the atmosphere regional model, with prescribed sea surface temperatures from reanalysis data. The second simulation was performed with the atmosphere-ocean coupled version which allows for considering the air-sea interactions over the Mediterranean Sea. The third run is a 100 years future climate simulation, again using the coupled model.

Strong differences in spatial distribution and magnitude of the moisture sources are observed for winter and summer seasons. During winter, the main source of evaporation is found over the sea areas, with approximately 40% of contribution from the Mediterranean Sea. A large part of the transported water comes from outside of the Mediterranean region (catchment + basin). During summer, the moisture comes predominantly from terrestrial areas, between 41% and 46%,

[1] Submitted to *Climate Dynamics*. Elizalde, A. and Jacob, D.

with a larger recycling ratio and a decrease of the amount of transported water into the Mediterranean region. Nevertheless, the evaporation produced inside the Mediterranean region represents 53% of the total evaporation involved in the Mediterranean hydrological cycle, with no significant difference between seasons despite their different hydrological regimes. Moreover, although the scenario simulation shows a general increase in evaporation and decrease in precipitation, the percentage of recycled water exhibits only a slight negative difference (-0.21% in winter and -0.74% in summer) in the climate projection.

4.1 Introduction

This work investigates marine evaporation conditions and sources of evaporation for Mediterranean catchment rainfall through tracking of the water vapor transport in the Mediterranean region. The Mediterranean Sea, due to its negative water budget, acts as a moisture provider for the Mediterranean area. Several studies have contributed to investigate the origin and areas of deposition of the transported water vapor in this region, and to infer the governing mechanisms of the water cycle. The marine evaporation is determined by different conditions that affect the surface: sea surface temperature (SST), atmospheric circulation, humidity, air temperature and wind speed. The spatial distribution and the time variability of these factors produce a very characteristic evaporation pattern of the Mediterranean Sea which influences the atmosphere and acts as forcing mechanism for the sea, being responsible for the Mediterranean thermohaline circulation.

To assess and understand the processes governing the water fluxes out of and into the Mediterranean Sea is a challenging task. The Mediterranean region includes several complex boundary conditions: complicated orography, intricate coastlines and narrow straits, in such a way that high resolution information is needed in order to resolve processes at medium and small-scales.

The components of the hydrological cycle have been analyzed extensively, in particular the fresh water budget, its temporal and spatial variability over the Mediterranean Sea (Colacino and Dell'Osso 1977; Mariotti et al. 2002; Somot et al. 2008; Jin and Zangvil 2009; Mariotti et al. 2008; Romanou et al. 2010) and Black Sea (Kara et al. 2008). The products of marine evaporation are transported to land areas by advection influencing local precipitation. In the Mediterranean catchment, the influence of Atlantic and Mediterranean evaporation on land rainfall largely depends on the location of the area, the season, the atmospheric conditions and circulation (Schicker et al. 2010). Moreover, large-scale pressure systems, northern fronts and extratropical cyclones from the Atlantic affect European and western Mediterranean catchments (Reale et al. 2001), as shown by the strong correlation between the precipitation in these areas and the North Atlantic Oscillation index (NAO) (Fernández et al. 2003). On the other hand, the correlation between NAO and the eastern catchment rainfall is poor since the evapo-

rative sources for rainfall are found in the eastern Mediterranean Sea itself. This phenomenon has been studied at regional/local-scale showing that the orography is an important factor that limits the eastward moisture transport. In the case of the Alpine region, the mountain range acts as a barrier, steering the winds and producing orographic precipitation by the upwards forced mechanical motion. Therefore, the northern and southern Alpine slopes present different hydrological regimes due to the different influence by Atlantic and Mediterranean water masses (Sodemann and Zubler 2010).

The water cycle budget is influenced by processes at local scale in coastal areas as well. In autumn, warm Mediterranean SSTs produce strong evaporation in the basin, the moist air at the coast is lifted by winds following the terrain profile upslope producing strong rainfall when cold air pools are found at high levels (Millán et al. 2005). This phenomenon has been described for the western Mediterranean coast, but is present in many parts of the basin. Since the Mediterranean coastlines run for approximately 47,027 km, and cover large parts of the Mediterranean catchment, the local-scale processes have an important influence on the whole Mediterranean hydrological cycle.

Previous works address the large to mesoscale moisture transport inside the Mediterranean region using coarse resolution datasets (~1°x1°) either for short periods of time or specific regions (Schicker et al. 2010; Sodemann and Zubler 2010). In this work, we assess the water transport inside the Mediterranean catchment using two 42 years simulation at a high resolution (0.22°x0.22°), one from a stand-alone version of the atmosphere regional climate model (ARCM) and a second using a coupled atmosphere-ocean-hydrology version with a high resolution ocean model (~0.1°x0.1°). Since the coupled model achieves the connection between the three earth components: land-atmosphere-ocean, the new tool can be considered as a Regional Climate System Model (RCSM). The goal is to understand and to assess the evaporation sources that contribute to land precipitation. For this, a Lagrangian-based method developed by Dirmeyer and Brubaker 1999 is used. The method calculates quasi-isentropic backward trajectories and has been applied previously in other studies (Brubaker et al. 2001), especially for the Mediterranean region with regard to heavy rainfall spells (Reale et al. 2001).

The analysis covers winter and summer seasons, where the Mediterranean climate presents opposite hydrological regimes. This work contributes to understanding the role of the Mediterranean Sea as a component of the Mediterranean hydrological cycle, and the impact of climate change on this cycle.

The data is discussed in Section 4.2. The backwards trajectory method for water vapor tracking is presented in Section 4.3. Results are shown in Section 4.4 and conclusions are drawn in Section 4.5.

4.2 Observations and model data

As pointed out by Dirmeyer and Brubaker (1999), for tracking trajectories of air parcels it is essential to use accurate data with high resolution in both time and space. Reanalysis datasets have been highlighted as a suitable option, if not the ideal one, since they include gridded data based on assimilated observations at a high temporal resolution. However, for this study, reanalysis data have major disadvantages (Fernández et al. 2003). Its spatial resolution in the best case, like for the ERA-Interim reanalysis (ECMWF 2009), is 0.7 degrees, and the covered time period is limited to 20 years in the postindustrial era. For longer time periods, resolution ranges from 1.125° to 1.9° for the ERA40 (Uppala et al. 2005) and NCEP (Kalnay et al. 1996) reanalysis. For the Mediterranean region, where complex orography and coastlines play an important role, such resolutions are too coarse. In the numerical model simulations that were performed for this work, the resolutions are 0.22° and 0.10° for atmosphere and ocean grids respectively. This allows for resolving small-scale processes and producing high-resolution gridded information for precipitation and evaporation. Although it is known that the regional climate models may misrepresent processes related to precipitation (like soil moisture-precipitation feedbacks, residence time of moisture advection etc.), we argue that high-resolution regional climate model simulations are an improvement on the relatively coarse reanalysis datasets.

The variables considered are precipitation, evaporation, surface pressure, wind components, specific humidity, and potential temperature at a frequency of 6 hours. Three different climate model simulations comprising the Mediterranean region were performed to create three climatological datasets. The simulations were performed with a regional atmospheric model and a coupled atmosphere-ocean model driven by reanalysis data and global climate model simulations.

Two simulations use the reanalysis ERA40 from the European Center of Medium Range Weather Forecast (ECMWF) (Uppala et al. 2005) as lateral boundary conditions. The first of these two simulations was carried out with the stand-alone version of the atmospheric regional climate model REMO (Jacob 2001; Jacob et al. 2007) for the period 1961 to 2001. For this run (hereinafter referred to as ARCM), the ERA40 data was used to prescribe the surface boundary conditions as well. The second simulation was performed using the same atmospheric model coupled to a regional version of the ocean model MPI-OM (Maier-Reimer 1997; Marsland et al. 2003) for the Mediterranean Sea. Since the coupled model achieves the connection between the three earth components: land-atmosphere-ocean, the new tool can be considered as a Regional Climate System Model (RCSM).

Heat, moisture and momentum fluxes are passed from REMO to MPI-OM and MPI-OM returns SSTs to the atmospheric model with a coupling frequency of 6 hours. For the coupled simulation the ERA40 reanalysis is used as lateral boundary conditions for the atmosphere as well. For the regional version of MPI-OM, the climatological dataset by Levitus et al. (1998) is

used to impose temperature and salinity boundary conditions at the Atlantic Ocean as a buffer zone.

The coupled model also includes a hydrological discharge model (HDmodel) (Hagemann and Dümenil 1998) which calculates discharge values for each Mediterranean and Black Sea river catchment based on the fast and slow component of the runoff calculated by REMO.

The third run considered in this study is a downscaled future climate simulation from a global run using the global climate ECHAM5/MPI-OM model and the A1B emissions scenario. It consists of a 100 years simulation that covers the period 1951 to 2050. For the present study climatological statistics for the time slices 1961-1990 and 2021-2050 were analyzed.

The resolution of the models are 0.22° and ~0.10° for REMO and MPI-OM respectively. All models have been developed at the Max Planck Institute for Meteorology.

The observational datasets used in the present work for model validation are: for wind speed and evaporation the HOAPS dataset from the World Data Center for Climate (Andersson et al. 2007), and the OAFlux dataset from the Woods Hole Oceanographic Institution (Yu et al. 2008). HOAPS is a completely satellite based global dataset with 0.5° resolution covering the years 1987 to 2005. OAFlux is a global dataset based on satellite and atmospheric reanalysis blended sources with a resolution of 0.25° for wind and 1° for evaporation from 1958 to 2001. For the sea surface temperature (SST), the climatological MEDATLASII dataset dedicated to the Mediterranean Sea is used. Its resolution is 0.2° (MEDAR/MEDATLAS. 2002).

For land precipitation, three monthly gridded datasets have been considered: the Climatic Research Unit database (CRU) version TS 3.0 from the University of East Anglia (CRU 2008), precipitation data from the Global Precipitation Climatology Centre (GPCC) at the German Weather Service (Rudolf et al. 1994), and the Global Historical Climatology Network version 1.02, produced and documented by J. Willmott and Kenji Matsuura (WILLMAT) (Willmott and Matsuura 2001). Their coverage is worldwide at a resolution of 0.5°x0.5°.

4.3 Moisture divergence and water vapor transport

To investigate the water transport in the Mediterranean region two calculations have been performed: the divergence of water vapor is evaluated, and a Langragian-based method to trace trajectories of water vapor backwards is applied.

The divergence has been calculated as follows:

$$\frac{\partial W}{\partial t} + \nabla \cdot Q = E - P \tag{4.1}$$

Here W is the vertically integrated total water content calculated as the sum of the vertically integrated liquid water content and specific humidity, Q is the horizontal transport of the moisture, and ∇ refers to the divergence operator. E and P are the accumulated evaporation and precipitation respectively. The time interval corresponds to the time resolution of the datasets. In this case, for both reanalysis and model data the time interval is 6 hours. The integration of W over long time periods tends to be at least one order of magnitude smaller than $E - P$. This leads to the interpretation of the moisture divergence $\nabla \cdot Q$ as source (positive) when E exceeds P clearly, and sink (negative) when P exceeds E clearly.

Moreover, the Langragian-based method by Dirmeyer and Brubaker (1999) was applied to the model data. The method consists in tracing backwards selected air parcels along quasi-isentropic trajectories. The selection of the air parcel height is based on a random humidity-weighted approach calculated from an cumulative probability function of the vertical moisture distribution. Each air parcel is submitted backwards in time. The moisture uptake is calculated by the rate of the local evaporation where the air parcel is passing by, and the total precipitable water at the original grid box of the trajectory given evaporation exceeds precipitation. The evaporation sources for winter and summer precipitation in the period from 1961-2001 were thus calculated.

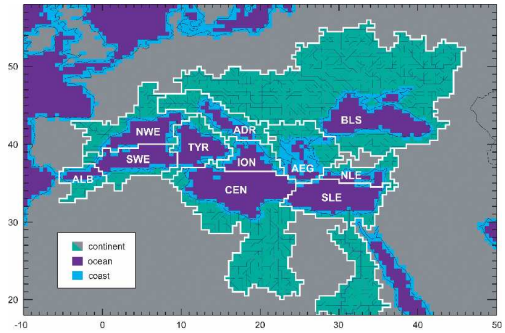

Figure 4.1: Mediterranean and Black Sea subcatchments by Ludwig et al., 2009

This procedure was applied for every grid box inside the Mediterranean subcatchments defined by Ludwig et al. (2009). Their boundaries are presented in Figure 4.1 and their definition is given in Table 4.1.

Table 4.1: Mediterranean and Black Sea subcatchments from Figure 4.1

Subcatchment name	Short name
Alboran	ALB
South-Western	SWE
North-Western	NWE
Tyrrhenian	TYR
Adriatic	ADR
Ionian	ION
Central	CEN
Aegean	AEG
North-Levantine	NLE
South-Levantine	SLE
Total Mediterranean	MED
Black Sea	BLS

4.4 Results

4.4.1 Present climate

Precipitation

Figure 4.2 shows yearly time series for mean precipitation over land areas in the Mediterranean catchment only. An ensemble of observation datasets, ARCM and RCSM simulations are plotted for winter and summer seasons. The range of uncertainty in gray is enlarged by the CRU dataset which shows largest precipitation of the three datasets, WILLMAT and GPCC data are strongly correlated. Both model versions are able to reproduce the yearly variability in precipitation for both seasons. In general, the RCSM experiment produces up to 0.24 mm/day more precipitation than the ARCM run for winter, and up to 0.17 mm/day less during summer. This is related to the different SSTs in the two simulations. During winter, the RCSM simulation exhibits warmer SSTs compared to the atmosphere stand-alone model simulation, implying an increase in heating of the near surface air and an increase of its moisture holding capacity. This allows for transporting larger volumes of water vapor at low levels. The relation reverses during summer due to the colder SSTs of the RCSM simulation. The transfer of heat and moisture from the surface to the air is reduced, damping convective activity and reducing the water vapor availability.

The precipitation distribution over the Mediterranean subcatchments is shown in Figure 4.3 for the observations datasets, RCSM and ARCM. Mediterranean subcatchments located at the

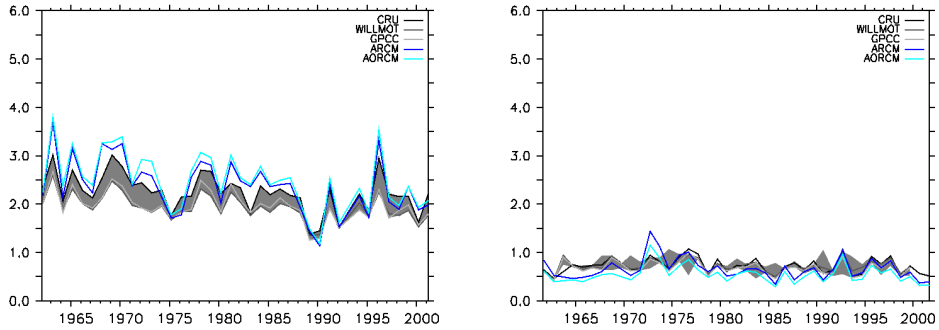

(a) Winter **(b)** Summer

Figure 4.2: Precipitation time series (mm/day) for observations (CRU, WILLMOT and GPCC), ARCM and RCSM for the period 1961-2001. The gray shaded area represents the range of uncertainty from observed data

north of the Mediterranean Sea receive higher rainfall during winter: south Italy and the west coast of Greece (ION), the east coast of the Adriatic Sea (ADR), the coasts at the Aegean Sea (AEG) and northern Levantine (NLE). All these areas experience mainly north-eastward winds and exhibit abrupt orographic changes near the coast. Both model versions produce larger precipitation values than observed, in particular the RCSM simulation.

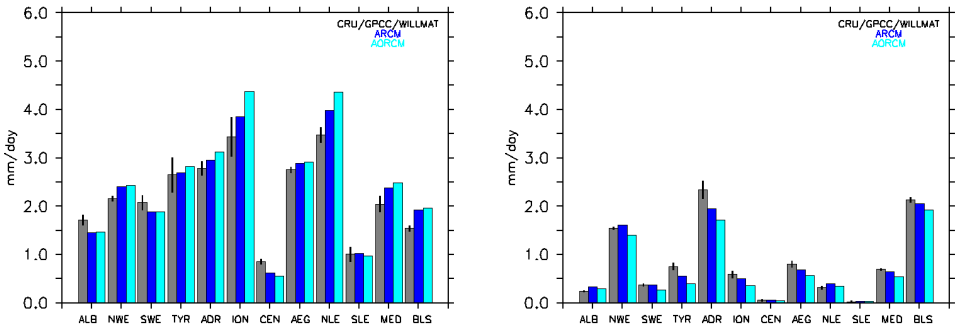

(a) Winter **(b)** Summer

Figure 4.3: Mean precipitation (mm/day) for each subcatchment (1961-2001). The ensemble of observation datasets is in gray color, ARCM in dark blue and RCSM in cyan. The standard deviation of the ensemble is represented by the small black bar

In summer, the dry season in the Mediterranean climate, the reduction of precipitation is not

homogeneous over the whole region. The NWE, ADR and BLS subcatchments show the highest precipitation. Both Mediterranean catchments (NWE and ADR) are under the influence of the Alpine mountain range system, where heavy precipitation takes place over the intra-Alpine region (Hofinger et al. 2000). In any case, the RCSM simulation has less precipitation than the ARCM run.

Water vapor divergence

In Figure 4.4 the water vapor divergence and convergence is presented for ERA40 reanalysis data and the ARCM simulation for winter and summer seasons. Since the RCSM simulation is similar to the ARCM simulation the comparison is made separately below. The spatial resolution of the data are the original ones, no interpolation was applied. Areas of sources/divergence and sinks/convergence of moisture are represented by positive and negative values and colored in red and blue respectively.

In the Mediterranean basin the divergence of the water vapor is permanent during the whole year. It is driven by the deficit in the water budget; that is, negative $E - P$ values, and the seasonal changes in this factor.

The difference between seasons regarding the Mediterranean Sea water vapor divergence is based on the reversed situations regarding the air and water temperatures at the air-sea interface. In winter, due to the large heat storage capacity of the Mediterranean Sea, the heat gained during summer keeps the Mediterranean SST warmer than the air temperature. This increases the gradient of the water vapor pressure between the surface and the near surface air which enhances the upward latent heat flux, and therefore, the transport of moisture into the atmosphere. During summer, the relation is reversed. Although $E - P$ remains negative, a reduction in E leads to a decrease of the water flux and smaller values of the water vapor divergence.

Areas with strongest divergence correspond mainly to two regions: the Eastern Mediterranean and the Golf of Lion. At the Eastern Mediterranean, the water vapor divergence is mainly due to thermal processes as explained above, with the specific characteristic of warmer SST than the rest of the whole basin. This regional warming is produced by the gain of heat of the water masses during their easterly travel steered by currents. From the Gibraltar Strait crossing the west and center basins following the African coast until they reach the eastern basin. The higher increase of the air-sea temperature gradient in this area triggers the enhancement of the evaporation. At the Golf of Lion the divergence enhancement is based on dynamical processes. The evaporation, that directly depends on the wind stress, is enhanced by the strong north-easterly winds steered through the channel formed by the Pyrenees and the Alpine mountain ranges.

Over land in winter, either westerly fronts bring cold and damp air from the Atlantic or easterly

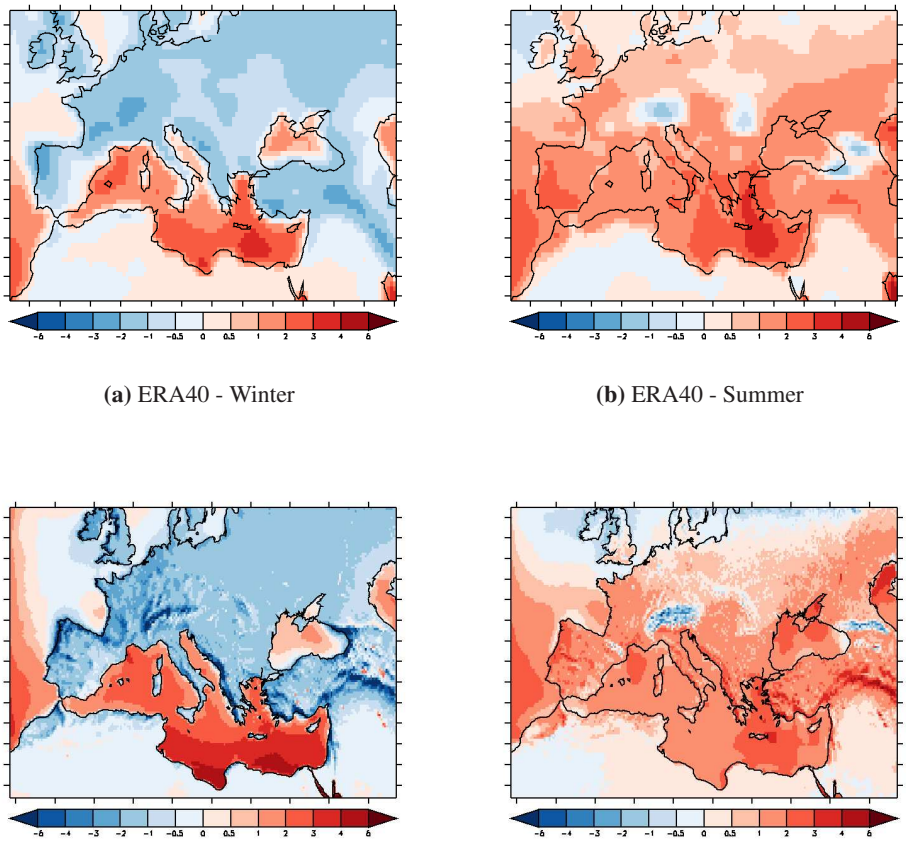

(a) ERA40 - Winter

(b) ERA40 - Summer

(c) ARCM - Winter

(d) ARCM - Summer

Figure 4.4: Moisture divergence (mm/day) for winter and summer for the driving dataset (ERA40) at its original resolution and ARCM simulation, for the reference period 1961-2001. Positive values in red color indicate water divergence and negative values in blue are convergence

fronts bring very cold and dry air towards Europe. The cold temperature is crucial with respect to the convergence of water vapor. The colder temperature limits the surface fluxes reducing the heat exchange and evaporation, whereas the large-scale systems bring moisture producing precipitation. The convergence is lower at the plain regions of Europe and almost neutral over Africa. During summer, the circulation is characterized by the southerly flow that brings dry and warm air from African regions. The dryness of the air and the reduced cloudiness produce surface heating that enhances evaporation, leading to a divergent situation. There is an exception in those regions where the moisture from the Atlantic is still predominant, like the northern slope of the Alps.

The orography plays an important role regarding the convergence of moisture. The moist air, that generally had traveled over large sea regions collecting moisture, is lifted mechanically by the mountain ranges. At upper levels, the water vapor condensates due to the lower temperature forming clouds and producing precipitation. By using a high-resolution dataset (Figure 4.4c), it is possible to observe this situation as a large positive convergence, more than -6 mm/day, at the windward slopes in the Cantabric, Alpine, Dinaric Alps, Pindos, Taurus and Caucasus mountain ranges, whereas for the reanalysis data (Figure 4.4a) this process is misrepresented due to the smoothed orography. Here convergence values are limited to no more that -2 mm/day. The mechanical blocking and steering of the wind flow due to the orography impacts the local water budget and mesoscale moisture transport, and should therefore not be neglected.

The impact of the active air-sea interaction on the water vapor flux divergence can be observed in Figure 4.5. Values of moisture divergence from the ARCM simulation are compared with those from the RCSM simulation. The field is separated in land, Mediterranean basin, Black Sea and the Atlantic regions. As in Figure 4.4, it is possible to identify the different seasonal hydrological regimes: larger values over land during winter and lower values during summer, and slightly larger values over the Mediterranean region in winter compared to summer.

Major differences between the two simulations are observed over land at larger values of convergence (negative values). Comparing to Figure 4.5 these values correspond to orographic precipitation areas due to the larger precipitation seen in the RCSM simulation. The RCSM model version produces warmer SSTs which warms the near surface air temperature and allows for an increase of water vapor holding capacity. Thus more precipitation can form when the water vapor is transported by advection, especially at the coastal regions. For the Mediterranean and Black Seas, the divergent water vapor transport is reduced in the RCSM due to the decrease of the evaporation (as shown in Table 4.2). The Atlantic basin shows no difference since the SST is prescribed for this area in both cases. During summer, the situation over water is reversed.

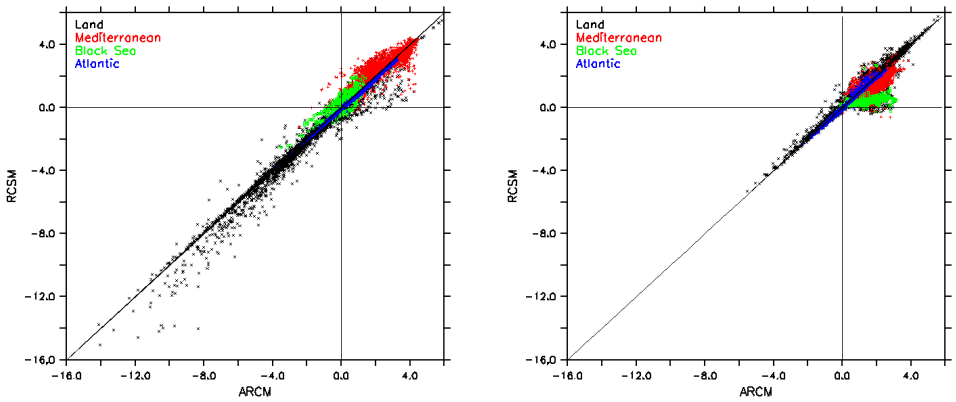

(a) Winter **(b)** Summer

Figure 4.5: Comparison between RCSM and ARCM for multiyear seasonal mean of moisture divergence (mm/day) over the period 1961-2001. The moisture divergence diagnostic has been masked per areas: land, Mediterranean Sea, Black Sea and Atlantic basin are colored in black, red, green and blue respectively

Table 4.2: Seasonal mean evaporation (mm/day) over the Mediterranean Sea for: observation datasets HOAPS3 (1988-2005), OAFlux (1961-2001), reanalysis ERA40 (1961-2001), and simulations ARCM and RCSM (1961-2001)

	HOAPS	OAFlux	ERA40	ARCM	RCSM
spring	2.00	2.06	2.60	2.10	1.96
summer	3.24	2.34	3.11	2.05	1.51
autumn	4.05	3.98	4.66	3.97	3.74
winter	3.68	3.78	4.37	4.36	4.46

Water vapor transport

To investigate the water vapor transport in the Mediterranean region, we have calculated the backwards trajectories of air parcels to identify the evaporation sources of land precipitation in the Mediterranean and Black Sea catchments using the delimitations by Ludwig et al. (2009) (Figure 4.1). This calculation has been performed for the winter (December-January-February or DJF) and summer (June-July-August or JJA) season separately.

Figures from 4.6 to 4.7 show the spatial distribution of seasonal accumulated evaporation sources for each subcatchment from the ARCM simulation. In order to do a spatial comparison between RCSM and ARCM models, evaporation source spatial averages have been calculated over land and sea areas where the evaporation uptake is produced. Over land, the total land area is considered. Moreover, the evaporation source located in the subcatchment itself is used to calculated the recycling ratio (RR). Over Sea, the averaged over total marine area is considered as well as the basin areas: Atlantic, Mediterranean and Black Sea. Tables 4.3 and 4.4 summarize these averages of each area as percentages with respect to the total precipitation in each subcatchment for the winter and the summer seasons. In the tables, the Mediterranean catchment row refers to the mean of the quantities of all Mediterranean subcatchments.

The seasonal hydrological cycle regimes discussed in Section 4.4.1 become evident again in this analysis: the marine evaporation is the main contributor during the winter months, whereas the terrestrial evaporation is most important for the summer months. This shows that the surface conditions regulate the water flux into the atmosphere. On the other hand, the mesoscale circulation governs the spatial distribution of the moisture sources.

In winter, in general, land evaporation is reduced. Instead, the main source of evaporation is found over the sea. Several features are remarkable from the Figure 4.6. Each subcatchment receives moisture from the Atlantic and the Mediterranean Sea in more or less amounts, depending on its location regarding the Mediterranean Sea. The mechanisms that bring moisture from the Atlantic and the Mediterranean Sea to the subcatchments are related to the winter pressure systems. Low pressure systems partly originate in the Mediterranean basin, but most of them are formed over the Atlantic open sea and travel eastwards along the northern part of Europe. In some cases their trajectory diverts into the Mediterranean area (Hillman and LTD 1962). During the eastwards low pressure displacement, the counterclockwise circulation transports absorbed moisture from the Mediterranean Sea into southern Europe. In this way the Mediterranean Sea becomes an active and important component of the European and Mediterranean hydrological cycle.

Mountain ranges play a passive role in the water cycle. The Alpine mountains block the transport of moisture from the Atlantic to the Mediterranean region by reducing the air humidity and forcing orographic precipitation and/or steering the winds in different directions. This can be seen when analyzing the North West, Adriatic, Tyrrhenian and Ionian catchments (Fig-

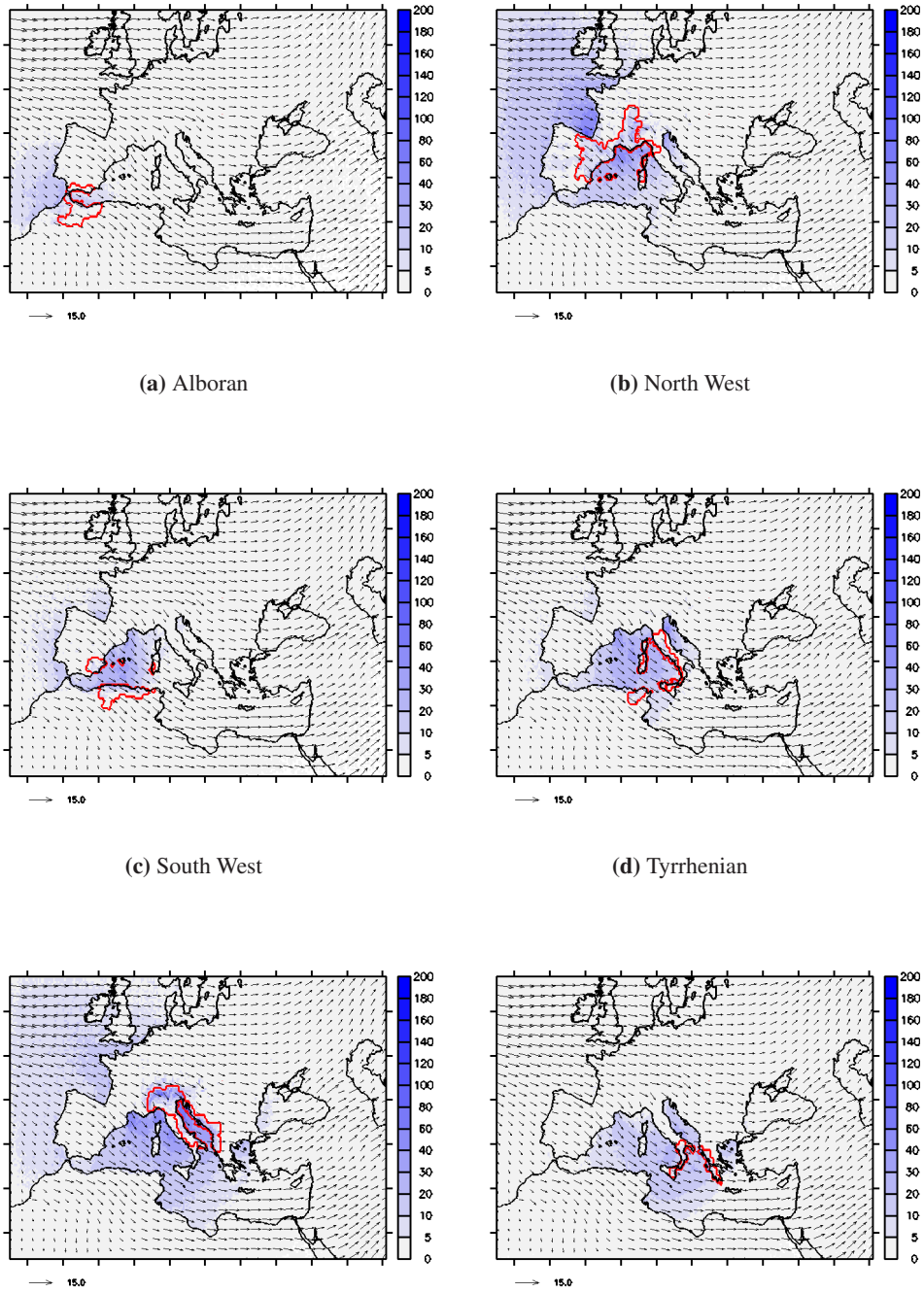

(a) Alboran

(b) North West

(c) South West

(d) Tyrrhenian

(e) Adriatic

(f) Ionian

Figure 4.6: Accumulated evaporation sources distribution (mm) for individual subcatchments for winter season for the ARCM simulation. Arrows show the mean wind flow (m/s) associated to this season

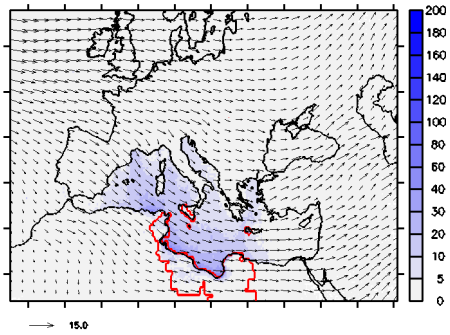

(g) Central

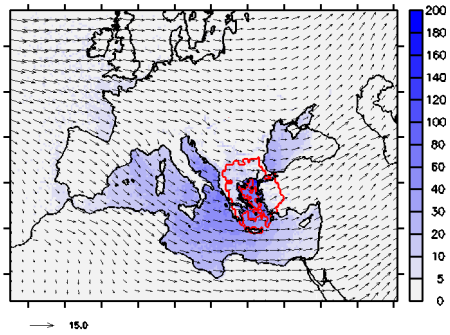

(h) Aegean

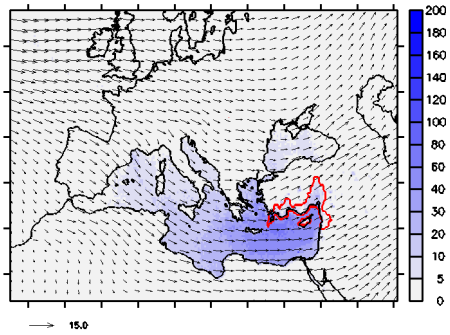

(i) North Levantine

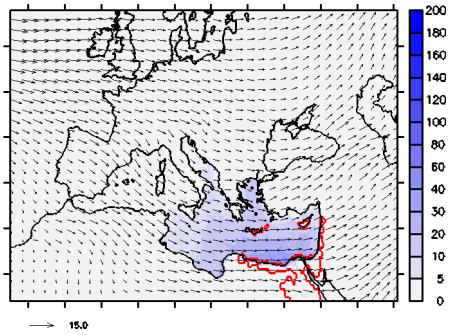

(j) South Levantine

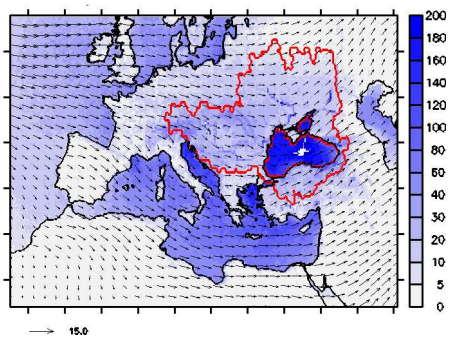

(k) Black Sea

Figure 4.6: Continues

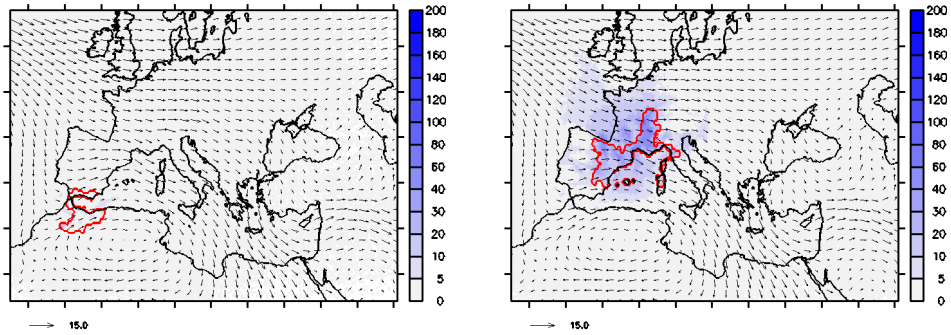

(a) Alboran **(b)** North West

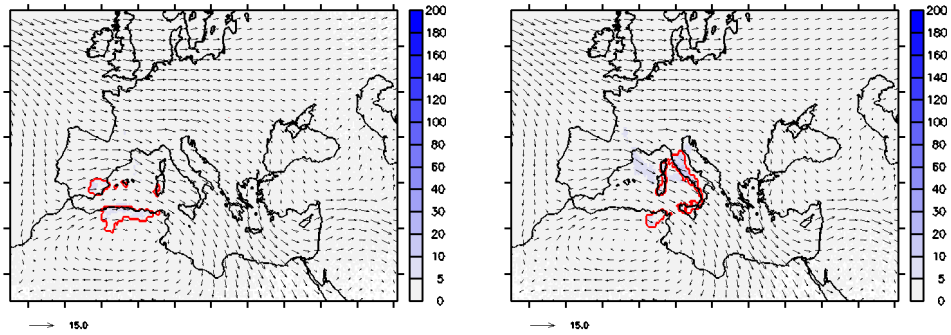

(c) South West **(d)** Tyrrhenian

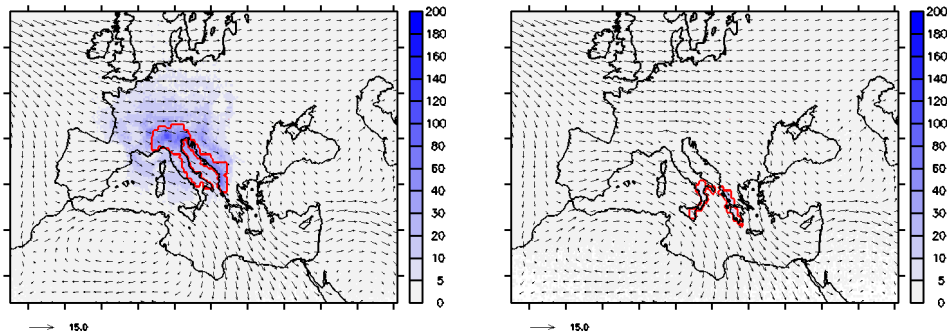

(e) Adriatic **(f)** Ionian

Figure 4.7: Same as in Figure 4.6 for summer season

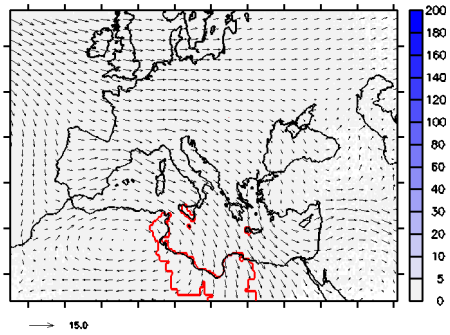

(g) Central

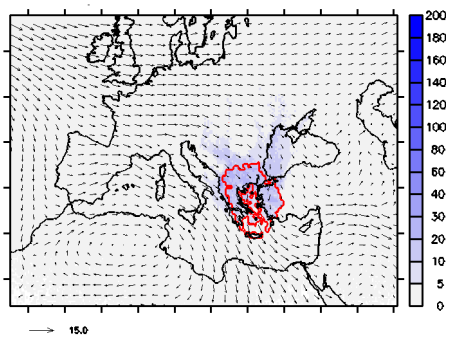

(h) Aegean

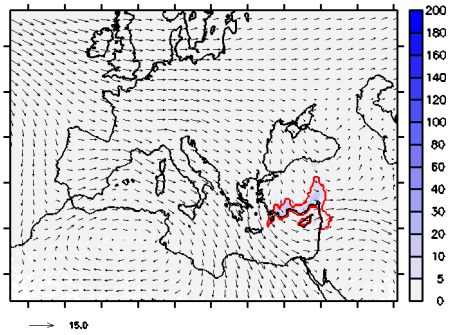

(i) North Levantine

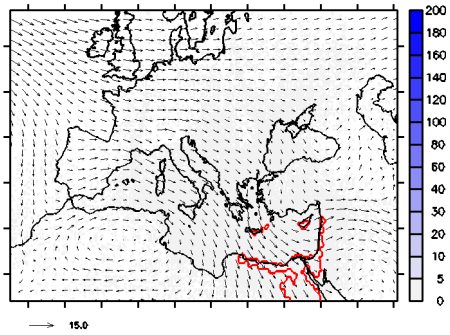

(j) South Levantine

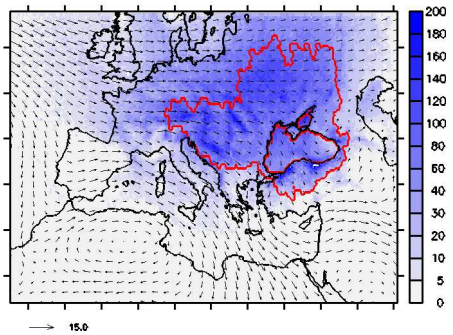

(k) Black Sea

Figure 4.7: Continues

ures 4.6b, 4.6e, 4.6d and 4.6f). From the Table 4.3, the Atlantic evaporation contributes to precipitation over the North West and Adriatic catchments approximately with 51% and 40% respectively, whereas its influence is reduced in the Tyrrhenian and Ionian catchments to 31% and 25% respectively. This feature is confirmed following down the Atlantic and Mediterranean columns in the table. The more into the east of the Mediterranean (down the column), the lower the influence from the Atlantic and the higher the contribution from the Mediterranean Sea. Besides the orographic steering, the variability of the large-scale easterly air flow into south-eastern Europe also contributes to this characteristic. In total, the Mediterranean Sea evaporation contribution to the land precipitation is approximately 40% in winter.

In summer, the land evaporation accounts for the major amount of moisture into the atmosphere. The contribution of the local evaporation, that is, the recycling ratio, is proportionally three times larger compared to winter (Table 4.4). The typical pressure systems in summer contribute to this situation: low pressure frequency at the Mediterranean region decreases to 70% compared to winter (Hillman and LTD 1962). Thus anticyclones are more persistent over Europe and the Mediterranean regions. Sometimes extended anticyclonic systems, located at the north or east or at both places of Europe, produce a cut off with regard to the easterly Atlantic depressions. As a consequence, light winds are observed over the Mediterranean basin, and together with the thermal state of the air-sea interface the marine evaporation is reduced. In this case, the percentage of evaporation stemming from the Mediterranean Sea is reduced to 25.8% (ARCM) and 22.1% (RCSM).

The Mediterranean recycled water is considered as the water that completes the hydrological cycle inside the Mediterranean catchment. This water vapor is generated by evaporation in the terrestrial and marine areas in the Mediterranean region and contributes to the land precipitation, which in turn eventually is converted into local evaporation or runoff routed towards the sea and summed as freshwater input into the Mediterranean sea. We computed the total Mediterranean recycled water as the sum of the marine evaporation from the Mediterranean sea plus the land evaporation produced over the Mediterranean catchment at each subcatchment (MCRR). This is then integrated over all subcatchments. We obtain for the ARCM/RCSM experiments 52.9/53.1% in winter and 53,5/52.2% in summer. That means, around 53% of the evaporation produced in the Mediterranean region contributes to the precipitation inside the catchment for both seasons. Thus, despite the exchanged roles of the terrestrial and marine evaporation during the two seasons, the percentage of recycled water stays at a very similar ratio.

4.4.2 Future climate impact

In the following paragraphs precipitation and water transport are analyzed for the scenario simulation. For this the historical period 1961 to 1990 and the climate projection period from

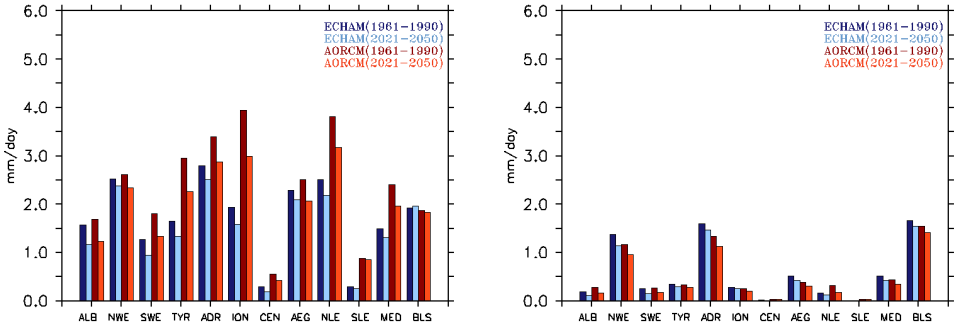

(a) Winter **(b)** Summer

Figure 4.8: Mean precipitation (mm/day) for each subcatchment. ECHAM and RCSM datasets are plotted in blue and red colors respectively. Dark and light color tones refer to historical (1961-1990) and future scenario (2021-2050) periods respectively

2021 to 2050 using the RCSM model version are considered.

Precipitation

Figure 4.8 shows mean precipitation for each Mediterranean subcatchment from the RCSM simulation and from the driving global climate model ECHAM5/MPI-OM. The main difference between models is during winter, there the RCSM produces more precipitation than the global model simulation over the whole Mediterranean region: 61% comparing the historical simulations and 49% comparing the scenario simulations. In the case of the Black Sea catchment, the RCSM produces less precipitation than the global model in both periods, therefore the difference between models is negative: -2.6% comparing historical simulations and -7.1% comparing scenario simulations.

During summer, the signal is not homogeneous for all the subcatchments, but the mean over the whole Mediterranean catchment exhibits a difference of -13.7% and -19% between the historical period and the scenarios.

A reason for this difference could be explained by the smoothed orography in the ECHAM5 /MPI-OM model. This may have an influence on the near surface circulation and orographic precipitation processes. Moreover, different Mediterranean Sea conditions in both simulations may lead to such precipitation differences as well, especially in those regions which stand under the influence of the Mediterranean Sea like the Tyrrehenian, Ionian, North and South Levantine subcatchments. Since a detailed comparison between both simulations is beyond the scope of

this work, it is not possible to reach a definite conclusion regarding this issue.

The future climate scenario exhibits a decrease in precipitation in comparison with the historical simulation for all the subcatchments. The exception is the Black Sea catchment during winter for the ECHAM5/MPI-OM simulation. The decrease in precipitation over the whole Mediterranean region is more pronounced in winter, -0.18 mm/day for ECHAM5/MPI-OM and -0.45 mm/day for the RCSM simulation. This represents between 12% (ECHAM5/MPI-OM) and 18.7% (RCSM) of reduction in water availability over the Mediterranean region.

Water vapor transport

Analogous calculations as in the previous Section have been performed for air parcel trajectories to analyze the moisture transport and the evaporation sources of land precipitation for the historical (1961-1990) and the scenario (2021-2050) simulations. Tables 4.5 and 4.6 summarize the results for all the subcatchments.

As can be observed from a comparison of the Tables 4.3 and 4.4 with Tables 4.5 and 4.6, the climatological values from the RCSM simulation driven by reanalysis and that one from the historical simulation driven by the global climate model are very similar. The largest differences in precipitation is 0.2 mm/day in summer for the mean value over the Mediterranean catchment. The evaporation source differences are not higher than 2%.

The percentage of the total evaporation sources found in the future climate compared with the historical simulation is slightly reduced for both seasons. This reduction is about -2.6% in winter and -0,8% in summer. Less moisture uptake inside the domain suggests an increase of the transported water vapor through the lateral boundaries of the domain, which implies a larger contribution from the Atlantic.

Inside the domain, a generalized decrease of terrestrial moisture uptake can be detected in the future climate scenario. For the Mediterranean catchment the reduction is -0.95% in winter and -1.6% in summer. Only few subcatchments show a slight increase in local evaporation, mainly those located at the central Mediterranean (ION, AEG, NLE and SLE).

Despite the reduction in total evaporation sources and its terrestrial component, the marine contribution shows a different behavior. In winter, the Black Sea catchment has more contributions from the Atlantic and the Black Sea, and less from the Mediterranean Sea. The Mediterranean catchment, however, receives more moisture from the Mediterranean and Black seas. In summer the Black Sea experiences a similar situation as in winter, but the Mediterranean Sea receives larger contributions from the three basins. The increase of the marine evaporation is connected to the SST warming. The SST increases the temperature gradient at the air-sea interface enhancing the latent heat flux and therefore the evaporation. These results

Table 4.3: The evaporation source averages on each area as percentages with respect to the total precipitation in each subcatchment for winter. All the values are percentages except for the precipitation at the first column in mm/day. Consecutive columns refer to percentages per areas at: the whole domain, only over land, only the Mediterranean catchment (Mediterranean catchment recycling ratio - MCRR), only the subcatchment (recycling ratio - RR), only over sea, only at the Atlantic, Mediterranean Sea and Black Sea. The Mediterranean catchment row at the bottom refers to the mean of the quantities of all Mediterranean subcatchments. *-Indicates that the difference in the averaged values between RCSM and ARCM is statistically significant with a 95% significance level

	Prec	**Evap**	**Land (MCRR/RR)**	**Sea**	**Atlantic**	**Medit**	**Black Sea**
Alboran							
ARCM	1.42	68.88	9.84 (6.43/4.42)	59.05	47.43	11.62	0.07
RCSM	1.47*	68.65*	9.58 (5.92*/4.26*)	59.07*	47.01	12.06*	0.05
North West							
ARCM	2.39	80.76	11.98 (9.59/6.13)	68.78	52.09	16.69	0.20
RCSM	2.43	80.30	11.57* (9.06*/5.92*)	68.73	50.83*	17.90*	0.18
South West							
ARCM	1.87	85.35	11.28 (11.54/5.70)	74.07	41.21	32.86	0.26
RCSM	1.88	84.89	10.84* (10.60*/5.31*)	74.05	40.07*	33.98*	0.22
Tyrrhenian							
ARCM	2.67	79.88	9.89 (13.58/6.03)	69.99	31.76	38.23	0.58
RCSM	2.82*	78.92*	9.18* (12.38*/5.74)	69.74*	30.82	38.93*	0.49
Adriatic							
ARCM	2.92	86.76	14.64 (15.20/8.17)	72.12	40.19	31.92	1.27
RCSM	3.12*	86.14*	13.79* (14.23*/7.60*)	72.34*	38.11	34.23*	1.15
Ionian							
ARCM	3.86	72.74	7.67 (11.77/3.82)	65.07	25.36	39.71	1.43
RCSM	4.37*	71.56*	7.04* (10.78*/3.70*)	64.51*	24.27*	40.24*	1.24
Central							
ARCM	0.62	91.86	14.08 (20.17/12.44)	77.78	19.86	57.90	0.87
RCSM	0.56*	91.87*	13.87* (18.78*/11.45*)	78.00*	18.52*	59.46*	0.83
Aegean							
ARCM	2.90	83.29	11.09 (16.21/9.21)	72.19	28.91	43.28	4.06
RCSM	2.92	83.34	10.52* (15.41*/8.69*)	72.82	28.29*	44.53*	4.23
North Levantine							
ARCM	4.01	87.64	9.73 (13.69/4.54)	77.91	21.07	56.84	2.67
RCSM	4.36*	87.02*	9.09 (13.06*/4.52*)	77.93*	20.85*	57.08*	2.74*
South Levantine							
ARCM	1.02	93.08	9.45 (18.19/8.40)	83.63	20.00	63.63	1.25
RCSM	0.97*	93.41*	9.08* (16.92*/7.42*)	84.33*	18.81*	65.52*	1.26
Black Sea							
ARCM	1.93	98.07	23.75 (9.55/14.96)	74.32	44.92	29.39	12.45
RCSM	1.96*	98.50*	22.49* (9.35*/14.08*)	76.01*	44.66*	31.35*	13.52*
Mediterranean Catchment							
ARCM	**2.37**	**83.02**	**10.97 (13.64/6.89)**	**72.06**	**32.79**	**39.27**	**1.27**
RCSM	**2.49***	**82.61***	**10.46* (12.71/6.46*)**	**72.15***	**31.76**	**40.39***	**1.24**

Table 4.4: Same as Table 4.3 for summer

	Prec	**Evap**	**Land (MCRR/RR)**	**Sea**	**Atlantic**	**Medit**	**Black Sea**
Alboran							
ARCM	0.35	80.89	32.03 (19.92/14.27)	48.86	26.69	22.14	0.06
RCSM	0.29*	79.86*	34.09* (20.66*/14.78*)	45.78*	27.38*	18.44*	0.04*
North West							
ARCM	1.63	75.52	43.14 (22.40/18.81)	32.37	22.74	9.63	0.07
RCSM	1.40*	76.96*	46.00* (23.71*/20.00*)	30.96*	23.42*	7.53*	0.02*
South West							
ARCM	0.38	80.43	32.04 (22.68/14.72)	48.39	20.68	27.67	0.06
RCSM	0.27*	79.98*	36.87* (24.73*/15.84*)	43.10*	21.07*	22.03*	0.04*
Tyrrhenian							
ARCM	0.58	82.02	36.73 (23.70/13.79)	45.30	17.67	27.62	0.17
RCSM	0.40*	85.52*	43.50* (27.14*/15.99*)	42.02*	18.22*	23.78*	0.05*
Adriatic							
ARCM	2.01	85.93	58.79 (29.23/20.28)	27.14	15.72	11.42	0.38
RCSM	1.71*	87.60*	63.21* (31.64*/22.32*)	24.39*	15.37*	9.02*	0.13*
Ionian							
ARCM	0.52	82.52	44.10 (26.64/13.04)	38.42	15.82	22.62	1.37
RCSM	0.36*	86.01*	51.84* (31.60*/16.23*)	34.17*	14.82*	19.35*	0.42*
Central							
ARCM	0.06	93.17	28.33 (27.47/18.26)	64.85	14.51	50.17	0.85
RCSM	0.05*	86.49*	32.68* (28.32*/18.74*)	53.81*	13.29*	40.52*	0.22*
Aegean							
ARCM	0.72	91.06	61.65 (30.22/23.86)	29.41	18.64	10.77	6.78
RCSM	0.57*	93.77*	70.23* (33.85*/26.33*)	23.54*	14.26*	9.28*	2.73*
North Levantine							
ARCM	0.41	95.51	57.36 (32.40/21.21)	38.15	16.46	21.69	5.93
RCSM	0.35*	94.48*	62.13 (34.60*/22.88*)	32.35*	13.14*	19.21*	2.10*
South Levantine							
ARCM	0.04	100.00	18.96 (42.81/37.31)	81.04	26.91	54.13	0.31
RCSM	0.03*	100.00*	22.50 (45.00*/39.64*)	77.50*	26.07*	51.43*	0.00*
Black Sea							
ARCM	2.05	89.55	72.03 (5.29/44.23)	17.52	15.04	2.48	5.36
RCSM	1.92*	89.88*	76.26 (5.67/46.12*)	13.63*	11.74*	1.89*	2.32*
Mediterranean Catchment							
ARCM	**0.67**	**86.71**	**41.31 (27.75/19.56)**	**45.39**	**19.58**	**25.79**	**1.60**
RCSM	**0.54***	**87.07***	**46.31* (30.12/21.27*)**	**40.76***	**18.70***	**22.06***	**0.57***

Table 4.5: Same as Table 4.3 for historical (1961-1990) and scenario (2021-2050) climate for winter. *-Indicates that the difference in the averaged values between historical and scenario simulation is statistically significant with a 95% significance level

	Prec	**Evap**	**Land (MCRR/RR)**	**Sea**	**Atlantic**	**Medit**	**Black Sea**
Alboran							
Historical	1.69	60.12	9.12 (5.15/3.65)	51.00	40.99	10.02	0.11
Scenario	1.24*	55.63*	8.58* (5.14*/3.24*)	47.04*	34.68*	12.36	0.12
North West							
Historical	2.61	78.93	12.20 (9.24/6.17)	66.73	47.75	18.99	0.18
Scenario	2.34	73.02*	10.07* (8.10*/5.08*)	62.96*	42.93*	20.03	0.23
South West							
Historical	1.81	83.56	11.44 (10.52/5.39)	72.11	38.83	33.28	0.30
Scenario	1.34*	80.07*	10.25* (10.17*/5.31*)	69.82*	35.68*	34.13*	0.22
Tyrrhenian							
Historical	2.95	76.93	8.93 (11.22/5.36)	67.99	29.04	38.95	0.42
Scenario	2.26*	72.36*	8.06* (11.22*/5.55*)	64.30*	26.25*	38.05*	0.47
Adriatic							
Historical	3.40	84.36	13.28 (13.39/6.66)	71.09	35.05	36.04	0.66
Scenario	2.88*	80.15*	12.07* (12.52*/6.24*)	68.08*	33.24*	34.83*	0.88
Ionian							
Historical	3.94	73.41	6.98 (10.23/3.68)	66.43	23.29	43.14	0.85
Scenario	3.00*	68.85*	6.59* (10.35*/3.99*)	62.26*	22.57*	39.68*	1.05
Central							
Historical	0.55	90.82	13.11 (17.08/9.46)	77.71	18.01	59.70	0.95
Scenario	0.43*	92.88*	11.42* (16.93*/9.24*)	81.46*	17.27*	64.16*	0.98
Aegean							
Historical	2.51	85.64	10.41 (16.28/9.54)	75.23	26.99	48.24	3.61
Scenario	2.07	83.30*	10.49 (15.96*/9.60*)	72.80*	28.43	44.37*	4.08
North Levantine							
Historical	3.81	84.99	8.86 (13.25/5.05)	76.13	19.20	56.93	2.55
Scenario	3.18*	85.78	8.47* (13.52/5.23*)	77.31	20.96	56.35	3.24
South Levantine							
Historical	0.88	90.92	8.41 (16.07/6.99)	82.51	19.21	63.32	1.43
Scenario	0.85	91.85	7.17 (15.82/6.61)	84.68	19.38	65.29	1.61
Black Sea							
Historical	1.87	98.67	23.15 (9.73/14.91)	75.52	43.14	32.38	13.85
Scenario	1.83	97.98	22.79 (8.96/14.16)	75.19	45.26	29.93	14.17
Mediterranean Catchment							
Historical	**2.41**	**80.97**	**10.27 (12.24/6.20)**	**70.69**	**29.84**	**40.86**	**1.11**
Scenario	**1.96***	**78.39**	**9.32 (11.97/6.01)**	**69.07**	**28.14**	**40.92**	**1.29**

Table 4.6: Same as Table 4.5 for summer

	Prec	**Evap**	**Land (MCRR/RR)**	**Sea**	**Atlantic**	**Medit**	**Black Sea**
Alboran							
Historical	0.28	73.23	33.48 (19.60/12.98)	39.75	20.73	18.98	0.04
Scenario	0.17*	71.32*	28.75* (18.19*/12.71*)	42.57*	22.69*	19.82*	0.07*
North West							
Historical	1.17	77.75	48.08 (26.40/21.44)	29.67	21.18	8.48	0.04
Scenario	0.96*	74.85*	45.93* (24.52*/19.38*)	28.92*	20.54*	8.39*	0.02*
South West							
Historical	0.27	71.60	33.89 (21.23/11.84)	37.70	15.94	21.76	0.04
Scenario	0.18*	69.29*	29.59* (18.41*/10.00*)	39.71*	18.06	21.71*	0.06
Tyrrhenian							
Historical	0.33	83.42	39.95 (27.47/16.97)	43.47	16.51	26.98	0.03
Scenario	0.28	80.17	38.91 (25.63*/15.13*)	41.26	15.95	25.35	0.08
Adriatic							
Historical	1.34	89.63	64.83 (37.53/26.74)	24.79	13.22	11.57	0.10
Scenario	1.13*	88.97*	65.67* (36.66*/26.61*)	23.30*	12.38*	10.92*	0.12
Ionian							
Historical	0.25	86.56	46.29 (32.77/18.08)	40.27	15.21	25.01	0.17
Scenario	0.20	83.20*	48.24 (32.32*/17.51*)	34.97*	14.21*	20.76*	0.55
Central							
Historical	0.04	86.80	30.62 (26.12/15.17)	56.18	12.92	43.26	0.56
Scenario	0.03	93.01	30.88 (25.00/15.07*)	62.13	13.97	48.16	0.37
Aegean							
Historical	0.39	95.29	69.33 (38.35/29.35)	25.96	13.13	12.83	1.84
Scenario	0.31*	93.18*	67.75* (34.33*/26.71*)	25.42*	13.61	11.81*	2.46
North Levantine							
Historical	0.32	94.08	61.41 (35.85/23.33)	32.67	11.63	21.03	1.76
Scenario	0.18*	95.49*	57.85* (38.81*/28.06*)	37.64*	13.29*	24.35*	1.92*
South Levantine							
Historical	0.03	98.98	22.37 (42.71/35.59)	76.61	26.78	49.83	0.00
Scenario	0.03*	100.00*	20.73* (43.50*/38.21*)	79.27*	27.64*	51.63	0.00
Black Sea							
Historical	1.55	94.00	80.96 (7.97/49.23)	13.04	9.90	3.14	2.71
Scenario	1.42	93.13*	80.50 (6.92*/50.13)	12.63	10.29	2.34*	3.02
Mediterranean Catchment							
Historical	**0.44**	**85.73**	**45.03 (30.80/21.15)**	**40.71**	**16.73**	**23.97**	**0.46**
Scenario	**0.35***	**84.95**	**43.43 (29.74/20.94)**	**41.52**	**17.23**	**24.29**	**0.56**

are in agreement with the findings by other authors (Mariotti et al. 2008; Sanchez-Gomez et al. 2009).

For both, the ARCM and the RCSM experiment, approximately 53% in winter and 54% in summer of the water is recycled in the Mediterranean hydrological cycle, with a difference of -0.21% in winter and -0.74% in summer in the future climate projection.

4.5 Discussion and conclusions

The water transport in the Mediterranean region is investigated for present and future climate conditions. A Lagrangian based method to calculate backward trajectories of air parcels is applied to find the moisture sources for precipitation over land inside the Mediterranean catchment. The considered data are high-resolution datasets (0.22° x 0.22°) from an atmosphere stand-alone regional climate model (ARCM) and a coupled atmosphere-ocean regional climate model (RCSM). The atmospheric component of the model consists of the regional climate model REMO, while the ocean is a regional version of the global ocean model MPI-OM.

The simulated precipitation in both versions of the regional model is well represented regarding temporal and spatial distributions. A larger amplitude in the yearly cycle is simulated for the coupled version where the interactive SSTs change the evaporation uptake of the atmosphere. For the future climate projection, a decrease in precipitation is observed. This signal is stronger for the RCSM version compared to the global climate model ECHAM5/MPI-OM.

The divergence and convergence of the water vapor over the Mediterranean region is marked by the geography and seasonal meteorological conditions. Over the Mediterranean Sea, all year long, divergence of the water mass is found. Its time and space variability depends on the seasonal temperature of the water and the corresponding wind circulation. The largest divergence is observed over the eastern Mediterranean. Over land, mainly divergence takes place in summer, with some specific regions of convergence as exceptions. In winter, the moisture converges over all land areas with specific strong convergence areas due to orographic precipitation. These features are not observed in the low resolution ERA40 reanalysis dataset.

The permanent characteristic of water vapor divergence over the Mediterranean Sea makes it a moisture provider for the entire region. Nevertheless, the marine evaporation produced over the Mediterranean Sea does not contribute to the land precipitation in the same magnitude over all year. In summer, when its minimum is reached, land evaporation replaces the moisture supply from the sea as a main source. The evaporation over the basin is not spatially homogeneous either, but it is related to the SST distribution and wind patterns. The influence of the Mediterranean Sea is larger in the eastern regions.

In the future climate simulation for the Mediterranean region the amount of moisture uptake

over land is reduced, and slightly larger evaporation takes place over the Mediterranean and Black seas. This second effect, however, is not strong enough to produce a increase in the total evaporation. The result suggests an increase in water vapor transport into the Mediterranean region and a larger contribution from the Atlantic.

About 53% of the water involved in the Mediterranean hydrological cycle is evaporated over the Mediterranean region itself (catchment + basin). This percentage remains at the same value with almost no variation independently of the exchanged roles of the terrestrial and marine evaporation in summer and winter. A slightly decrease in the percentage of the recirculated water of -0.21% in winter and -0.74% in summer is detected in the scenario simulation.

Since uncertainties are implicit in the assumptions entering the water transport tracking method, an extension of the present work to other water transport tracking algorithms and an ensemble of climate model simulations is planned for the future. This hopefully will increase the confidence in the results presented here and lead to a more detailed understanding of the Mediterranean hydrological cycle.

Chapter 5

Does the Mediterranean Sea influence the atmospheric dynamics of the European summer climate? The anomalous summer 2003 as a testbed[1]

The European summer 2003 marks a notable anomaly and presents a rare opportunity to investigate dynamical interactions in the otherwise variable European climate. Not only air temperature and the hydrological cycle over the continent showed distinct signals, also the Mediterranean sea surface temperature (SST) was exceptionally warm during the period.

The traditional view on the role of the Mediterranean Sea in the climate system highlights the influence of the large-scale atmospheric circulation on the Mediterranean Sea. The question whether the Mediterranean Sea acts back on the atmospheric dynamics in the region is of central importance.

The case of the extremely anomalous summer 2003 allows for investigating the issue under realistic boundary conditions. In the present study we take advantage of a newly developed regional coupled atmosphere-ocean model consisting of the regional climate model REMO and a regional version of the global ocean model MPI-OM. This allows for a controlled experimental setup that simulates the summer 2003 realistically.

Experiments with prescribed historical versus climatological SST in the region suggest that the atmospheric circulation is not strongly sensitive to the state of the Mediterranean Sea, but its influence on the moisture balance and its role in the regional hydrological cycle is substantial. Warmer Mediterranean SSTs lead to enhanced evaporation and moisture transport in the atmosphere.

[1] Submitted to *Climate Dynamics*. Tomassini, L. and Elizalde, A.

Results of regional coupled simulations with different ocean initial conditions imply that due to the strong stratification of the surface waters in summer the response time of the upper layers of the Mediterranean Sea to atmospheric forcing is rather short. We conclude that the role of the Mediterranean Sea in the European summer climate is mostly passive. In winter, however, since the upper layers of the Mediterranean Sea are well mixed, the memory of the Mediterranean SSTs stretches over longer timescales which implies a potential for actively governing regional climate characteristics to some extent.

5.1 Introduction

The atmospheric dynamics over Europe is characterized by high variability on a wide range of timescales. It is therefore difficult to identify signals in order to quantify specific interactions of different components of the regional climate system. The summer of 2003 represents such a signal and provides the rare opportunity to investigate the interrelation of certain variables under anomalous conditions.

It is not fully understood why the large-scale circulation during summer 2003 showed the observed structure (Black et al. (2004)). The anomalous anticyclonic conditions over Europe were caused by a northward displacement of the subtropical Azores anticyclone which extended from the mid-Atlantic through to eastern Europe. At the same time, the Icelandic low was further south than normal. The streamfunction anomalies in the European Centre for Medium-Range Forecast (ECMWF) analysis show an alternating sign from South America to Europe and beyond suggesting a Rossby-wave signal propagating from tropical America. The intensification of the Azores anticyclone was accompanied by a regional northward shift and intensification in the west African ITCZ and a southward shift in the summer extratropical storm track (Black et al. (2004), Cassou and Terray (2005))).

Cassou and Terray (2005) describe two geopotential anomaly patterns which are responsible for hot conditions in Europe and show that they occur with higher probability if the outgoing longwave radiation anomalies that were present in summer 2003 are imposed in the tropical Atlantic. A similar configuration consisting in a southward shift of the Scandinavian jet and a northward displacement of the Mediterranean jet were described by Baldi et al. (2006) as being responsible for high temperatures over the Mediterranean basin. A location of the Mediterranean jet over the Alps causes anticyclonic vorticity south of the mountain range forcing strong subsidence and adiabatic warming of the troposphere over the Mediterranean.

A comparable pattern results from canonical correlation analysis (CCA) of Mediterranean summer air temperature and other large-scale variables (Xoplaki et al. (2003)). The positive phase of the first mode shows positive geopotential height anomalies over the European continent

with centre over the Alps and northern Italy, and negative anomalies south of Iceland. It is responsible for anticyclonic conditions, subsidence and stability related to warm Mediterranean summers. The second CCA pattern of sea level pressure in the study by Della-Marta et al. (2007) is similar to the first CCA stationary wave pattern of Xoplaki et al. (2003) and shown to be associated with the situation in summer 2003. However, as discussed in Della-Marta et al. (2007), sea level pressure variability explains only about 30% of heat wave variability for the period 1880 to 2003.

Neither ENSO nor the Indian dipole mode were abnormal in Summer 2003. Instead, from mid-July to early August the European anomaly can be related to the summer northern annular mode NAM (Ogi et al. (2004)). However, in May and June the summer NAM index stayed close to its climatological mean. In general, from a global perspective, Mediterranean summer variability is described to a large degree be the so-called East-Atlantic pattern (Lionello et al. (2006a), Dünkeloh and Jacobeit (2003), NOAA-CPC (2003)) which can be considered as a southward shifted NAO pattern and incorporates a strong subtropical link. The positive pressure anomaly over central and southern Europe representative for this pattern agrees with the situation in summer 2003.

This suggests that although the situation of summer 2003 matches certain features of European atmospheric summer variability, the dimension of the event was unusual. One could hypothesize that a possible reason for the extent of the extraordinary conditions consisted in an amplification by an anomalous state of the surrounding oceans. The Mediterranean sea surface temperatures built up quickly at the end of April and beginning of May 2003 (Grazzini and Viterbo (2003)). They grew further in May and rapidly became very large in the first week of June. The area covered by the anomaly expanded and at the end of July effected almost the whole basin with the Aegean Sea as an exception. Subsequently Mediterranean sea surface temperatures persistently exceeded climatological values by 2 to 3 $^{\circ}$C.

Although it is clear that atmospheric dynamical conditions played an important role in the development of the European summer of 2003, the question arises in what way and to what extent the anomalous Mediterranean SSTs acted back on the atmosphere. The fact that the event had a large-scale characteristics that was not confined to the Mediterranean Sea lead Xoplaki et al. (2003) to the conclusion that the Mediterranean Sea was a passive element in the system. Similarly, since in contrast to the banded pattern of Atlantic radiative flux anomalies, the Mediterranean SST pattern amplified most rapidly between May and June and hardly changed between July and August, Black et al. (2004) suggested that SST anomalies responded passively to radiative flux anomalies.

On the other hand, Black and Sutton (2007) show that an ensemble of global atmosphere model simulations forced by the observed summer 2003 sea surface temperatures reproduces the atmospheric conditions in the mean, although the anomaly over Europe is considerably weaker in their setup. An experiment with Mediterranean sea surface temperatures set to climatolog-

ical values exhibits a significant influence of Mediterranean SSTs on the atmosphere when compared to the historical control integration for summer 2003. Similarly, Feudale and Shukla (2007) achieved to simulate the summer 2003 heat wave to a certain extent by forcing a global atmospheric general circulation model with observed sea surface temperatures. An experiment with observed SST anomalies over the Mediterranean Sea only reproduces the upper level anticyclone over central Europe, even though in a weaker form. The resulting temperature anomalies showed about half of the amplitude compared to the experiment with global SST anomalies prescribed. Also Li (2006) reports significant effects of Mediterranean sea surface changes on the global atmospheric circulation. The described experiments are however confined to the month of January.

Somewhat contrary to these results, Jung et al. (2006) concluded in a study based on comparable modelling experiments that the Mediterranean plays a minor role, if any, in maintaining the anomalous atmospheric circulation as observed in the summer of 2003. In contrast, the perturbations of the humidity fields caused by the Mediterranean SST anomalies proved to be significant.

But even if the European summer climate is sensitive to Mediterranean Sea surface temperatures, this does not answer the question whether the role of the Mediterranean Sea is active or passive. The high Mediterranean SSTs could have been merely a consequence of the warm temperature of the atmosphere. The question whether the Mediterranean Sea actively influences the European summer climate and in what ways can only be answered using a coupled atmosphere-ocean model. The issue is intimately connected with the question about the memory in the upper layers of the Mediterranean Sea. If the surface waters of the Mediterranean Sea do not remember their past state, then this implies that they are driven by the atmosphere.

The aim of the present work is not to give an explanation of the anomalous atmospheric conditions of summer 2003, but to explore the role of the Mediterranean Sea in the European summer climate. Employing a regional model allows for a controlled experimental setup that focuses on regional processes and guarantees, due to the realistic boundary forcing, that the characteristics of the summer 2003 are reproduced realistically. Various sensitivity experiments are performed within this framework using an atmosphere-only and a newly developed regional coupled ocean-atmosphere model for the Mediterranean area.

The paper is structured as follows. Section 2 gives an overview over the climate model and the performed experiments. In Section 3 the climate model is validated. Not the climate (which is tuneable to some degree), but the simulated anomalies are compared to observations. Moreover the result of a canonical covariance analysis is presented which motivates the following modelling studies. The first part of Section 4 is devoted to the question whether the European summer climate is sensitive to Mediterranean SSTs. This is investigated using a regional atmospheric model and prescribed SSTs. The second part of the section treats the central question of this study. The role and the memory of the Mediterranean Sea is examined using the regional

coupled atmosphere-ocean model. A section containing the main conclusions completes the paper.

5.2 Climate model and experiments

5.2.1 Climate model

For the present study we use a recently developed regional coupled atmosphere-ocean climate model consisting of the regional atmosphere model REMO, a regional version of the Max Planck Institute for Meteorology global ocean model MPI-OM, and the hydrological discharge (HD) model. The OASIS3 software is used to couple the system. In the standard coupling configuration REMO calculates fluxes of heat, momentum and freshwater separately for the sea ice covered and ice free fractions of a grid box and receives in turn SST and sea ice properties from the ocean model. The coupling is updated every 6 hours for all variables except for the freshwater discharge that is updated daily. Figure 5.1 shows a schematic of the coupled model.

REMO (Jacob et al. 2001) is a three-dimensional, meso-scale atmospheric circulation model which solves the discretized primitive equations of atmospheric motion. It is based on the Europa-Modell of the German Weather service (Majewski, 1991) and the physical parameterizations are taken from the global climate model ECHAM-4. REMO is a hydrostatic model and can be used for a horizontal resolution up to 10km. In the present study the model is run at a resolution of 25 km. In the vertical, 31 levels are used for the experiments. As a limited area model, REMO needs lateral boundary forcing data like temperature, wind, surface pressure and moisture. At the surface boundary, the treatment of soil hydrology is based on a simple bucket scheme, whereas, over the sea, REMO uses the sea surface temperature calculated on-line by the oceanic component for the Mediterranean Sea and Black Sea and prescribed values in other areas.

The HD (Hydrological Discharge) Model is a routing scheme, which has been developed at the Max Planck Institute for Meteorology by Hagemann and Duemenil (1998). It accounts for the lateral waterflow on the land surface in global climate model applications. It is part of the coupled atmosphere-ocean model, providing the ocean component with freshwater input from the surface river system. The model describes the translation and retention of the lateral discharge within the river system as a function of spatially distributed land surface characteristics.

The oceanic component of the coupled model consists in a regional version of the Max Planck Institute Ocean Model (Mars-Land et. al, 2002), which is a primitive equation model. It has a free surface and uses a mass flux boundary condition for salinity. A simple bottom boundary layer scheme is included as well as the standard set of subgrid-scale parameterizations. The horizontal resolution is about 10 km. 30 vertical levels are used. The original global model was

modified and limited to the Mediterranean Sea area. The domain covers the Mediterranean and Black Seas. The communication with the global ocean is performed by nesting the Mediterranean Sea model in the Atlantic by means of an Atlantic box.

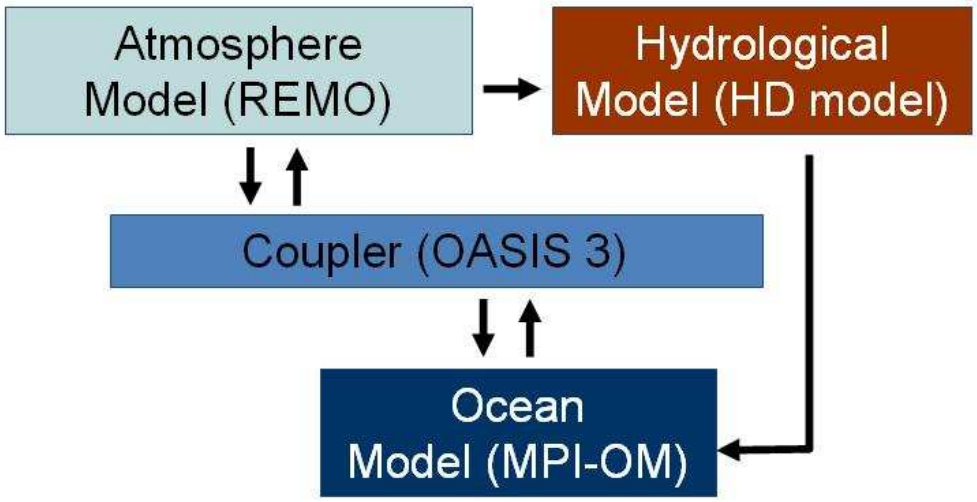

Figure 5.1: Schematic of the regional coupled atmosphere-ocean model including a hydrological discharge model.

5.2.2 Experiments

All the simulations discussed in this study are performed with limited area models. The model domain is evident from the subsequent figures. The atmospheric model REMO is forced at the lateral boundary by ERA40 reanalysis (Uppala et al. (2005)) for the simulation period January 1958 to August 2002, and ERA Interim reanalysis (Simmons et al. (2007)) from September 2002 to December 2003. Accordingly, the sea surface temperatures are taken from the respective reanalysis in the uncoupled, atmosphere-only simulations. For the coupled runs, the Atlantic sea surface temperatures are also prescribed and derived from the reanalysis. Using reanalysis data as forcing has the advantage that the climate model is able to realistically simulate the historic evolution of the climate. Moreover, the fact that the boundary conditions are fixed allows for a controlled experimental setup and a focus on regional climate interactions.

Simulations for the period 1958 to 2003 are performed with the uncoupled atmospheric model as well as with the coupled atmosphere-ocean model. In addition, several sensitivity experiments are conducted in order to assess the influence of Mediterranean sea surface temperatures in the uncoupled as well as the coupled simulations. The experiments are summarized in Table 5.1. In the uncoupled case, a simulation (UNC-CLISST) was performed for 2003 with fixed climatological SSTs for the Mediterranean Sea. The SST climatology was derived from the reanalysis for the period 1958 to 2000. To mimic this setup in the situation of the coupled

Table 5.1: Simulations that were performed for this study.

Acronym	Time period	Description
UNC-CLIM	1958-2003	uncoupled model, prescribed historical SSTs
UNC-CLIMSST	2003	uncoupled model, climatological Mediterranean SSTs
CPL-CLIM	1958-2003	coupled model, lateral ERA40 forcing
CPL-INICOLD	2003	coupled model, cold Mediterranean Sea initialisation
CPL-INIWARM	2003	coupled model, warm Mediterranean Sea initialisation

model, two runs are performed with different Mediterranean Sea initial conditions. Both runs are initialized in January 2003. One simulations is initialized with a relatively cold state of the Mediterranean Sea taken from January 1 of 1978 (CPL-INICOLD), the other run is initialized with a relatively warm state of the Mediterranean Sea taken from January 1 of 1989 (CPL-INIWARM).

5.3 Observations and modelling of summer 2003

Pressure anomalies in summer 2003 were barotropic in nature. Figure 5.2 shows the geopotential height anomalies for 500 hPa and 850 hPa as present in a 50km resolution simulation with the regional climate model REMO over the European domain driven by ERA 40 reanalysis and ECMWF operational analysis. The geopotential height simulated by the model essentially reproduces the reanalysis and analysis and can therefore be considered to be very close to observations.

In June high pressure was located over Central Europe and an intensification of the Iceland low can be observed. It was situated west of the UK in June and July and further southwest in August. During June and July, extratropical cyclones tracked further south than average before deflecting polewards around the anticyclonic ridge over central Europe (Black et al. (2004)). July shows persistent temperature anomalies, the pressure distribution was rather slack over central Europe, associated with weak synoptic forcing, with a still somewhat strengthened low over the northern Atlantic and a weak high pressure anomaly over the Mediterranean Sea. In August an amplification by Rossby waves reinforced the pre-existing anticyclone over Europe (Grazzini et al. (2003)) and resulted in a blocking-like situation. A weak low-pressure anomaly over northeastern Europe favoured the transport of moist air towards the east of the continent.

These pressure anomalies are reflected in the anomalies for temperature and precipitation (Figure 5.3). For daily mean temperature, precipitation and sea level pressure version 4 of the data compiled by Haylock et al. (2008) are used in the following. Anomalies are calculated with respect to the reference period 1958 to 2000. In June Central Europe experienced strong

positive temperature anomalies, while colder air was advected to the northeastern parts of the continent. In July positive anomalies covered most of western Europe with the exception of Portugal. Strongest anomalies occur around the Mediterranean basin and in northern Scandinavia. In August the positive temperature anomalies again dominated over central Europe including Italy.

The sign of the precipitation anomalies in summer 2003 was mostly negative. In June central and eastern Europe receive less than average precipitation, with the exception of northwestern France and Greece. In July the rainfall signal is weaker. On the western coasts of France and the Iberian Peninsula the rainfall anomaly is slightly positive. Dry conditions prevail mainly in southern France and Italy, and to a somewhat larger extent in Scandinavia and northeastern Europe, the centre of the high-pressure system. The anomaly pattern in August again resembles the situation in June, although in August the negative anomaly does not affect the Iberian Peninsula and is stronger over the British Islands. In the northeast of the continent the low-pressure anomaly causes above average precipitation.

In Figure 5.4 a comparison of the temperature anomalies simulated by the regional uncoupled model (top row) and the regional coupled model (bottom row) to the observed anomalies are displayed. The simulated pattern agree well with observations. Also details like the slight negative anomaly over Portugal in July are reproduced. The general positive anomalies tend to be somewhat underestimated by the models, especially in June and August. In July there are regions in central and eastern areas of the continent with stronger than observed positive anomalies. Especially in June the coupled simulation shows some distinct improvements over the uncoupled run.

The SST anomaly in the coupled model is somewhat smaller than in the uncoupled model which uses prescribed SSTs from ERA-40 (Uppala et al. (2005)) and Era-Interim (Simmons et al. (2007)). The differences in the anomaly are between 0 and 1.5 degrees Celsius and occur most pronouncedly in June and close to coast lines. Several issues have to be taken into account with this regard. One is the fact that SST in the coupled model is defined as a mean over the first, about 12m thick layer, while in the reanalysis it is supposed to be the mean from about 0 to 0.5 meter depth (Reynolds et al. (2002)). Another point is the interpolation error due to the coarse resolution of the reanalysis, especially close to the coast. Indeed, the higher resolution is one of the motivations for developing regional coupled models. Also the distribution of incoming solar radiation over the upper layers of the ocean in the coupled model is affected by uncertainty, but a detailed investigation of this question is beyond the scope of the present work. Moreover, the realistic simulation of evaporation in the coupled model (see below) indicates that atmosphere-ocean interactions are well represented in the coupled model.

Also for precipitation the coupled model generally outperforms the uncoupled setup (Figure 5.5). The positive bias with respect to the observations is reduced in some regions like southern France, the Iberian Peninsula, and parts of Italy. This could be related to the fact that the

SSTs in the coupled model exhibit a cold bias. Consequently absolute evaporation and ocean-atmosphere moisture fluxes are reduced. But the differences between the coupled and the uncoupled run do not form a particularly systematic picture. Both simulations reproduce the rainfall deficit in the Mediterranean region during summer 2003. Also specific features like the slight positive anomalies in northwestern France agree with the observations.

There are little differences in simulated sea level pressure anomalies between the coupled and the uncoupled model (Figure 5.6). Generally the model overestimates sea level pressure over the land masses of Central Europe. This is true for all months of summer 2003 indicating that the bias is mostly independent of the temporal development of the event and not related to Mediterranean SSTs. Also evaporation over the Mediterranean Sea is well simulated (Figure 5.7) by the climate models. Here we use OAFlux data (Yu et al. (2008)) in a one degree resolution for comparison. Due to the coarser grid cells of the observations that are mapped to the finer model grid interpolation errors occur mostly along the coast lines (but of course to a certain extent also in the interior of the Mediterranean Sea). Negative biases tend to be somewhat more pronounced in the coupled model compared to the simulation with prescribed SSTs, especially in July in the Western Mediterranean. Since surface winds are very similar in the coupled compared to the uncoupled simulation (and agree well with OAFlux observations), the differences can be attributed mainly to the weaker anomaly in sea surface temperatures simulated by the coupled regional model.

In order to investigate the relation between temperature and precipitation in Europe on one side, and Mediterranean SSTs on the other side, a canonical covariance analysis (Wilks (2006)) was performed on the observations. Figure 5.8 shows the normalized first canonical patterns for the analysis of observed 2-meter temperature and Mediterranean SSTs (top row), and the analysis of observed precipitation and the same Mediterranean SST fields (bottom row). The explained variance of the temperature pattern is 59.5 %, for the corresponding SST pattern 31.3 %, and for the precipitation pattern 52.8 %.

It is striking how closely the first canonical patterns for temperature, precipitation, and also Mediterranean SSTs resemble the anomalies in summer 2003. Both SST patterns, the one from the analysis including the observed temperature, and the one based on the analysis with observed precipitation, are very similar and very alike to the anomalies in summer 2003, with larger positive values in the western part of the basin and especially the Gulf of Lion and the Adriatic Sea. The temperature anomalies in summer 2003 extended somewhat more into the European continent compared to the canonical pattern. For precipitation, the general negative signal in the observations agrees very well with the first pattern from the canonical covariance analysis, and even the slight positive anomalies over northwestern France, Greece, and Sicily match the conditions during summer 2003. Also the weakening of the signal over the Iberian Peninsula is present in the canonical pattern as well as in the observed anomalies in summer 2003.

Of course this statistical analysis does not imply that Mediterranean SST anomalies influence temperature and precipitation over Europe. The question arises whether the Mediterranean Sea responds passively to the atmospheric dynamics that governs temperature and precipitation over the continent, or whether is plays an active role and impacts the summer climate in the Mediterranean region and north of the Alps. This subject is discussed in the following section by means of different modeling experiments.

5.4 Results of the sensitivity experiments

In this section the results of two sensitivity experiments are presented. The first discusses the role of the prescribed SSTs in the uncoupled atmospheric model, the second investigates the sensitivity of the climate to initial ocean conditions in the coupled regional model.

5.4.1 Uncoupled SST experiment

In the experiment UNC-CLIMSST (see Table 5.1) the atmospheric boundary forcing is the one from the year 2003, as derived from the ERA-Interim reanalysis, but the prescribed sea surface temperatures in the domain are defined, for every 6-hourly coupling time step, as climatological means over the period 1958 to 2002. This simulation is compared to the uncoupled simulation with the historical 2003 sea surface temperatures as lower boundary conditions, called UNC-CLIM.

Figure 5.9 displays the difference between the two experiments for various quantities. Black dots indicate regions where the differences are larger than one standard deviation of the respective seasonal values over the time period 1958 to 2000 in the uncoupled simulation. The surface temperature reflects the strong SST anomaly of summer 2003 in the Mediterranean Sea and parts of the Atlantic Ocean. Over land, however, temperature is reduced in the historical simulation. The areas of reduced temperature over land match quite consistently with regions of increased precipitation, indicating that it is a cause of evaporative cooling. The rainfall surplus in the run with higher SSTs comes with enhanced evaporation over the ocean and some land areas. This is consistent with a positive signal in vertically integrated water vapor. For vertically integrated cloud liquid water the response is less local. Moisture is partly transported away from the Atlantic and Mediterranean area. The signal in sea level pressure is quite strong and results in a surface heat low over the warmer SSTs and slight high pressure ridges over parts of central and eastern Europe. However, in higher levels of the atmosphere this response of higher pressure over land is not present anymore.

The left panel in the upper row of Figure 5.10 displays the vertical velocity at 500 hPa in the uncoupled simulation with the historical SSTs of the year 2003 (UNC-CLIM). Negative

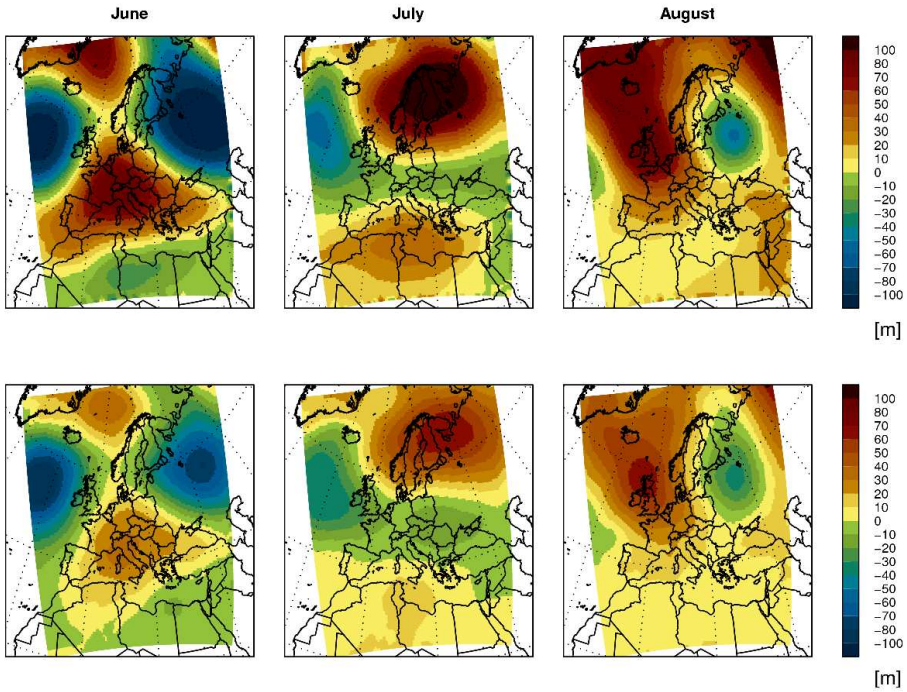

Figure 5.2: Anomalies for geopotential height at 500 hPa (top row) and 850 hPa (bottom row) in summer 2003 compared to the period 1958 to 2000. Shown are the results from a regional climate model simulation driven by ERA40 reanalysis and ECMWF operational analysis.

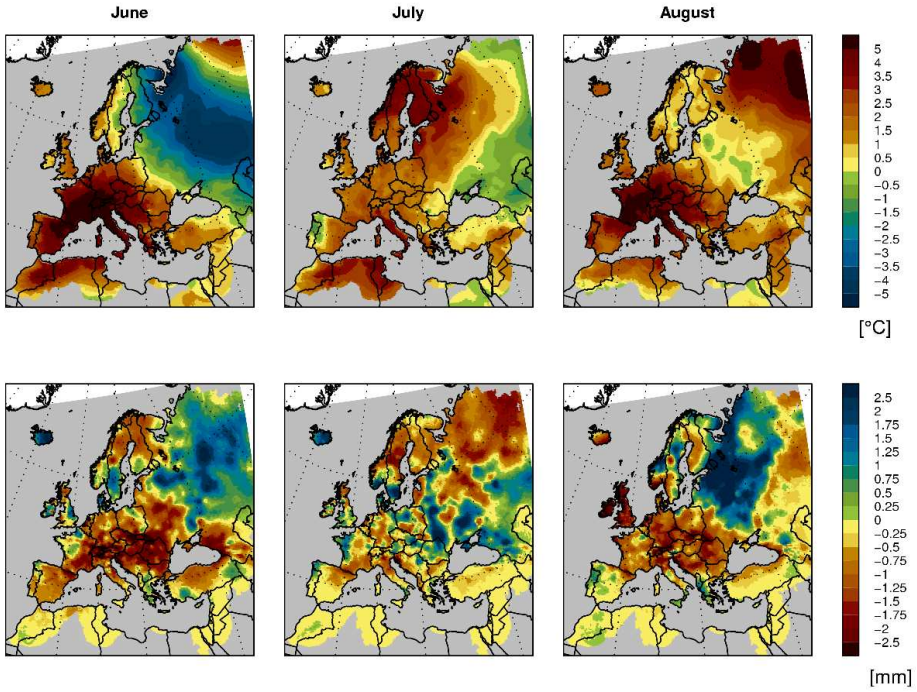

Figure 5.3: Observed anomalies for 2-meter temperature (top row) and precipitation (bottom row) in summer 2003 compared to the period 1958 to 2000.

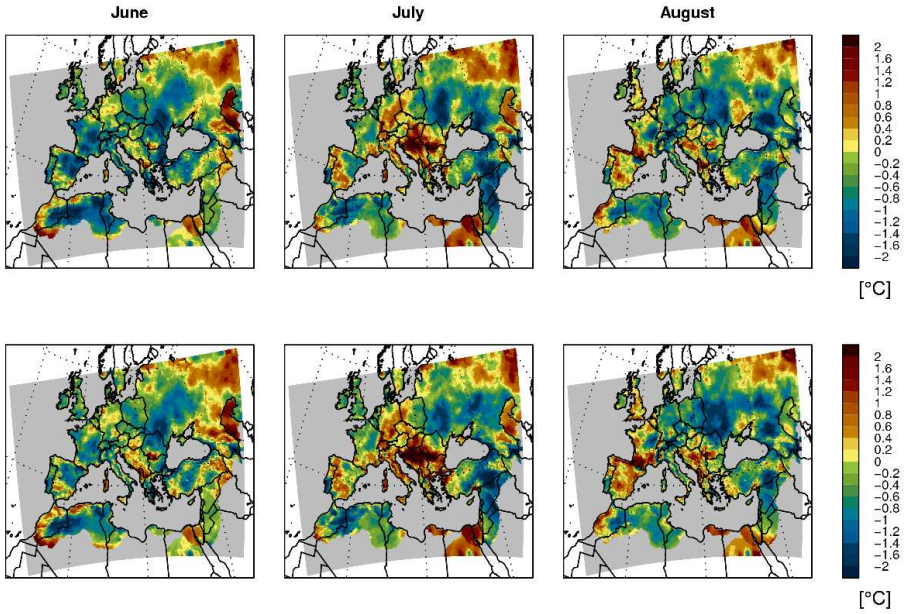

Figure 5.4: The top row shows the difference of the 2003 temperature anomaly in the uncoupled simulation versus the observed anomaly. In the bottom row the difference of the 2003 temperature anomaly in the coupled simulation versus the observed anomaly is displayed.

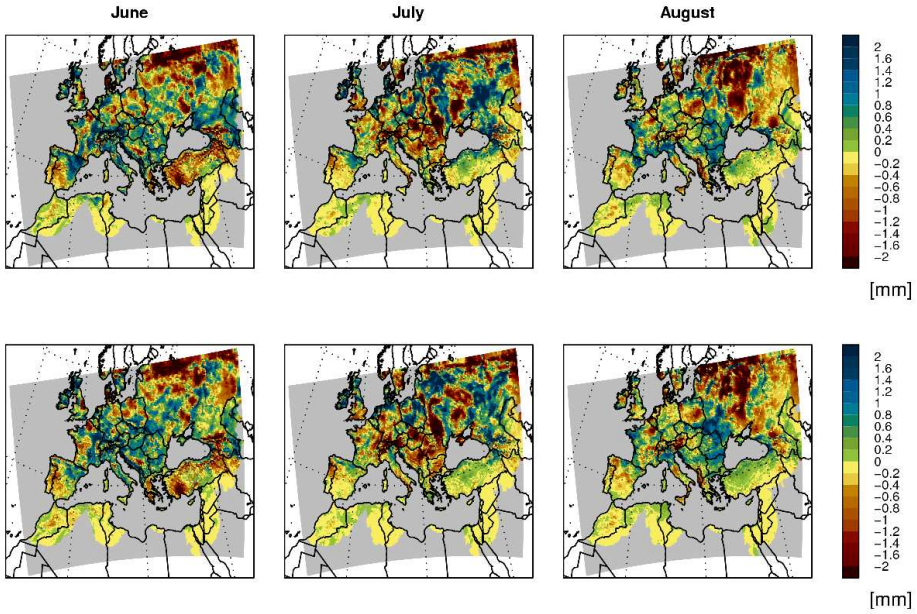

Figure 5.5: The top row shows the difference of the 2003 precipitation anomaly in the uncoupled simulation versus the observed anomaly. In the bottom row the difference of the 2003 precipitation anomaly in the coupled simulation versus the observed anomaly is displayed.

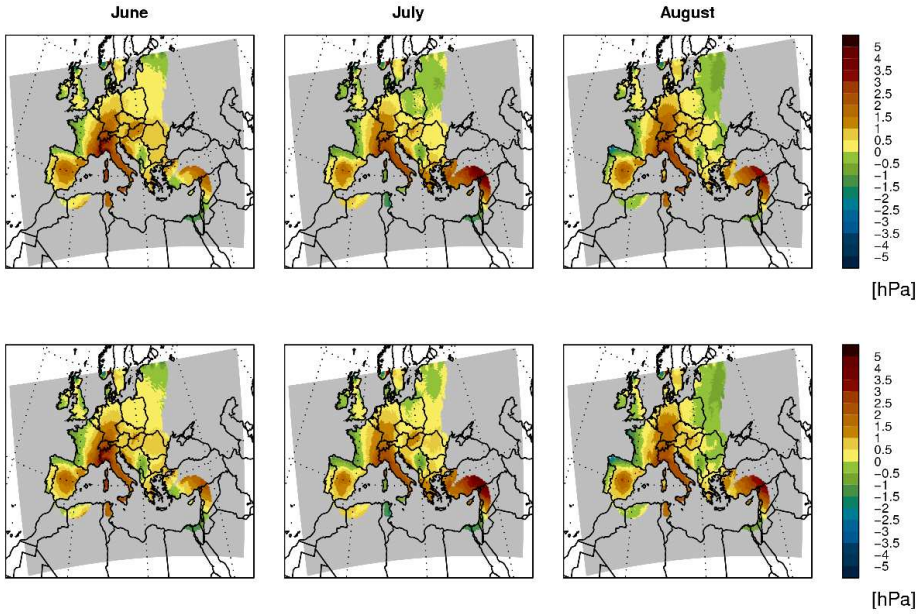

Figure 5.6: The top row shows the difference of the 2003 sea level pressure anomaly in the uncoupled simulation versus the observed anomaly. In the bottom row the difference of the 2003 sea level pressure anomaly in the coupled simulation versus the observed anomaly is displayed.

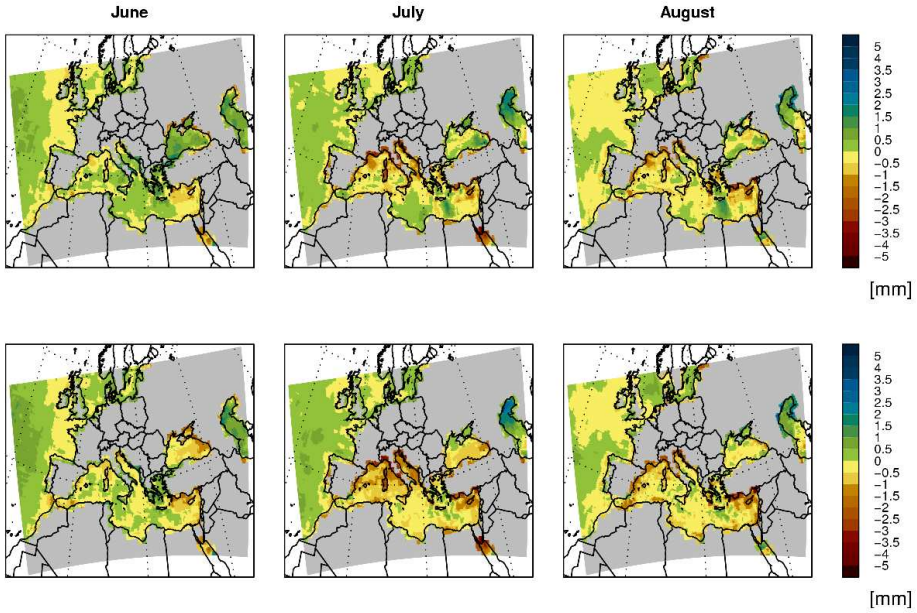

Figure 5.7: The top row shows the difference of the 2003 evaporation anomaly in the uncoupled simulation versus the observed anomaly. In the bottom row the difference of the 2003 evaporation anomaly in the coupled simulation versus the observed anomaly is displayed. Negative biases along the coast line are due to errors in the interpolation from the coarse, one degree observational data set to the 25 km grid of the climate model.

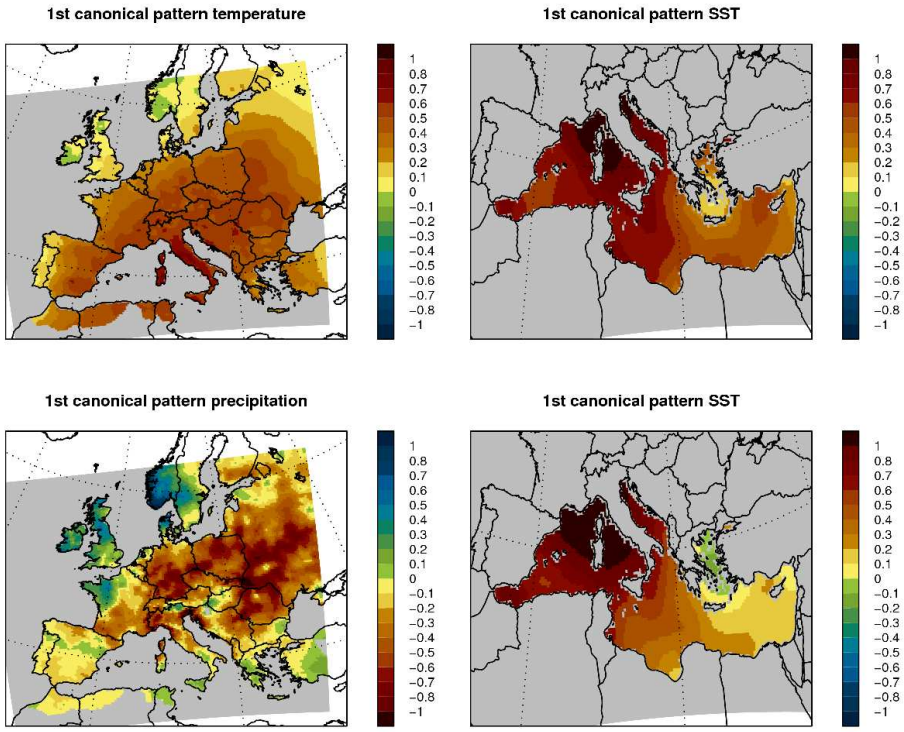

Figure 5.8: Upper row: Normalized first canonical patterns for 2-meter temperature (left) and corresponding Mediterranean SSTs (right). Bottom row: Normalized first canonical patterns for precipitation (left) and corresponding Mediterranean SSTs (right).

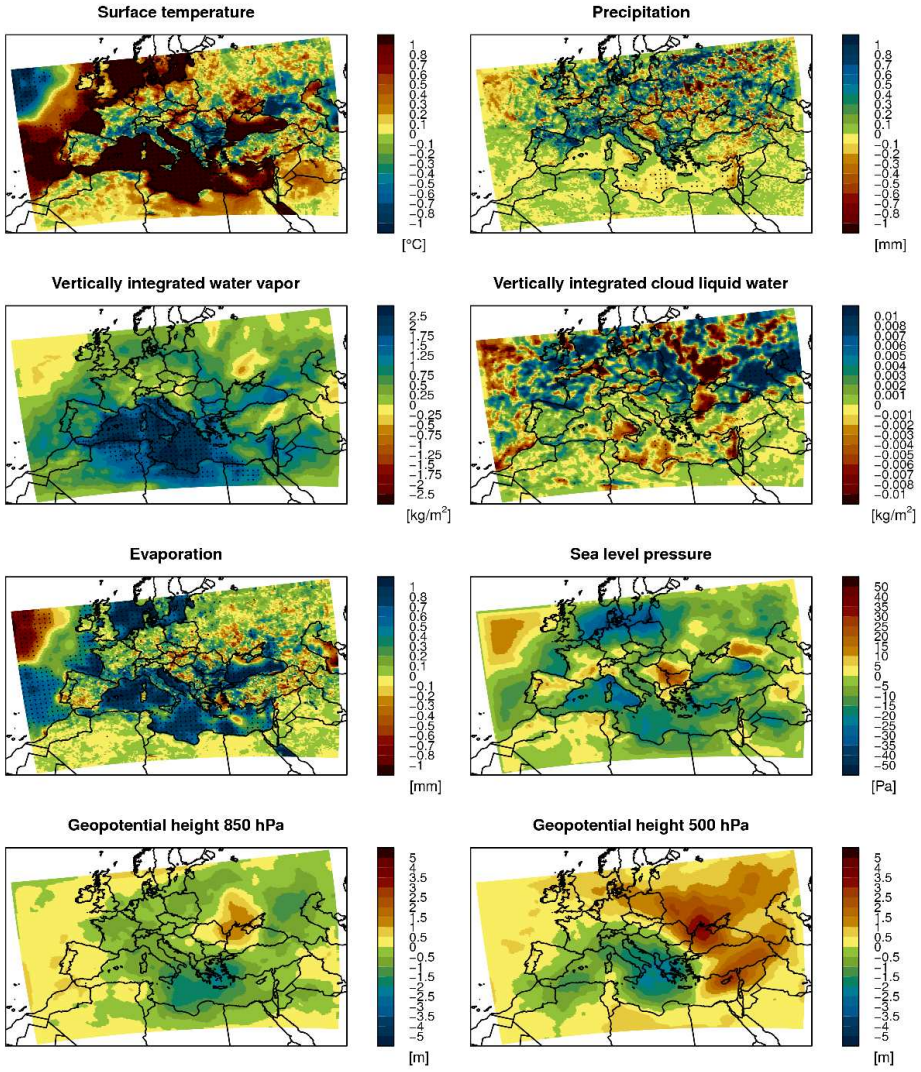

Figure 5.9: Difference between the uncoupled historical run and the uncoupled simulation with climatological SSTs for various quantities. Black dots indicate regions where the differences are larger than one standard deviation of the seasonal values over the time period 1958 to 2000 in the uncoupled simulation.

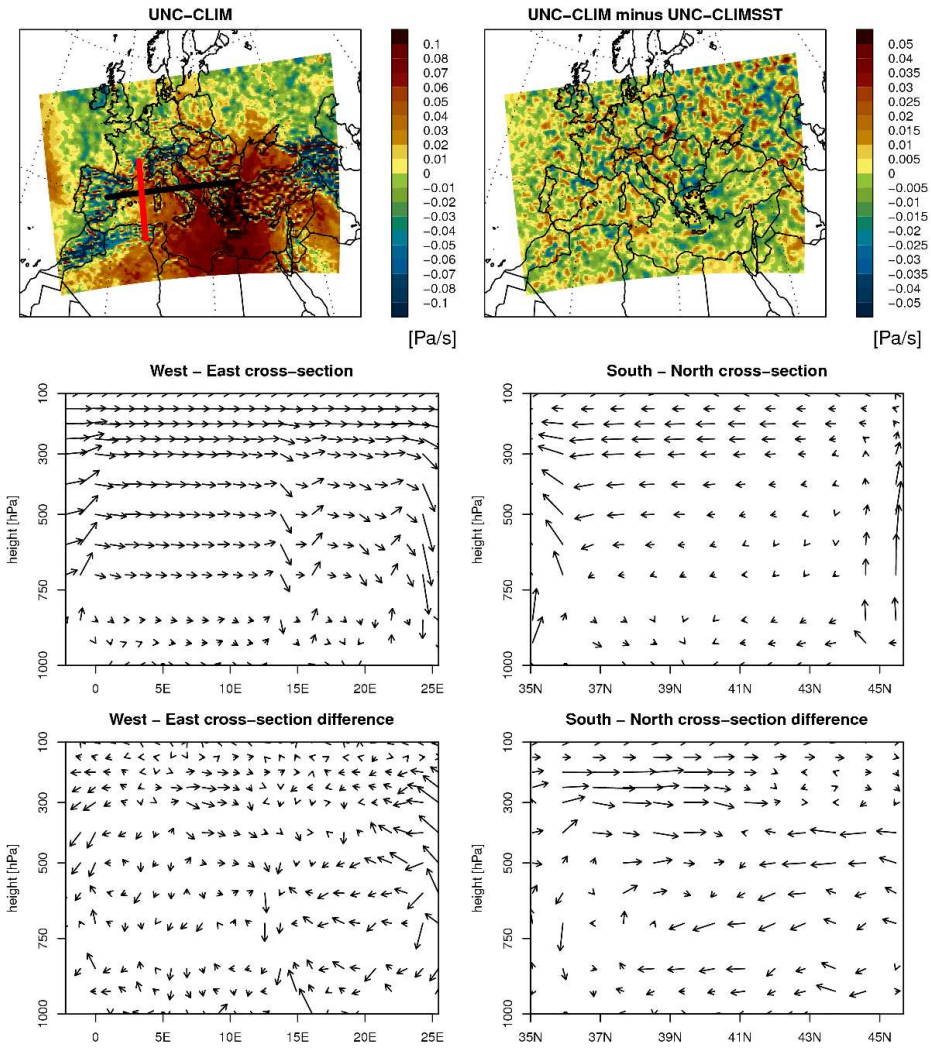

Figure 5.10: Top row left panel: vertical velocity at 500 hPa in the UNC-CLIM simulation. Also indicated are two cross-sections. Top row right panel: difference in vertical velocity at 500hPa between UNC-CLIM and UNC-CLIMSST. Middle row: zonal-vertical wind for the West-East cross-section and meridional-vertical wind for the South-North cross-section in the case of the UNC-CLIM simulation. Bottom row: difference to the UNC-CLIMSST simulation. In the difference plots the arrows are stretched by a factor of 6.

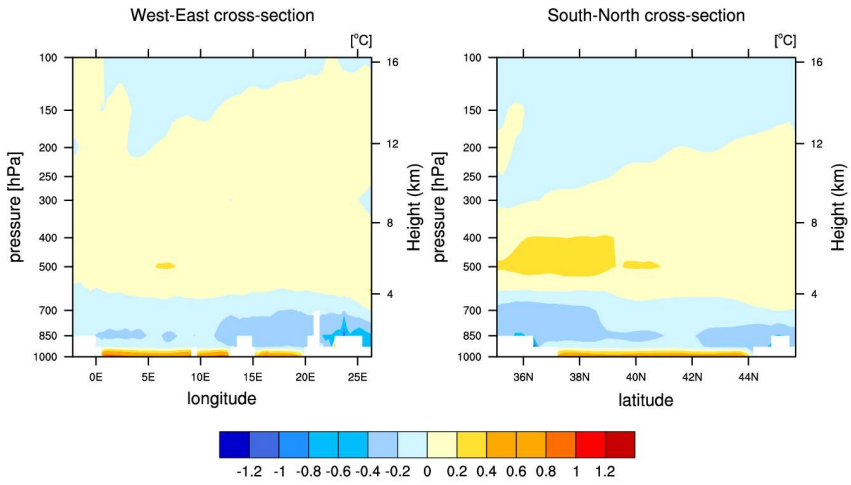

Figure 5.11: Differences in the atmospheric temperature profiles for the West-East cross-section (left panel) and the South-North cross-sections (right panel).

values correspond to upward motion, positive values to downward motion. One can observe a large area of subsidence over the Mediterranean Sea, while over land areas convective activity dominates in many parts. Also indicated in the panel are two cross-sections, one from the South to the North (red line), and one from the West to the East (black line). The right panel shows the difference in vertical wind velocity at 500 hPa between UNC-CLIM and UNC-CLIMSST. No systematic pattern can be identified at this level of the atmosphere.

The panels in the middle row of Figure 5.10 show the zonal-vertical wind for the West-East cross-section, and the meridional-vertical wind for the South-North cross-section in the case of the UNC-CLIM simulation. Convective motion over the Iberian Peninsula was prevalent in summer 2003. At the western flank of Italy subsidence dominates, while over the eastern part of the country the air is rising. In eastern Europe around the Bosporus there is a region of strong subsidence also over land. The mean wind tends to transport moisture from west to east. However, at lower levels, which contain most of the moisture, this mean transport is rather unincisive. Similarly, in the meridional direction, the north to south flow of the air is restricted to higher altitudes of the atmosphere. Over the land areas of northern Africa and southern France convective motion is triggered by heating of the surface.

The difference between UNC-CLIM and UNC-CLIMSST (bottom row of the figure) is rather small in magnitude, mainly restricted to land areas, and does not indicate a consistent change in circulation. The motion of the air over Italy is slightly enhanced in the UNC-CLIM experiment. The subsidence over the eastern land regions covered by the West-East cross-section is somewhat weakened by the colder SSTs in UNC-CLIMSST at lower levels of the atmosphere, and strengthened at higher altitudes. This could be related to the excess of rainfall and the effectively colder surface temperatures in the UNC-CLIM experiment over this areas compared

to UNC-CLIMSST.

The atmospheric temperature profiles for the two cross-sections (Figure 5.11) confirm that the differences in the SSTs induce differences in air temperature mainly in the lowest levels of the atmosphere and mostly over the Mediterranean Sea. This feature will attenuate sea breezes during daytime and intensify land breezes at night. In the level around 800 hPa a slight cooling can be observed which is possibly due to advection of colder air as a compensating motion to the warming of the surface. This is supported by the left panel in the bottom row of Figure 5.10. Another reason for the weak negative signal in temperature is the enhanced evaporation due to increased moisture content of the atmosphere.

The change in the water budget in a column of air can be written as

$$\frac{dW}{dt} = E(t) - P(t) - Div(t), \tag{5.1}$$

where W denotes the vertically integrated water content, E the surface evaporation, P precipitation, and Div the divergence of the moisture flux. Positive values of Div imply that the water column at a specific location acts as a moisture source for surrounding regions. In the upper panel of Figure 5.12 the divergence of the moisture flux is displayed for the UNC-CLIM experiment, the lower panel shows the difference in moisture flux divergence between UNC-CLIM and UNC-CLIMSST. During summer 2003 not only the Mediterranean Sea, but also most of western, central, and eastern Europe acted as a source of moisture to the atmosphere, except for the Alps. That is, assuming that the change in the water content of the air column over the whole season is small, evaporation exceeded precipitation in most areas (see Equation 5.1). The lower panel confirms that evaporation was larger over the Mediterranean Sea and areas of the Atlantic ocean in the simulation with warmer, historical SSTs. This moisture was partly transported to the land masses. Especially mountainous regions like the Alps, the Pyrenees, the Italian Apennine, and the Greek Pindus mountain range benefit from the moisture excess in the UNC-CLIM experiment.

The arrows in the plot indicate the direction and strength of the vertically integrated mean moisture transport over the summer 2003. In the mean, moisture is mainly transported from the west to the east in the western part of the continent, and from north to south in the east of the Mediterranean catchment. However, this does not exclude that for specific rainfall events the source of moisture could come from other directions. Generally, this circulation pattern of moisture is strengthened in the UNC-CLIM simulation, indicating that the warmer SSTs intensify the hydrological cycle in the region.

As already mentioned above, the seasonal mean moisture transport does not capture the effect of cyclones that move moisture, in the course of specific rainfall events, in directions that do not coincide with the seasonal mean flow. Therefore we calculated the moisture source for

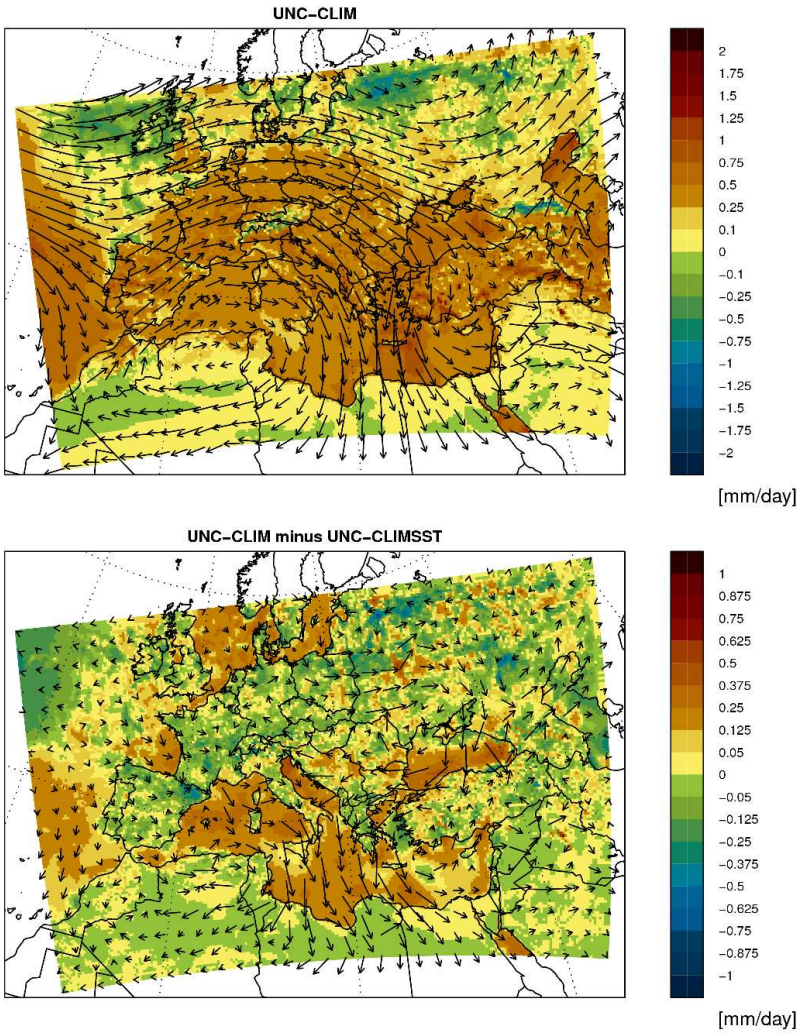

Figure 5.12: Upper panel: Colour shading indicates moisture divergence in the UNC-CLIM experiment. Arrow show the flux of moisture by advection. Lower panel: the same quantities as in the upper panel, but the differences between UNC-CLIM and UNC-CLIMSST are shown. In the difference plot arrows are scaled by a factor of 10.

all the rainfall events for specific Mediterranean subcatchments, namely "Southern France", "Adriatic", and "Aegean". The subcatchment boundaries and the results of the analysis are presented in Figure 5.13. The method is based on a Lagrangian backtracking algorithm which follows air parcels along their back-trajectories. More details about the method can be found in Elizalde and Jacob (2011).

All three catchments receive more precipitation in the UNC-CLIM simulation than in UNC-CLIMSST. The subcatchment "Southern France" (top row) receives part of the moisture from the Atlantic Ocean, but a substantial contribution comes from the Mediterranean Sea, although this is not to be expected considering the mean moisture flux (Figure 5.12). The third main moisture source is local land evaporation in the subcatchment itself and surrounding areas. The surplus of moisture in UNC-CLIM (top row, right panel) stems to a large part from the Mediterranean Sea, but also excess evaporation over the Bay of Biscay and land areas in southern France play a significant role.

The situation is similar for the Adriatic subcatchment (middle row). Here the Mediterranean Sea, and especially the Adriatic Sea, contribute most to the precipitation increase in UNC-CLIM compared to UNC-CLIMSST. In contrast, for the Aegean subcatchment, the excess of moisture can be tracked mostly to the Black Sea and land areas north and northeast of the subcatchment, in accordance with the mean moisture flow.

In order to asses whether the increase in precipitation of UNC-CLIM compared to UNC-CLIMSST is caused by addition precipitation events, or simply by increased rainfall intensities, Figure 5.14 shows precipitation time series for the three selected subcatchments. Indeed, the rainfall events are mostly more intense in the UNC-CLIM simulation. In some cases, they last significantly longer, like for instance around August 8 in the Adriatic subcatchment. The excess of moisture in the atmosphere strengthens and maintains the formation of precipitation for longer periods of time in some incidents.

5.4.2 Coupled ocean initial condition experiment

In the following section we investigate the memory of the Mediterranean Sea and its influence on surrounding land areas. This is the central point in the question whether the Mediterranean Sea plays an active role in shaping the European summer climate. If the Mediterranean Sea upper ocean temperatures are driven by the atmosphere, then this means that the Mediterranean Sea is a passive component of the system. The Mediterranean Sea may only be an active agent in the regional climate system if there is memory in the surface temperatures of the Mediterranean Sea that is rooted in the lower levels of the water body. This key question can only be examined with the regional ocean-atmosphere coupled climate model.

In the experiment CPL-INICOLD the Mediterranean Sea was initialized on January 1st of the

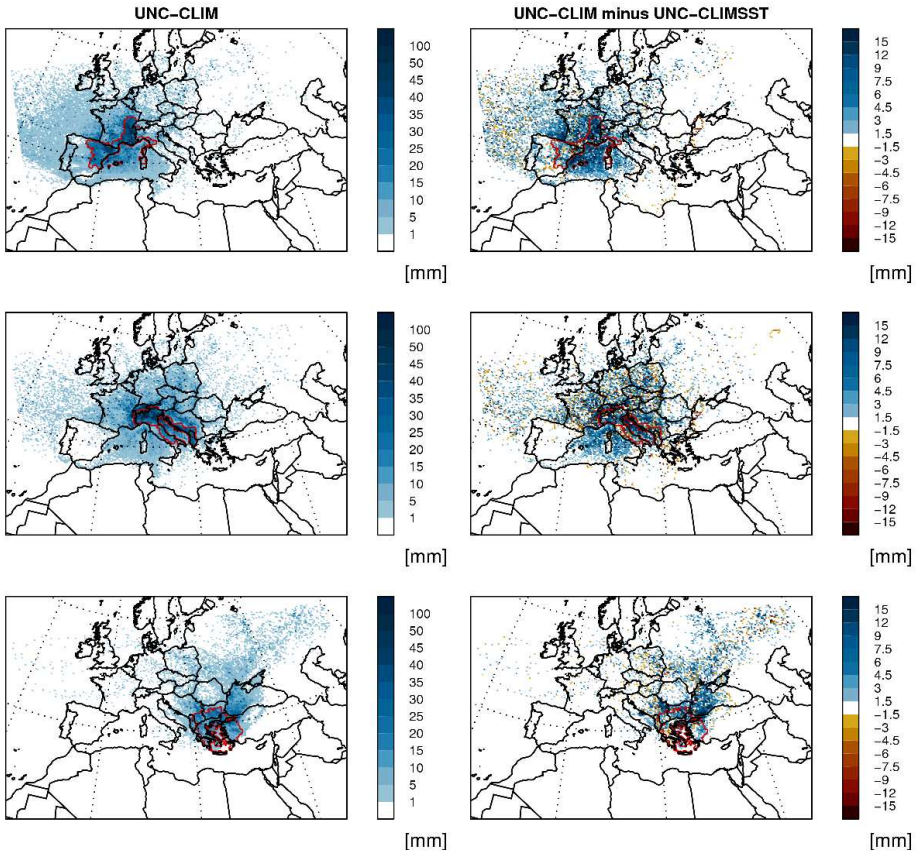

Figure 5.13: Moisture source for all rainfall events for three Mediterranean subcatchments. Left column: mean over summer 2003 for UNC-CLIM. Right column: difference of UNC-CLIM and UNC-CLIMSST.

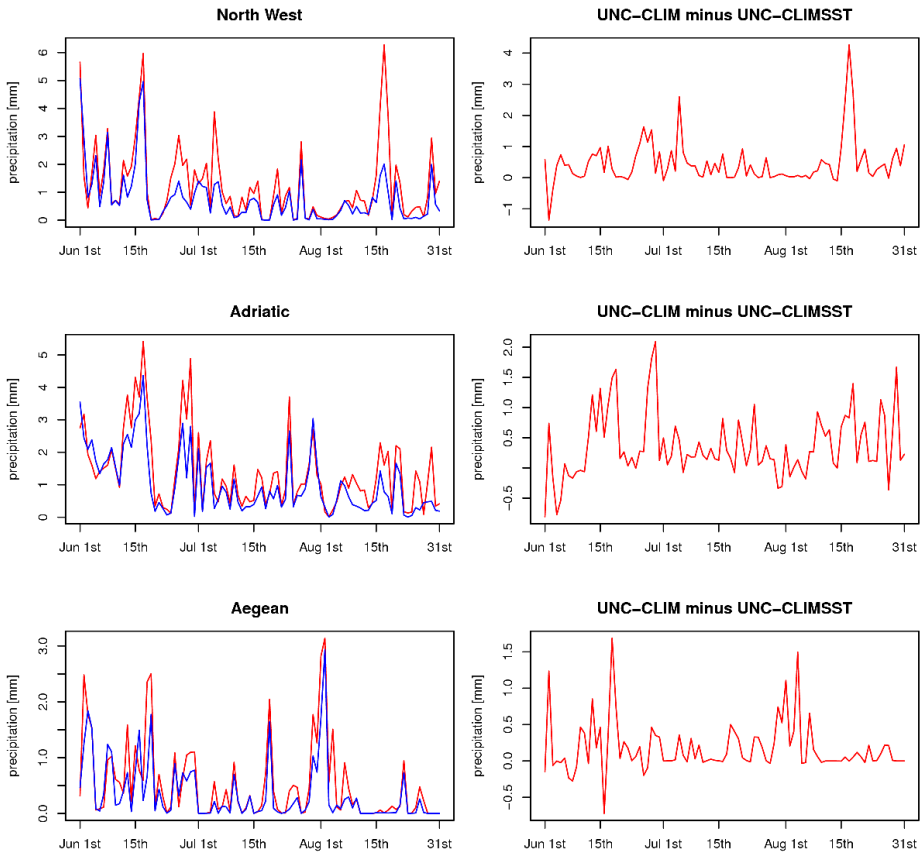

Figure 5.14: Precipitation time series for the three selected subcatchments during summer 2003.

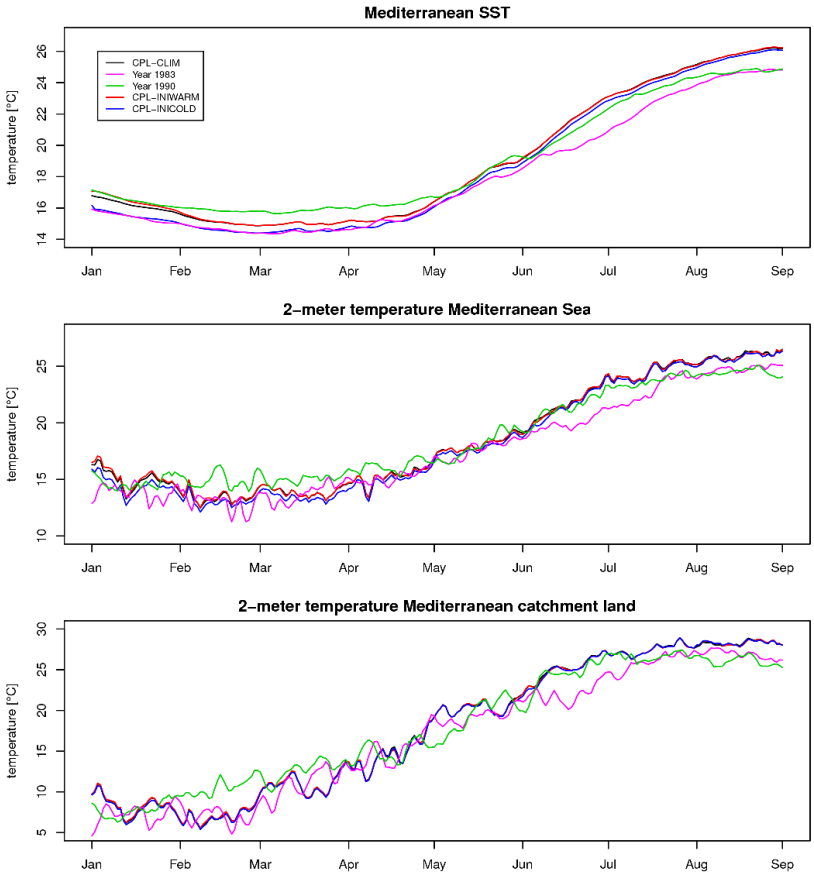

Figure 5.15: Daily time series of Mediterranean SST (top panel), 2-meter temperature over the Mediterranean Sea (middle panel), and 2-meter temperature over the land part of the Mediterranean catchment (bottom panel) for the year 2003. Indicated are the experiments CPL-CLIM, COL-INICOLD, CPL-INIWARM as well as the historical years 1983 and 1990.

year 2003 with the state of the Mediterranean Sea of January 1st, 1983, which was a year with a cold ocean state on that date. Analogously, for the experiment CPL-INIWARM the Mediterranean Sea was initialized on January 1st of the year 2003 with the state of the Mediterranean Sea of January 1st, 1990, which was a year with a warm ocean state on that date. These two runs are compared with the historical coupled simulation for the year 2003 and the historical coupled simulations of the years 1983 and 1990 in Figure 5.15. The upper panel shows the developement of the Mediterranean SST for January 1st to the end of August, the mid row displays 2-meter temperature averaged over the area of the Mediterranean Sea, and the bottom panel depicts 2-meter temperature averaged over the land part of the total Mediterranean catchment.

Remarkably, Mediterranean SSTs in CPL-INICOLD are substantially different from the SSTs in CPL-INIWARM until the beginning of June, although the atmospheric forcing is the same in both experiments. In May, SSTs rise in accordance with atmospheric temperatures for the simulations with the 2003 atmospheric conditions. The comparison with the cold year 1983, which possesses a rather cold atmosphere also in summer, shows that the reaction time of SSTs to atmospheric forcing is much shorter in summer than in winter. While in winter the differences in SSTs between CPL-INICOLD and CPL-INIWARM remain over several months despite the identical atmospheric conditions, the SSTs of CPL-INICOLD and the year 1983 rapidly diverge in summer due to the different atmospheric temperatures. Similarly, in summer the differences in SSTs between the year 1983 and the year 1990 quite closely follows the differences in 2-meter temperature over the Mediterranean Sea. However, although the 2-meter temperature is almost the same from mid July, the SST only converges in the beginning of August, implying a reaction time of SSTs to atmospheric temperatures of about three weeks.

This suggests that due to the stable stratification of the surface layers of the Mediterranean Sea, the response time of the upper most levels of the water body is shorter in summer compared to winter. The surface layers are closely connected to the atmosphere. In winter, however, the upper part of the Mediterranean Sea is less stable and therefore heat is more easily transported across layers. This results in a longer memory of the upper layers of the Mediterranean Sea which can potentially impact the 2-meter temperatures in the region.

This interpretation is supported by the time series of the heat content of the Mediterranean Sea down to different depths (Figure 5.16). Down to 200 meter and also 100 meter, the heat content in CPL-INICOLD is still substantially different from the one in CPL-INIWARM at the end of the summer. Even down to 50 meter one can observe a difference in the heat content at the end of August. At the upper most levels, however, as indicated by the heat content down to 10 meter, the two simulations are very close to each other already during June and hardly distinguishable in August. Similarly, in summer the year 1883 catches up with the year 1990 only in the upper most layer, which is disconnected from the water below. In contrast, during the winter months, the differences in heat content between CPL-INICOLD and CPL-

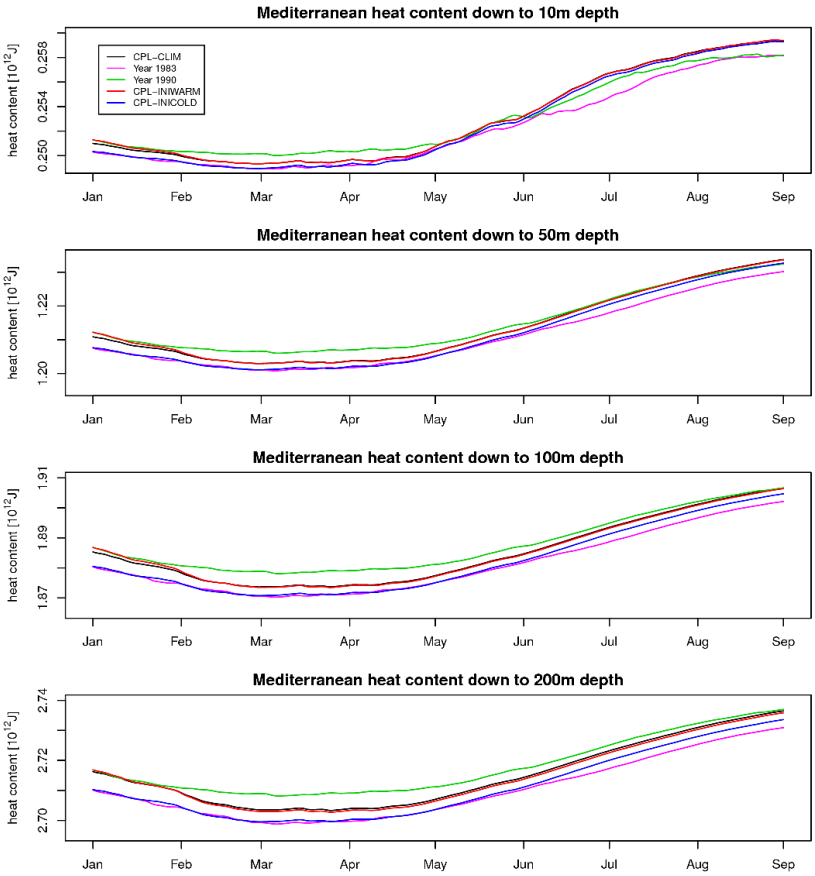

Figure 5.16: Daily time series of Mediterranean heat content down to different depths for the year 2003. Indicated are the experiments CPL-CLIM, COL-INICOLD, CPL-INIWARM as well as the historical years 1983 and 1990.

INIWARM are similar in relative terms in all four layers.

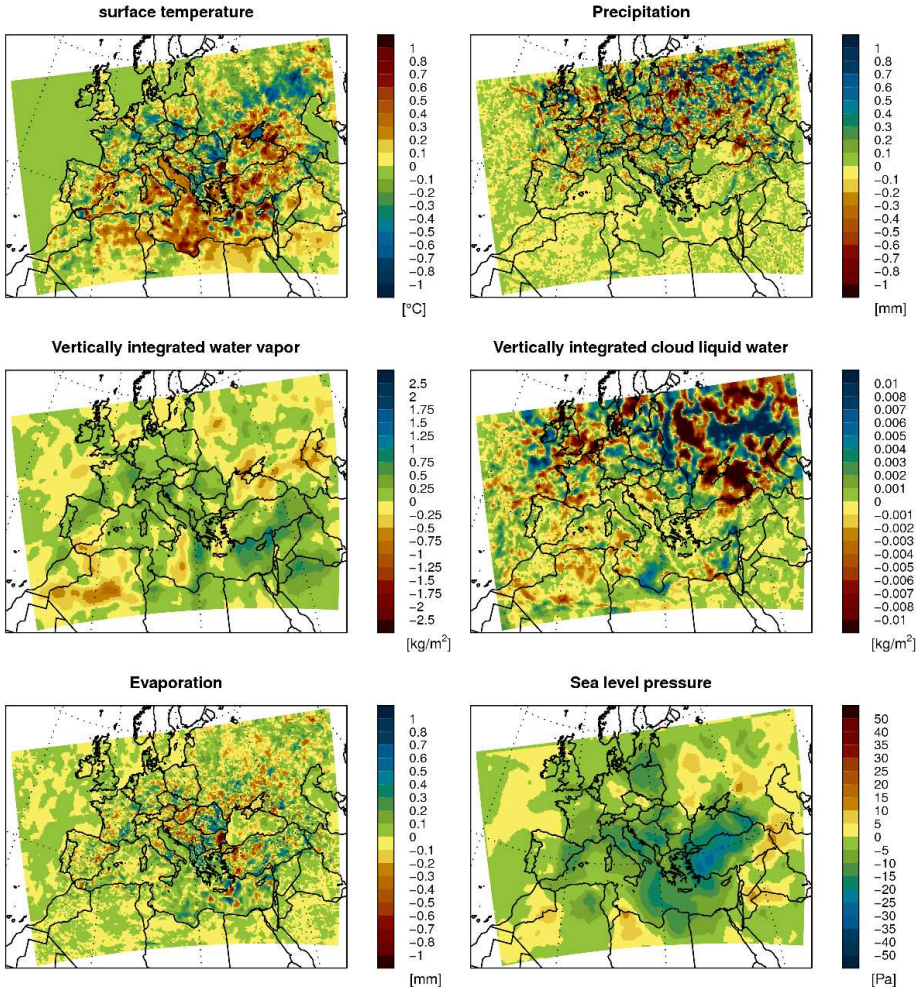

Figure 5.17: Mean difference between CPL-CLIM and CPL-INICOLD over summer 2003 for various quantities.

Figure 5.17 shows the difference between the historical simulation CPL-CLIM and CPL-INICOLD for various quantities. The response is similar to the effect of changed SSTs in the experiments with the uncoupled model, but smaller in magnitude. Over land, the signal is

insignificant.

5.5 Discussion and conclusions

The present study treats the question whether the Mediterranean Sea plays an active role in shaping the European summer climate. There are two aspects to this issue. In a first step we investigate the impact of Mediterranean SSTs on the climatic characteristics of the European land areas during summer. However, even if SSTs substantially influence the regional climate, the Mediterranean Sea surface waters could still be driven entirely by the atmospheric conditions. In that case the atmosphere would govern the regional heat and moisture budget. In summer 2003, for instance, the Mediterranean SSTs were anomalously high. In a second step we therefore study if this could actually have been different. Colder Mediterranean SSTs could have had established only if there is memory in the surface layers of the Mediterranean Sea during summer which remembers the state of the ocean in the winter or spring before. While the first question of the influence of Mediterranean SSTs on the climate can be tackled with an atmospheric model and prescribed Mediterranean SSTs, the second, more vital matter can only be explored using a coupled atmosphere-ocean model.

With respect to the sensitivity of the European summer climate to Mediterranean SSTs our study essentially confirms the conclusions of Jung et al. (2006). Warmer SSTs produce a heat low at the surface, evaporation is enhanced and consequently the moisture content of the atmosphere is increased. The heat low over the water induces a modest high pressure anomaly over parts of the continent, but this signal is weak and restricted to the lowest levels of the atmosphere. Altogether the general circulation is not substantially modified by different Mediterranean SSTs. Although convective activities over land masses are affected, they are not very consistently altered according to a defined large-scale dynamic response to the change in SSTs. However, in some areas, like in eastern parts of the Mediterranean basin where subsidence is weakened in the experiment with colder SSTs, a regional signal can be identified.

The main impact of the Mediterranean SSTs on European summer climate becomes evident when analyzing the effect on the moisture balance of the atmosphere. The mean moisture transport is intensified in the simulations with historical, anomalously warm SSTs. But also the eddy transport induces enhanced moisture advection and precipitation over land, as shown by the result of the moisture tracking analysis. In general, the excess moisture does not induce additional rainfall events, but precipitation is intensified and in some cases prolonged.

The initial condition experiments with the regional coupled ocean-atmosphere model suggest that in summer 2003 the role of the Mediterranean Sea was essentially passive in nature. At the beginning of 2003 the Mediterranean Sea is indeed relatively warm in our historical coupled simulation (which does not necessarily need to be in accordance with observations). How-

ever, it cools in the course of spring and water temperatures become rather low in April. The Mediterranean SSTs then follow quite closely the rising air temperatures in May. Deeper layers of the Mediterranean actually remain colder than average, but due to the strong stratification of the water in summer, heat from the surface is not transported effectively to deeper levels. In winter, when the water column in the Mediterranean Sea is less stable, heat exchange can occur more easily across layers. In that case, mixing processes vertically redistribute energy gained at the surface which induces a longer memory in the SSTs in winter.

One can therefore conclude that although the Mediterranean SSTs were indeed distinctly above average in summer 2003, this was most probably due to the anomalously warm conditions of the atmosphere. It was not an extraordinary state of the Mediterranean Sea which actively enhanced the heat wave over Europe. This finding is in line with the study of Hertig and Jacobeit (2011) which shows that the predictability of temperature and precipitation in the Mediterranean region is very limited, even when global sea surface temperature patterns are taken into account. Our work supports the view that seasonal predictions of European summer climate based on Mediterranean SSTs have only modest prospect.

Chapter 6

Conclusions and outlook

6.1 Conclusions

This dissertation addresses the processes involved in the Mediterranean water cycle and the role of the Mediterranean Sea. For this purpose, a new regional atmosphere-ocean-hydrology coupled model has been developed to simulate the Mediterranean climate. In the new model the regional atmosphere climate model REMO (ARCM, in the stand-alone version), the hydrological model HDmodel and the Max Planck Institute Ocean Model MPI-OM are fully coupled. Due to the fact that the model accomplishes to join the atmosphere, ocean and land components, it has been named as Regional Climate System Model (RCSM). For the first time, the Mediterranean water cycle has been simulated in a closed hydrology system. Moreover, the high resolution allows a better representation of the orography and detailed SST pattern. Finally, the interactive air-sea feedback is included in the calculation of the sea surface fluxes.

The capability of the RCSM and the ARCM to simulate the water cycle in the Mediterranean Region has been analyzed. Both models are able to reproduce the main characteristics of the components of the hydrological cycle. The values obtained for the heat and freshwater fluxes are in agreement with those found by Mariotti et al. (2002) and Sanchez-Gomez et al. (2011) without any necessity to apply flux corrections.

The improvements of the RCSM allow to overcome previous deficiencies on existing climate simulations, as discussed in Chapter 1, and to address the following questions:

What are the impacts of the improved resolution and the inclusion of the air-sea feedbacks on the simulation of the water budget?

It has been shown that, on the one side, a detailed representation of the orography in the models improves the simulation of both the processes involved in the orographic precipitation and the moisture advection. More realistic patterns of the water vapor convergence and divergence are produced in comparison with coarse resolution data sets. Therefore a detailed spatial pattern for precipitation is achieved. Nevertheless, precipitation is one of the most difficult variables

to simulate, and it is the main reason for the biases in the land water budget. Although some individual rivers present biases in their simulated discharge due to precipitation, the total river discharge in the Mediterranean catchment is very well calculated.

On the other hand, a detailed information of the SSTs improves the correlation of the marine evaporation with its driving components. This is especially true in the sea areas near to the coast. A higher correlation demonstrates as well the interactivity of the simulated thermal and dynamic processes at the RCSM.

What is the role of the Mediterranean Sea for precipitation in the Mediterranean region?

The permanent characteristic of the water vapor divergence over the Mediterranean Sea shows that the Mediterranean Sea to acts as a moisture source for the entire region. The seasonal variability of the moisture divergence is driven by the atmospheric moisture content and thermal state between the atmosphere and the sea. The maximum evaporation rate takes place at end of autumn beginning of winter and the minimum happens at the beginning of summer. The atmospheric eddy transport induces the moisture advection to the land areas, where the precipitation is influenced by the orography as shown by the results of the moisture tracking analysis. This implies that the precipitation over the Mediterranean catchment is not formed with water vapor from Mediterranean Sea evaporation in the same proportion throughout the year. The contribution of the Mediterranean basin is larger in winter than in summer, the opposite behavior to the land evaporation.

Up to 53% of the water of the hydrological cycle is recycled inside the Mediterranean region. This concept is defined here as the Mediterranean Catchment Recycled Ratio (MCRR). This percentage remains nearly constant throughout the year independently of the exchanged roles of the terrestrial and marine evaporation sources.

From the study focused on the summer 2003 it can be concluded that the atmospheric general circulation in the Mediterranean region is not substantially modified by the Mediterranean SST. Moreover, the Mediterranean SST follows quite closely the rising air temperatures in May of that year. Both results suggest that it was not an extraordinary state of the Mediterranean Sea which actively enhanced the heat wave over Europe and that the Mediterranean Sea only played a passive role. This finding is in line with the recent study of Hertig and Jacobeit (2011).

How is the Mediterranean hydrological cycle affected by anthropogenic climate change?

As discussed in Chapter 1, the changes on large-scale circulation induce a decrease of the moisture transport into the Mediterranean region. The RCSM shows a negative trend in precipitation for the future climate. As a consequence of the decrease of water availability, the deficit on the land water budget induces a reduction in the total river discharge up to 23% with respect to present climate. Over the Mediterranean Sea, the freshwater loss increases up to 21% due to the decrease in precipitation and the river discharge, but not to an increase of marine

evaporation, which shows only a weak signal. The decrease of land water budget and increase of the freshwater loss agree with the findings of Mariotti et al. (2002) and Sanchez-Gomez et al. (2009). Except for the change in the marine evaporation, which is larger in Mariotti et al. (2002) and Sanchez-Gomez et al. (2009) findings.

Furthermore, the negative trend in the precipitation induces a soil dryness which reduces the terrestrial evaporation, jointly with the slight increased evaporation from the Mediterranean Sea, leading to a slight shift between the land and sea roles in the hydrology cycle at the future climate projection. The MCRR does not show significant changes.

Final comments

The models analyzed here are able to reproduce the main characteristics of the physical processes involved in the Mediterranean hydrological cycle and the sea surface fluxes. On the one hand, the RCSM improves the representation of the air-sea feedbacks, which are important for the simulation of the surface fluxes. On the other hand, another source of uncertainty is introduced into the climate simulation due to the intrinsic model variability and internal model errors. Nevertheless, the ability of the RCSM to produce its own SSTs makes it more advantageous to the stand-alone atmospheric model with regard to the assessment of the Climate Change response. The RCSM keeps more independence from the SSTs signal of its driving model in the future climate simulations. This study can be considered as the first step towards the use of a new modeling tool and further model development will overcome current deficiencies.

6.2 Outlook

The effects of the sea spray has not been taken into account, but probably they should not be neglected. Andreas (2002) found that during wind speeds of about 10 m s^{-1} approximately 10% of the total latent heat flux was originated from sea spray. For the wind speed range 15-18 m s^{-1}, the sea-spray-mediated flux accounted for as much as 10-40% of the total flux. At the Mediterranean Sea, the RCSM simulates wind speeds up to 14-26 m s^{-1} with an occurrence frequency up to 10% in the Gulf of Lions. The sea spray effect could have two sorts of impacts. On the one side, it enhances the evaporation rate, on the other hand, it helps cooling the surface water which could enhance the dense water formation at the Mediterranean Sea. Experiments including a sea spray parametrization could help to improving the representation of the surface fluxes.

The analysis of the Mediterranean and Black Seas was restricted to their interaction with the atmosphere, but not to the seas themselves. The study of the thermohaline circulation and water

masses formation will be useful for a better understanding of the SSTs behavior, and will yield estimates of sea level rise or changes in deep water ventilation of the Mediterranean Sea.

Due to the high computational costs of the RCSM only a limited number of simulations could be carried out. Even though some effort has already been dedicated to improve the model, still some technical work is needed, like the interpolation method for variables exchange and the optimization of parameters for sub-grid scale e.g. vertical mixing that can reduce the model biases.

Since uncertainties are implicit in the assumptions entering the water transport tracking method, an extension of the present work to other water transport tracking algorithms and the analysis of an ensemble of climate model simulations is planned for the future. This hopefully will increase the confidence in the results presented here and lead to a more detailed understanding of the Mediterranean hydrological cycle.

Bibliography

Adler, R., Huffman, G., Chang, A., and et al. (2003). The Version-2 Global Precipitation Climatology Project (GPCP) monthly precipitation analysis (1979-present). *J. Hydrometeor.*, 4 (6):1147–1167.

Aldrian, E., Sein, D., Jacob, D., Gates, L., and Podzun, R. (2005). Modelling Indonesian rainfall with a coupled regional model. *Climate Dynamics*, 25(1):1–17.

Alpert, P., Baldi, M., Ilani, R., Krichak, S., Price, C., Rodo, X., Saaroni, H., Ziv, B., Kishcha, P., Barkan, J., Mariotti, A., and Xoplaki, E. (2006). *Relations between Climate Variability in the Mediterranean Region and the Tropics: ENSO, South Asian and African Monsoons, Hurricanes and Saharan Dust. Mediterranean Climate Variability*, chapter in chap 2, pages 149–177. Mediterranean Climate Variability. Elsevier.

Andersson, A., Bakan, S., Fennig, K., Grassl, H., Klepp, C.-P., and Schulz, J. (2007). Hamburg Ocean Atmosphere Parameters and Fluxes from Satellite Data, HOAPS3 monthly mean. *Data Center for Climate*.

Andersson, A., Fennig, K., Klepp, C., Bakan, S., Graßl, H., and Schulz, J. (2010). The Hamburg Ocean Atmosphere Parameters and Fluxes from Satellite Data – HOAPS-3. *Earth Syst. Sci. Data Discuss.*, 3(1):143–194.

Andreas, E. L., a. J. D. (2002). The signature of spray in the HEXOS turbulent heat flux data. *Bound.-Layer Meteor.*, 103:303–333.

Baldi, M., Dalu, G., Maracchi, G., Oasqui, M., and Cesarone, F. (2006). Heat waves in the Mediterranean: a local feature or a large-scale effect? *Int. J. Clim.*, 26:1477–1487.

Barron, C. and Smedstad, L. (2002). Global river inflow within the Navy Coastal Ocean Model. *Proc. Oceans 2002 MTS IEEE Conf., 29 to 31 October*, pages 1472–1479.

Berry, D. and Kent, E. (2009). A New Air-Sea Interaction Gridded Dataset from ICOADS With Uncertainty Estimates. *Bull. Amer. Meteor. Soc.*, 90:645–656.

Black, E., Blackburn, M., Harrison, G., Hoskins, B., and Methven, J. (2004). Factors contributing to the summer 2003 European heatwave. *Weather*, 59:217–223.

Black, E. and Sutton, R. (2007). The influence of oceanic conditions on the hot European summer of 2003. *Climate Dynamics*, 28(1):53–66.

Bojariu, R. and Giorgi, F. (2005). The North Atlantic Oscillation signal in a regional climate simulation for the European region. *Tellus A*, 57(4):641–653.

Brubaker, K. L., Dirmeyer, P. A., Sudradjat, A., Levy, B. S., and Bernal, F. (2001). A 36-yr Climatological Description of the Evaporative Sources of Warm-Season Precipitation in the Mississippi River Basin. *Journal of Hydrometeorology*, 2(6):537–557.

Buongiorno Nardelli, B. and Salusti, E. (2000). On dense water formation criteria and their application to the Mediterranean Sea. *Deep Sea Research Part I: Oceanographic Research Papers*, 47(2):193–221.

Cassou, C. and Terray, L. (2005). Tropical Atlantic influence on European heat waves. *J. Climate*, 18:2805–2811.

Colacino, M. and Dell'Osso, L. (1977). Monthly mean evaporation over the Mediterranean sea. *Meteorology and Atmospheric Physics*, 26(2):283–293.

CRU (2008). Climate Reseach Unit Datasets. Technical report, University of East Anglia Climate Research Unit (CRU). CRU Datasets. British Atmospheric Data Centre, 2008, Date of citation. Available from http://badc.nerc.ac.uk/data/cru.

Della-Marta, P. M., Luterbacher, J., von Weissfluh, H., Xoplaki, E., Brunet, M., and Wanner, H. (2007). Summer heat waves over western Europe 1880-2003, their relationship to large scale forcings and predictability. *Clim. Dyn.*, 29:251–275.

Dirmeyer, P. A. and Brubaker, K. L. (1999). Contrasting evaporative moisture sources during the drought of 1988 and the flood of 1993. *J. Geophys. Res*, 104(D16):19,383–19,397.

Dümenil Gates, L., Hagemann, S., and Golz, C. (2000). Observed historical discharge data from major rivers for climate model validation. Report 307, Max Planck Institute for Meteorology.

Dünkeloh, A. and Jacobeit, J. (2003). Circulation Dynamics of Mediterranean precipitation variability. *nt. J. Climatol.*, 23:1843–1866.

ECMWF (2009). ERA-Interim Re-Analysis data. Technical report, European Centre for Medium-Range Weather Forecasts. British Atmospheric Data Centre. Available from http://badc.nerc.ac.uk/data/ecmwf-era-interim/.

Elizalde, A. and Jacob, D. (2011). Water vapor transport and precipitation over the Mediterranean region. *Submitted to Climate Dynamics.*, -:–. submitted.

Elizalde, A., Sein, D., Mikolajewicz, U., and Jacob, D. (2010). Technical Report: Regional atmosphere-ocean-hydrology coupled climate model. Max Planck

Institute for Meteorology. http://www.remo-rcm.de/fileadmin/user_upload/remo/UBA/pdf/TechnicalReport.pdf.

Fernández, J., Sáenz, J., and Zorita, E. (2003). Analysis of wintertime atmospheric moisture transport and its variability over southern Europe in the NCEP Reanalyses. *Climate Research*, 23(3):195–215.

Feudale, L. and Shukla, J. (2007). Role of Mediterranean SST in enhancing the European heat wave of summer 2003. *Geophys. Res. Lett.*, 34(3):L03811–.

Gibelin and Déqué (2003). Anthropogenic climate change over the Mediterranean region simulated by a global variable resolution model. *Climate Dynamics*, 20(4):327–339.

Gimeno, L., Drumond, A., Nieto, R., Trigo, R. M., and Stohl, A. (2010). On the origin of continental precipitation. *Geophys. Res. Lett.*, 37(13):L13804–.

Giorgi, F. (2006). Climate change hot-spots. *Geophys. Res. Lett.*, 33.

Giorgi, F. and Lionello, P. (2008). Climate change projections for the Mediterranean region. *Global and Planetary Change*, 63(2-3):90–104.

Grazzini, F., Ferranti, L., Lalaurette, F., and Vitart, F. (2003). The exceptional warm anomalies of summer 2003. *ECMWF Newsletter*, 99:2–8.

Grazzini, F. and Viterbo, P. (2003). Record-breaking warm sea surface temperature of the Mediterranean Sea. *ECMWF Newsletter*, 98:30–31.

Hagemann, S., Arpe, K., and Bengtsson, L. (2005). Validation of the hydrological cycle of ERA-40. *ERA-40 Project Report Series*, 24.

Hagemann, S. and Dümenil, L. (1998). A parametrization of the lateral waterflow for the global scale. *Climate Dynamics*, 14:17–31.

Hagemann, S. and Dümenil, L. (1999). Application of a global discharge model to atmospheric model simulations in the BALTEX Region. *Nordic Hydrology*, 30:209–230.

Hagemann, S. and Jacob, D. (2007). Gradient in the climate change signal of European discharge predicted by a multi-model ensemble. *Climatic Change*, 81:309–327.

Haylock, M. R., Hofstra, N., Klein Tank, A. M. G., Klok, E. J., Jones, P. D., and New, M. (2008). A European daily high-resolution gridded data set of surface temperature and precipitation for 1950–2006. *J. Geophys. Res.*, 113:–.

Hertig, E. and Jacobeit, J. (2011). Predictability of Mediterranean climate variables from oceanic variability. Part II: Statistical models for monthly precipitation and temperature in the Mediterranean area. *Clim. Dyn.*, 36:825–843.

Hewitt, C. D. and Griggs, D. J. (2004). Ensembles-Based Predictions of Climate Changes and Their Impacts. *Eos Trans. AGU*, 85(52).

Hibler, W. D. (1979). A dynamic thermodynamic sea ice model. *J. Phys. Oceanogr.*, 9:815–846.

Hillman, D. R. and LTD, S., editors (1962). *Weather in the Mediterranean, Volume I*. Her Majesty's Stationary Office - Meteorological Office.

Hofinger, S., Mayr, G. J., Dreiseitl, E., and Kuhn, M. (2000). Fine-Scale Observations of Summertime Precipitation in an Intra-Alpine Region. *Meteorology and Atmospheric Physics*, 72:175–184. 10.1007/s007030050014.

Hopkins, T. S. (1999). The thermohaline forcing of the Gibraltar exchange. *Journal of Marine Systems*, 20(1-4):1–31.

Hurrell, J. W. (1995). Decadal Trends in the North Atlantic Oscillation: Regional Temperatures and Precipitation. *Science*, 269 (No. 5224):676–679.

IPCC, C. . (2007). *Christensen, J.H. and B. Hewitson and A. Busuioc and A. Chen and X. Gao and I. Held and R. Jones and R.K. Kolli and W.-T. Kwon and R. Laprise and V. Magaña Rueda and L. Mearns and C.G. Menéndez and J. Räisänen and A. Rinke and A. Sarr and P. Whetton. Regional Climate Projections. In: Climate Change 2007: The Physical Science Basis.* Contribution of Working Group I to the Fourth Assessment Report of the Intergovernmental Panel on Climate Change [Solomon, S., D. Qin, M. Manning, Z. Chen, M. Marquis, K.B. Averyt, M. Tignor and H.L. Miller (eds.)]. Cambridge University. Press, Cambridge, United Kingdom and New York, NY, USA.

Jacob, D. (2001). A note to the simulation of the annual and interannual variability of the water budget over the Baltic Sea drainage basin. *Meteorology and Atmospheric Physics*, 77:61–73.

Jacob, D., Bärring, L., Christensen, O. B., Christensen, J. H., de Castro, M., Déqué, M., Giorgi, F., Hagemann, S., Hirschi, M., Jones, R., Kjellström, E., Lenderink, G., Rockel, B., Sánchez, E., Schär, C., Seneviratne, S. I., Somot, S., van Ulden, A., and van den Hurk, B. (2007). An intercomparison of regional climate models for Europe: model performance in present day climate. *Climatic Change*, 81:31–52.

Jacob, D. and Podzun, R. (1997). Sensitivity studies with the regional climate model REMO. *Meteorology and Atmospheric Physics*, 63:119–129.

Jin, F. and Zangvil, A. (2009). Relationship between moisture budget components over the eastern Mediterranean. *International Journal of Climatology*, 30(5):733 – 742.

Josey, S. A., Somot, S., and Tsimplis, M. (2011). Impacts of atmospheric modes of variability on Mediterranean Sea surface heat exchange. *J. Geophys. Res.*, 116(C2):C02032–.

Jung, T., Ferranti, F., and Tompkins, A. M. (2006). Response to the summer 2003 Mediterranean SST anomalies over Europe and Africa. *J. Climate*, 19:5439–5454.

Kalnay, E., Kanamitsu, M., Kistler, R., Collins, W., Deaven, D., Gandin, L., Iredell, M., Saha, S., White, G., Woollen, J., Zhu, Y., Leetmaa, A., Reynolds, R., Chelliah, M., Ebisuzaki, W., Higgins, W., Janowiak, J., Mo, K. C., Ropelewski, C., Wang, J., Jenne, R., and Joseph, D. (1996). The NCEP/NCAR 40-Year Reanalysis Project. *Bulletin of the American Meteorological Society*, 77(3):437–471.

Kara, A. B., Wallcraft, A. J., Hurlburt, H. E., and Stanev, E. (2008). Air-sea fluxes and river discharges in the Black Sea with a focus on the Danube and Bosphorus. *Journal of Marine Systems*, 74(1-2):74–95.

Kim, D. and Ramanathan, V. (2008). Solar radiation budget and radiative forcing due to aerosols and clouds. *J. Geophys. Res.*, 113(D2):D02203–.

Levitus, S., Boyer, T. P., Conkright, M. E., O'Brien, T., Antonov, J., Stephens, C., Stathoplos, L., Johnson, D., and Gelfeld, R. (1998). Introduction: NOAA Atlas NESDIS 18, Ocean Climate Laboratory, National Oceanographic Data Center U.S. Gov. Printing Office, Wash., D.C. *World Ocean Database*, 1.

Li, L. Z. X. (2006). Atmospheric GCM response to an idealized anomaly of the Mediterranean sea surface temperature. *Cli. Dyn.*, 27:543–552.

Lionello, P., Bhend, J., Buzzi, A., Della-Marta, P. M., Krichak, S. O., Jansa, A., Maheras, P., Sanna, A., Trigo, I. F., and Trigo, R. (2006a). Cyclones in the Mediterranean region: climatology and effects on the environment. In Lionello, P., Malanotte-Rizzoli, P., and Boscolo, R., editors, *Mediterranean climate variability*. Elsevier, Amsterdam.

Lionello, P., Malanotte, P., and Boscolo, R. (2006b). *Mediterranean Climate Variability*. Elsevier B.V.

Lionello, P. and Sanna, A. (2005). Mediterranean wave climate variability and its links with NAO and Indian Monsoon. *Climate Dynamics*, 25:611–623.

Ludwig, W., Dumont, E., Meybeck, M., and Heussner, S. (2009). River discharges of water and nutrients to the Mediterranean and Black Sea: Major drivers for ecosystem changes during past and future decades? *Progress In Oceanography*, 80(3-4):199–217.

Maier-Reimer, E. (1997). Design of a closed boundary regional model of the Arctic Ocean. *Bull. Amer. Meteor. Soc.: Workshop on polar processes in global climate*, 13:72.

Majewski, D. (1991). The Europa Modell of the Deutscher Wetterdienst. Technical report.

Malanotte-Rizzoli, P. and Bergamasco, A. (1991). The wind and thermally driven circulation

of the eastern Mediterranean Sea. Part II: the Baroclinic case. *Dynamics of Atmospheres and Oceans*, 15(3-5):355–419.

Malanotte-Rizzoli, P., Manca, B. B., D'Alcalà, M. R., Theocharis, A., Bergamasco, A., Bregant, D., Budillon, G., Civitarese, G., Georgopoulos, D., Michelato, A., Sansone, E., Scarazzato, P., and Souvermezoglou, E. (1997). A synthesis of the Ionian Sea hydrography, circulation and water mass pathways during POEM-Phase I. *Progress In Oceanography*, 39(3):153–204.

Manca, B. B., Kovacevic, V., Gacic, M., and Viezzoli, D. (2002). Dense water formation in the Southern Adriatic Sea and spreading into the Ionian Sea in the period 1997-1999. *Journal of Marine Systems*, 33-34:133–154.

Mariotti, A., Struglia, M. V., Zeng, N., and Lau, K.-M. (2002). The Hydrological Cycle in the Mediterranean Region and Implications for the Water Budget of the Mediterranean Sea. *Journal of Climate*, 13(13):1674–1690.

Mariotti, A., Zeng, N., Yoon, J.-H., Artale, V., Navarra, A., Alpert5, P., and Li, L. Z. X. (2008). Mediterranean water cycle changes: transition to drier 21st century conditions in observations and CMIP3 simulations. *Environmental Research Letters*, 3:044001 (8pp).

Marsland, S. J., Haak, H., Jungclaus, J. H., Latif, M., and Röske, F. (2003). The Max-Planck-Institute global ocean/sea ice model with orthogonal curvilinear coordinates. *Ocean Modelling*, 5(2):91–127.

McKnight, T. L. and Hess, D. (2000). *Climate Zones and Types: The Köppen System. Physical Geography: A Landscape Appreciation. Upper Saddle River, NJ: Prentice Hall. pp. 200–1. ISBN 0-13-020263-0.*

MEDAR/MEDATLAS., G. (2002). Mediterranean and Black Sea database of temperature salinity and bio-chemical parameters. *Climatological Atlas. IFREMER Edition (4 Cdroms).*

Mikolajewicz, U. (2011). Modeling Mediterranean Ocean climate of the Last Glacial Maximum. *Climate of the Past*, 7(1):161–180.

Mikolajewicz, U., Sein, D., Jacob, D., Königk, T., Podzun, R., and Semmler, T. (2005). Simulating Arctic sea ice variability with a coupled regional atmosphere-ocean-sea ice model. *Meteorologische Zeitschrift*, 14, No.6:793–800.

Millot, C. (1999). Circulation in the Western Mediterranean Sea. *Journal of Marine Systems 20 Ž1999. 423 – 442*, 20:423 – 442.

Millán, M. M., Estrela, M. J., Sanz, M. J., Mantilla, E., Martín, M., Pastor, F., Salvador, R., Vallejo, R., Alonso, L., Gangoiti, G., Ilardia, J. L., Navazo, M., Albizuri, A., Artíñano, B., Ciccioli, P., Kallos, G., Carvalho, R. A., Andrés, D., Hoff, A., Werhahn, J., Seufert, G.,

and Versino, B. (2005). Climatic Feedbacks and Desertification: The Mediterranean Model. *Journal of Climate*, 18(5):684–701.

Millán, M. M., José Sanz, M., Salvador, R., and Mantilla, E. (2002). Atmospheric dynamics and ozone cycles related to nitrogen deposition in the western Mediterranean. *Environmental Pollution*, 118(2):167–186.

Neppel, L., Pujol, N., and Sabatier, R. (2011). A multivariate regional test for detection of trends in extreme rainfall: the case of extreme daily rainfall in the French Mediterranean area. *Advances in Geosciences*, 26:145–148.

NOAA-CPC (2003). Northern Hemisphere teleconnection indices (1950-2003, monthly). http://www.cpc.ncep.noaa.gov/data/teledoc/telecontents.shtml.

Ogi, M., Yamazaki, K., and Tachibana, Y. (2004). The summer northern annular mode and abnormal summer weather in 2003. *Geophys. Res. Lett.*, 32.

Ohmura, A. and Wild, M. (2002). Is the Hydrological Cycle Accelerating? *Science*, 298(5597):1345–1346.

Peel, M. C., Finlayson, B. L., and McMahon, T. A. (2007). Updated world map of the Köppen-Geiger climate classification. *Hydrol. Earth Syst. Sci.*, 11(5):1633–1644.

Perry, G. D., Duffy, P. B., and Miller, N. L. (1996). An extended data set of river discharges for validation of general circulation models. *J. Geophys. Res.*, 101(D16):21339–21349.

Ramanathan, V., Crutzen, P. J., Kiehl, J. T., and Rosenfeld, D. (2001). Aerosols, Climate, and the Hydrological Cycle. *Science*, 294(5549):2119–2124.

Reale, O., Feudale, L., and Turato, B. (2001). Evaporative moisture sources during a sequence of floods in the Mediterranean region. *Geophys. Res. Lett.*, 28(10):2085–2088.

Reynolds, R. W., Rayner, N. A., Smith, T. M., Stokes, D. C., and Wang, W. (2002). An improved in situ and satellite SST analysis for climate. *J. Climate*, 15:1609–1625.

Rixen, M., Beckers, J.-M., Levitus, S., Antonov, J., Boyer, T., Maillard, C., Fichaut, M., Balopoulos, E., Iona, S., Dooley, H., Garcia, M.-J., Manca, B., Giorgetti, A., Manzella, G., Mikhailov, N., Pinardi, N., and Zavatarelli, M. (2005). The Western Mediterranean Deep Water: A proxy for climate change. *Geophys. Res. Lett.*, 32(12):L12608–.

Roderick, M. L. and Farquhar, G. D. (2002). The Cause of Decreased Pan Evaporation over the Past 50 Years. *Science*, 298(5597):1410–1411.

Roeckner, E., Arpe, K., Bengtsson, L., Christoph, M., Claussen, M., Dümenil, L., Esch, M., Giorgetta, M., Schlese, U., and Schulzweida, U. (1996). Report No. 218 The atmospheric general circulation model ECHAM4: Model description and simulation of present day climate. Technical report, Max Planck Institute for Meterology.

Romanou, A., Tselioudis, G., Zerefos, C. S., Clayson, C.-A., Curry, J. A., and Andersson, A. (2010). Evaporation–Precipitation Variability over the Mediterranean and the Black Seas from Satellite and Reanalysis Estimates. *Journal of Climate*, 23(19):5268–5287.

Rudolf, B., Rueth, W., and Schneider, U. (1994). Terrestrial precipitation analysis: Operational method and required density of point measurements. *NATO ASI Series, Vol I 26. Global Precipitation and Climate Change, M. Desbois and F. Desahmond, Eds., Springler-Verlag*, I 26:173–186.

Röske, F. (2006). A global heat and freshwater forcing dataset for ocean models. *Ocean Modelling*, 11(3-4):235–297.

Sanchez-Gomez, E., Somot, S., Josey, S., Dubois, C., Elguindi, N., and Déqué, M. (2011). Evaluation of Mediterranean Sea water and heat budgets simulated by an ensemble of high resolution regional climate models. *Climate Dynamics*, pages 1–20.

Sanchez-Gomez, E., Somot, S., and Mariotti, A. (2009). Future changes in the Mediterranean water budget projected by an ensemble of regional climate models. *Geophys. Res. Lett.*, 36(21):L21401–.

Sannino, G., Herrmann, M., Carillo, A., Rupolo, V., Ruggiero, V., Artale, V., and Heimbach, P. (2009). An eddy-permitting model of the Mediterranean Sea with a two-way grid refinement at the Strait of Gibraltar. *Ocean Modelling*, 30(1):56–72.

Schicker, I., Radanovics, S., and Seibert, P. (2010). Origin and transport of Mediterranean moisture and air. *Atmos. Chem. Phys.*, 10(11):5089–5105.

Sheffield, J. and Wood, E. (2008). Projected changes in drought occurrence under future global warming from multi-model, multi-scenario, IPCC AR4 simulations. *Climate Dynamics*, 31(1):79–105.

Simmons, A. J., Uppala, S. M., Dee, D. P., and Kobayashi, S. (2007). ERA-Interim: New ECMWF reanalysis prosucts from 1989 onwards. *ECMWF Newsletter*, 110:25–35.

Sodemann, H. and Zubler, E. (2010). Seasonal and inter-annual variability of the moisture sources for Alpine precipitation during 1995–2002. *Int. J. Climatol.*, 30(7):947–961.

Somot, S., Sevault, F., Déqué, M., and Crépon, M. (2008). 21st century climate change scenario for the Mediterranean using a coupled atmosphere-ocean regional climate model. *Global and Planetary Change*, 63(2-3):112–126.

Spagnoli, B., Planton, S., Déqué, M., Mestre, O., and Moisselin, J.-M. (2002). Detecting climate change at a regional scale: the case of France. *Geophys. Res. Lett.*, 29(10):1450–.

SRES (2000). *Nakicenovic, N. et al. Special Report on Emissions Scenarios: A Special Report of Working Group III of the Intergovernmental Panel on Climate*

Change. Cambridge University Press, Cambridge, U.K., 599 pp. Available online at: http://www.grida.no/climate/ipcc/emission/index.htm.

Stanev, E. V., Traon, P. L., and Peneva, E. L. (2000). Sea level variations and their dependency on meteorological and hydrological forcing: Analysis of altimeter and surface data for the Black Sea. *J. Geophys. Res*, 105:17,203–17,216.

Struglia, M. V., Mariotti, A., and Filograsso, A. (2004). River Discharge into the Mediterranean Sea: Climatology and Aspects of the Observed Variability. *Journal of Climate*, 17(24):4740–4751.

Svensson, C., Kundzewicz, Z. W., and Maurer, T. (2005). Trend detection in river flow series: 2. Flood and low flow index series. *Hydrolog. Sci. J.*, 50(3):811–824.

Theocharis, A., Klein, B., Nittis, K., and Roether, W. (2002). Evolution and status of the Eastern Mediterranean Transient (1997-1999). *Journal of Marine Systems*, 33-34:91–116.

Tomassini, L. and Elizalde, A. (2011). Does the Mediterranean Sea influence the atmospheric dynamics of the European summer climate? The anomalous summer 2003 as a testbed. *Submitted to Climate Dynamics.*, –:–.

Tsimplis, M. and Bryden, H. (2000). Estimation of the transports through the Strait of Gibraltar. *Deep-Sea Research Part I*, 47:2219 2242.

Ulbrich, W. e. a. (2006). *The Mediterranean climate change under global warming Mediterranean*. Climate Variability and Predictability ed P Lionello et al (Amsterdam: Elsevier).

Uppala, S., Kallberg, P., Simmons, A., Andrae, U., da Costa Bechtold, V., Fiorino, M., Gibson, J., Haseler, J., Hernandez, A., Kelly, G., Li, X., Onogi, K., Saarinen, S., Sokka, N., Allan, R., Andersson, E., Arpe, K., Balmaseda, M., Beljaars, A., van de Berg, L., Bidlot, J., Bormann, N., Caires, S., Chevallier, F., Dethof, A., Dragosavac, M., Fisher, M., Fuentes, M., Hagemann, S., Holm, E., Hoskins, B., Isaksen, L., Janssen, P., Jenne, R., McNally, A., Mahfouf, J.-F., Morcrette, J.-J., Rayner, N., Saunders, R., Simon, P., Sterl, A., Trenberth, K., Untch, A., Vasiljevic, D., Viterbo, P., and Woollen, J. (2005). The ERA-40 re-analysis. *Quart. J. Roy. Meteor. Soc.*, 131:2961–3012.

Valcke, S. (2006). *OASIS User Guide prism 2.5. PRISM Support Initiative No 3. 68pp*. CERFACS.

Vorosmarty, C. J., Fekete, B. M., and Tucker, B. A. (1998). Global River Discharge, 1807-1991, Version. 1.1 (RivDIS). Data set. *Available on-line http://www.daac.ornl.gov from Oak Ridge National Laboratory Distributed Active Archive Center, Oak Ridge, Tennessee, U.S.A.*

Wilks, D. S. (2006). *Statistical methods in athmospheric sciences*. Elsevier, Amsterdam.

Willmott, C. J. and Matsuura, K. (2001). Terrestrial air temperature and precipitation: Monthly and annual time series (1950–1999) Version 1.02. *online*.

Wüst, G. (1961). On the Vertical Circulation of the Mediterranean Sea. *J. Geophys. Res.*, 66(10):3261–3271.

Xoplaki, E., Gonzalez-Rouco, J. F., Luterbacher, J., and Wanner, H. (2003). Mediterranean summer air temperature variability and its connection to the large-scale atmospheric circulation and SSTs. *Climate Dyn.*, 20:723–739.

Yu, L., Jin, X., and Weller, R. A. (2008). Multidecade Global Flux Datasets from the Objectively Analyzed Air-sea Fluxes (OAFlux) Project: Latent and sensible heat fluxes, ocean evaporation, and related surface meteorological variables. *Woods Hole Oceanographic Institution, OAFlux Project Technical Report*, OA-2008-01:64pp.

Zhang, R.-H., Wang, G., Chen, D., Busalacchi, A. J., and Hackert, E. C. (2010). Interannual Biases Induced by Freshwater Flux and Coupled Feedback in the Tropical Pacific. *Monthly Weather Review*, 138(5):1715–1737.

Acknowledgements

Many people have contributed to this work in one way or the other. I am very thank to all of them because without their support I would not have been able to complete this step in my life.

I owe my deepest gratitude to my advisor, Prof. Dr. Daniela Jacob, who gave me the opportunity to become part of her working team, the freedom to explore by my own and advice guiding my studies. I would not have learned as much as I did without all her support. I am deeply grateful to Dr. Uwe Mikolajewicz for introducing me to oceanography, for shearing his knowledge and experience and for his patiently answering all my questions.
I am also indebted to Dr. Dmitry Sein and Irina Fast, who had infinite patience in teaching me about the coupled model and for their support solving the innumerable problems. I would not have been able to do my experiments without their great help. To Dr. Lorenzo Tomassini, for his insightful comments and constructive criticisms to my work, and to Dr. Stefan Hagemann for his advice and help using the hydrological model. A special thanks to Dr. Samuel Somot, from whom I received inspiration and motivation to continue on my track, and for transmitting me his enthusiasm for the Mediterranean issues.
I am also thankful to all my REMO group colleagues for their fruitful help in several ways: shearing expertise, nice discussions, a lot of support, helpful comments, but especially for the very nice day-to-day life. To Antje Weitz and Cornelia Kampmann, for their support in administrative issues and for cheering me up throughout my PhD.
Special thanks to my thesis reviewers, who kindly accepted to check part of my thesis. Thanks again for your time and effort to Christina Rieckers, Meike Strecker, Thomas Raub, Rossina Grim, Christopher Moseley and Christof Wilhelm.
I greatly value the friendship of several people who made my life in Hamburg a great experience. Sorry not to mention the large list, but I am sure you know who you are.
También quiero agradecer a Elena Padorno, por su amistad, continuado apoyo y anímos para seguir adelante. A Pilar García, simplemente por ser mi mejor amiga y estar ahí siempre, y a mi hermana Cynthia Elizalde, por alentarme con todo su cariño.
Finalmente, a mis padres Jorge Elizalde y Graciela Arellano, que cualquier cosa que diga para expresarles mi gratitud a su apoyo incondicional, se quedaría pequeña. Así que a ellos les dedico estos años de esfuerzo. Gracias.

This dissertation is dedicated to my parents Graciela and Jorge



ISSN 1614-1199